The Evolution of the Intergalactic Medium

Matthew McQuinn

Department of Astronomy, University of Washington, Seattle, Washington 98195; email: mcquinn@uw.edu

Annu. Rev. Astron. Astrophys. 2016. 54:313–62

First published online as a Review in Advance on July 22, 2016

The *Annual Review of Astronomy and Astrophysics* is online at astro.annualreviews.org

This article's doi: 10.1146/annurev-astro-082214-122355

Keywords

intergalactic medium, IGM, physical cosmology, large-scale structure, quasar absorption lines, reionization, Lyα forest

Abstract

The bulk of cosmic matter resides in a dilute reservoir that fills the space between galaxies, the intergalactic medium (IGM). The history of this reservoir is intimately tied to the cosmic histories of structure formation, star formation, and supermassive black hole accretion. Our models for the IGM at intermediate redshifts ($2 \lesssim z \lesssim 5$) are a tremendous success, quantitatively explaining the statistics of Lyα absorption of intergalactic hydrogen. However, at both lower and higher redshifts (and around galaxies) much is still unknown about the IGM. We review the theoretical models and measurements that form the basis for the modern understanding of the IGM, and we discuss unsolved puzzles (ranging from the largely unconstrained process of reionization at high z to the missing baryon problem at low z), highlighting the efforts that have the potential to solve them.

Contents

1. INTRODUCTION

Most cosmic matter resides in the void between galaxies known as the intergalactic medium (IGM). At present, roughly half of the dark matter resides in structures that can more or less be thought of as intergalactic (i.e., unvirialized objects and dark matter halos likely too small to contain a galaxy, taken here to be $<10^9\ M_\odot$). The present fraction of baryons that are intergalactic is probably much higher. At earlier cosmic times, the intergalactic reservoir was even larger as fewer massive halos had coalesced from it. By $z = 3$ (6), a much larger 80% (95%) of the dark matter was extragalactic. Eventually, before $z = 20$ or so, the first galaxies had yet to form, and so the term intergalactic is no longer applicable. This review starts at this time, a time for which observations are scant. It ends at the present, again an epoch with few observations, as the IGM has become so tenuous that only its densest constituents are visible. A major focus of this review is the intermediate epochs, when the Universe was one to a few billion years old. During these epochs a rich set of observations provide a fabulous test of IGM models.

An understanding of the IGM is relevant for many astrophysical disciplines. For the cosmologist, the IGM has been used to test our models of structure formation on the smallest comoving scales (Viel et al. 2005, Seljak et al. 2005), it induces anisotropies in the cosmic microwave background (CMB; Ostriker & Vishniac 1986, Hu 2000), and the astrophysical processes that shape the IGM can bias cosmological parameter inferences from galaxy clustering (Pritchard et al. 2007, Wyithe & Dijkstra 2011). For the large community interested in galaxy formation, the IGM is the trough from which galaxies feed, setting the minimum mass of galaxies (Rees 1986, Efstathiou 1992, Thoul & Weinberg 1996) and feeding some galaxies more than others (e.g., Kereš et al. 2005). In addition, the IGM can be used to measure the total ionizing photon production of galaxies (Haardt & Madau 1996, Miralda-Escudé 2003, Faucher-Giguère et al. 2008b, Becker & Bolton 2013) as well as galaxies' stellar nucleosynthetic yield, as a large fraction is ejected into the IGM (e.g., Peeples et al. 2014). For those who focus on our own Milky Way, aside from the obvious connection that the Milky Way too is fed by the same intergalactic spigot, we note that many of the physical processes at play in the IGM are simplified versions of those encountered in the interstellar medium (ISM).

An appeal of studying the IGM is that we have an excellent understanding of the cosmological initial conditions and of the equations that govern much of the subsequent evolution of what becomes the IGM. Although uncertain astrophysical processes certainly enter into the equations, for times well after reionization and densities less than ten times or so the cosmic mean, the consensus view is that astrophysical effects can essentially be ignored (as astrophysical radiation backgrounds are approximately uniform, and galactic mechanical feedback is mostly localized in the dense regions around the sources). This view (which has been tested extensively in the HI Lyα forest) enables intergalactic studies to search for subtle effects, potentially improving constraints on the cosmological initial conditions, on the sources of intergalactic heating and on how galactic winds operate.

The aim of this review is to highlight the developments that form the modern understanding of the IGM. This means covering a lot of ground (spanning from the cosmic dark ages to the present day) at the expense of only being able to discuss the major developments on each topic. However, this approach allows us to present a more holistic understanding of the IGM, which we think is particularly important as, e.g., the properties of the IGM at any epoch are connected to those at other epochs. For uncovered topics, we point the reader to the more comprehensive recent review by Meiksin (2009). There are also reviews from the past decade that overlap with topics covered in this review: Fan et al. (2006) on reionization, Bregman (2007) on the missing baryon problem, Morales & Wyithe (2010) on the high-redshift 21-cm signal, and Bromm & Yoshida (2011) on the first galaxies. We find, largely because of our focus on the history and properties of the IGM, that the overlap is not so substantial.

This review adopts a narrow definition of the IGM as being anything outside of the virial radius of galaxies and clusters (the medium between halos rather than the medium between galaxies). In terms of density, this means we are considering gas that has densities less than $\sim$200 times the mean cosmic density. We do not cover the literature on damped Lyα (DLA) systems (Wolfe et al. 2005, which are primarily on the outskirts of galactic disks), on the intracluster medium (Rosati et al. 2002, Kravtsov & Borgani 2012), or on the circumgalactic medium (Stocke et al. 2013, Werk et al. 2014). For many observations, however, the distinction between intergalactic and galactic/circumgalactic can be difficult. In fact, there is debate as to whether almost all of the intergalactic metal line absorption at $z \sim 0$ could actually arise from within virialized regions (Shull et al. 2012b, Prochaska et al. 2011). We use this pretext to opt out of a detailed summary of the extensive literature on metal absorption lines in quasar spectra, focusing primarily on pixel optical depth constraints on metal absorption (which are unquestionably probing intergalactic gas).

The calculations presented in this review assume the concordance flat ΛCDM cosmological model with $\Omega_m \approx 0.3$, $\Omega_b \approx 0.045$, $\sigma_8 \approx 0.8$, $n_s \approx 0.96$, and $Y_{\rm He} = 0.25$ (Planck Collaboration et al. 2015), although the precise value of these parameters depends on the study being summarized. We also assume the standard Fourier convention used in cosmology in which the (2π)'s only appear under the dk's. We now briefly overview the history of the IGM, and we use this overview to serve as an outline for ensuing sections.

1.1. A Brief Overview and Review Outline

Nearly scale invariant and Gaussian potential fluctuations (evolved from early times in a ΛCDM background Friedmann-Lemaître-Robertson-Walker cosmology with a photon-to-baryon ratio of a billion) explain the statistical properties of the CMB and the clustering of galaxies (Peebles 1980, Dodelson 2003), not to mention the nucleosynthetic yields of the Big Bang (Fields & Sarkar 2006). Also from CMB observations, we know that the cosmic gas "recombined" and became neutral around the Universe's 400,000th birthday ($z \approx 1{,}100$). Subsequently this gas cooled with

the expansion of the Universe. It is from these cold conditions that the IGM emerged, its structure largely the result of gravity acting on the primordial matter fluctuations.

The history of the IGM is tied to the history of star and supermassive black hole formation, as these objects are thought to be the primary sources of intergalactic heating, ionization, and metal enrichment. The first star likely formed in the rarest peak in the cosmological density field at a redshift of ∼70 (Naoz et al. 2006). This star and its more immediate brethren are thought to have formed in 10^5–10^7-$M_\odot$ halos—halos whose virialized gas is hot enough to cool and condense by exciting molecular hydrogen transitions. Gradually, more and more stars formed in the Universe. Trenti & Stiavelli (2009) estimate that the Universe reached a saturation level of PopIII star formation in minihalos of $\sim 10^{-5}$–$10^{-4}\,M_\odot$ year^{-1} comoving Mpc^{-3} at $z \sim 20$–30, with saturation set by their 11–13-eV radiative backgrounds destroying the molecular hydrogen coolant that had created them (Haiman et al. 2000). Such low star-formation rates are insufficient to ionize but a small fraction of the then neutral IGM, even for a top-heavy stellar population that simulations find is most likely (Abel et al. 2002; Greif et al. 2011). If some of these stars ended their lives in pair-instability supernovae or in other exotic stellar deaths, then they may be detectable in the IGM via their enrichment patterns (Heger & Woosley 2002, Kulkarni et al. 2013; see Section 2.6).

The first galaxies formed later in halos with masses of $\gtrsim 10^8\ M_\odot$, halos that could cool by more robust atomic transitions and that formed in abundance around $z \sim 10$ (Barkana & Loeb 2001, Bromm & Yoshida 2011). Unlike the diminutive dark matter halos that hosted the first stars, which likely formed only a handful of stars (Abel et al. 2002, Bromm & Larson 2004, Greif et al. 2011), these halos were able to harbor more sustained star formation (Mac Low & Ferrara 1999, Bromm & Yoshida 2011). It is thought that even our soon-to-be-launched large space telescope, the James Webb Space Telescope, will not be able to directly image galaxies in halos with $<10^{9-10}\,M_\odot$ at $z > 6$ (Kuhlen & Faucher-Giguère 2012, Behroozi & Silk 2015), and so the first galaxies may be most detectable through their impact on the IGM.

Once the first galaxies emerged, there was not much time before the IGM was affected by the associated radiative backgrounds. First, their ∼10-eV and soft X-ray backgrounds, respectively, pumped the hyperfine states of hydrogen and heated the gas in manners that are potentially observable with the 21-cm line of atomic hydrogen (e.g., Madau et al. 1997, Furlanetto et al. 2006). Next, their greater-than 13.6-eV photons photoionized nearly all the intergalactic hydrogen. Cosmological reionization also heated the IGM to tens of thousands of degrees Kelvin, smoothing the cosmic distribution of gas and affecting the subsequent formation of galaxies. We discuss observations that constrain reionization as well as theoretical models of this process in Section 3.

Once the cosmic hydrogen became reionized, a largely uniform metagalactic ionizing background quickly pervaded space and kept the intergalactic hydrogen highly ionized. It is thought that, at high redshifts, this background was sourced by stars but that by $z \sim 3$ quasars became important if not dominant. Over $2 < z < 5$, owing to several fortuitous factors, there is a wealth of absorption-line data for intergalactic hydrogen, helium, and select metals, far more intergalactic data than at other cosmic epochs. These data have been used to show that the structure of the low-density IGM is in quantitative agreement with cosmological simulations of the ΛCDM cosmology, to understand the evolution of the ionizing background, to measure the temperature of the IGM, and to constrain the intergalactic enrichment history. We discuss these observations of the intermediate redshift IGM in Section 2.

By lower redshifts still ($z \lesssim 2$), it again becomes difficult to observe the bulk of the intergalactic volume as cosmological expansion has further diluted most cosmic gas. In addition, structure formation shocks become more efficient at heating intergalactic gas, putting ∼50% in a warm-hot 10^{5-6}-K phase by the present (Cen & Ostriker 1999), which is a phase that is even more difficult to

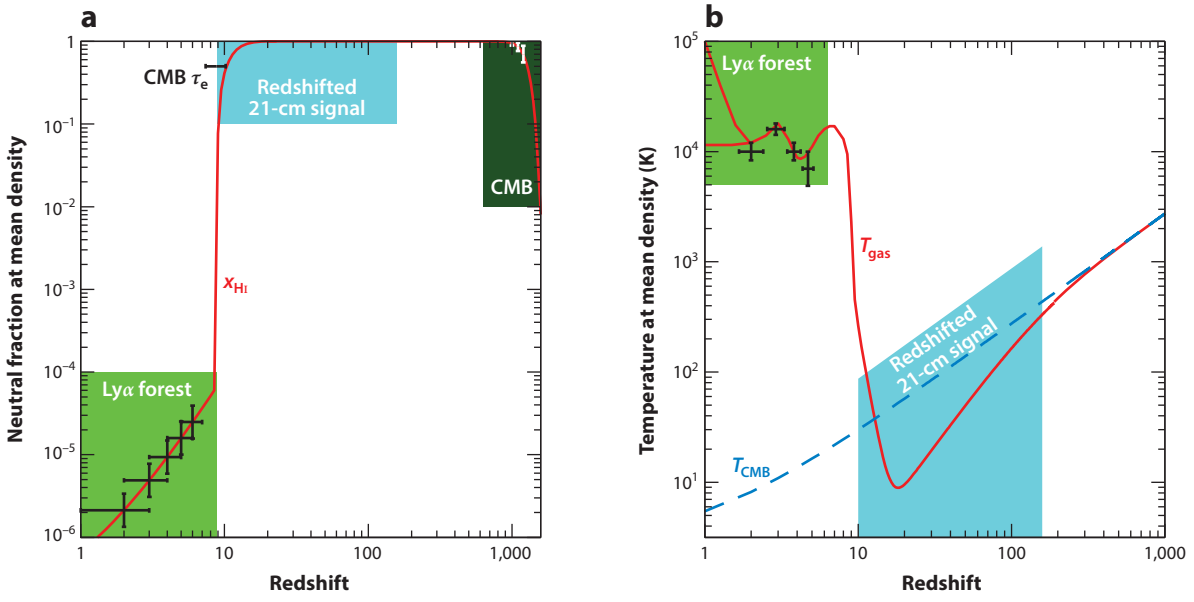

Figure 1

Diagram showing the ionization and thermal history of intergalactic gas. The red curves show a model of intergalactic gas. Error bars symbolize existing constraints, and the highlighted regions illustrate the potential purview of the named cosmological probe. In the temperature panel, the model curve bifurcates at low redshifts to indicate the intergalactic medium (IGM) temperature becoming multiphase.

probe observationally than the unshocked $\sim 10^4$-K photoionized one. The low-redshift IGM has had much more time to be affected by astrophysical processes, and these processes in turn shape gas accretion onto galaxies. Section 4 describes our understanding of the present-day IGM.

The solid curves in **Figure 1** show a theoretical model for the thermal and ionization history of the Universe. The highlighted regions represent the space that is potentially constrained by different cosmological probes. Error bars symbolize existing constraints. This review covers the IGM probes that appear in this figure as well as a few others.

2. THE IGM AT INTERMEDIATE REDSHIFTS, $z = 2$–5

Redshifts of $z = 2$–5 set the foundation for our understanding of intergalactic matter. This redshift range has been so important, firstly, because at $z \gtrsim 2$ the Lyα line (as well as some of the most useful metal lines, particularly CIV $\lambda\lambda$1548, 1551 Å, and OVI $\lambda\lambda$1032, 1038 Å) has redshifted sufficiently that it can be observed with ground-based optical telescopes and, secondly, because there are plenty of bright quasars that enable high signal-to-noise (S/N) spectra at high resolution. In addition, at these times the density and ionization state of the IGM are ideal for probing gas near the cosmic mean density with the HI Lyα forest. The Lyα forest spectral region of hundreds of quasars has been observed at high resolution with 10-m telescopes (see O'Meara et al. 2015) and the number has surpassed a hundred thousand at medium resolution with the Sloan telescope (Lee et al. 2013). These quasar spectra have been used to conduct precision tests of the Lyα forest (Section 2.1), to measure the HI column density distribution (Section 2.2), to constrain the thermal history of the IGM (Section 2.3), to constrain the metagalactic ultraviolet background (Section 2.4), to study the HeII Lyα forest (Section 2.5), and to measure the enrichment of intergalactic gas

(Section 2.6). This grab bag of measurements and tests, whose summary composes this section, forms the basis for our understanding of the IGM at intermediate redshifts.

2.1. The Lyα Forest

Soon after Schmidt (1965) detected several quasi-stellar objects at significant redshifts, it was realized that there should be hydrogen Lyα absorption in their spectra from intervening intergalactic gas (Bahcall & Salpeter 1965, Gunn & Peterson 1965, Scheuer 1965). However, it took until the mid-1990s for the study of the Lyα forest to reach maturity, following the commissioning of High Resolution Echelle Spectrometer (HIRES) on the Keck telescope (Vogt et al. 1994), which enabled resolved studies of the Lyα forest absorption (Hu et al. 1995, Kim et al. 1997, Kirkman & Tytler 1997), and also following the advent of cosmological hydrodynamics simulations in the emerging cold dark matter model (Cen & Ostriker 1992, Katz et al. 1992). (See Rauch 1998 for more on the history.) Indeed, calculations of mock Lyα forest spectra using the first cold dark matter simulations showed a forest of absorption much like that in the actual observations (Cen et al. 1994, Zhang et al. 1995, Hernquist et al. 1996, Miralda-Escudé et al. 1996), reinforcing this suggestion from earlier analytic models (Bi et al. 1992). This success led to the modern paradigm that the "trees" in the forest are the highly photoionized sheets, filaments, and halos that result from cosmic structure formation in a Universe with gravitationally dominant cold dark matter and with an approximately uniform ionizing background. This paradigm has been subjected to a battery of tests with hardly a chink in its armor. In the following we describe the latest comparisons and how they relate to our present understanding of the low-density IGM.

Figure 2 shows spectra of three of the brightest quasars at their respective redshifts, focusing on the Lyα forest spectral region. The hydrogen Lyα forest is a region in the spectrum of all high-redshift sources that appears blueward of the HI Lyα resonance in the frame of the source, observed at $1216\,(1+z)$ Å, where z is the redshift of the quasar. It corresponds to the absorption of intergalactic neutral hydrogen "clouds" along the quasar's sightline, with a cloud at redshift z_1 absorbing in Lyα at $1216\,(1+z_1)$ Å. It is typically studied in quasar spectra, with each spectrum probing the absorption of gas that lies ∼1 Gpc in front of the quasar (as foreground HI continuum absorption tends to eliminate the ultraviolet flux blueward of 912 Å, especially for $z \gtrsim 2$ sightlines). At each location, the Lyα optical depth corresponding to gas at a fixed density with a smooth line-of-sight gradient, $\mathrm{d}v/\mathrm{d}x$, in velocity (including the Hubble contribution) is given by

$$\tau_{\mathrm{Ly}\alpha} = 1.3\,\Delta_b \left(\frac{x_{\mathrm{HI}}}{10^{-5}}\right)\left(\frac{1+z}{4}\right)^{3/2}\left[\frac{\mathrm{d}v/\mathrm{d}x}{H(z)/(1+z)}\right]^{-1}, \tag{1}$$

where the optical depth is related to the absorption probability via $P = \exp(-\tau_{\mathrm{Ly}\alpha})$. Here, Δ_b is the baryonic density in units of the cosmic mean, and x_{HI} is the fraction of hydrogen that is neutral. Similarly, there are Lyβ, Lyγ, Lyδ, etc. HI absorption forests, corresponding to absorption into a progressively higher-n Rydberg state. With increasing n, the associated forest spans a progressively shorter path length (and falls on top of lower redshift, smaller-n forests) and is less absorbed (owing to smaller oscillator strengths).

Equation 1 shows that the Lα forest is sensitive to $x_{\mathrm{HI}} \sim 10^{-5}$ at $z = 3$, which translates to astonishingly low HI number densities of $n_{\mathrm{HI}} \sim 10^{-10}\ \mathrm{cm}^{-3}$. It turns out that over much of cosmic time such number densities occur in the low-density IGM (as is apparent from the spectra in **Figure 2**). In the postreionization IGM, x_{HI} is physically set by the balance between photoionization and recombination and is given by

$$x_{\mathrm{HI}} = \frac{\alpha_A n_e}{\Gamma}, \tag{2}$$

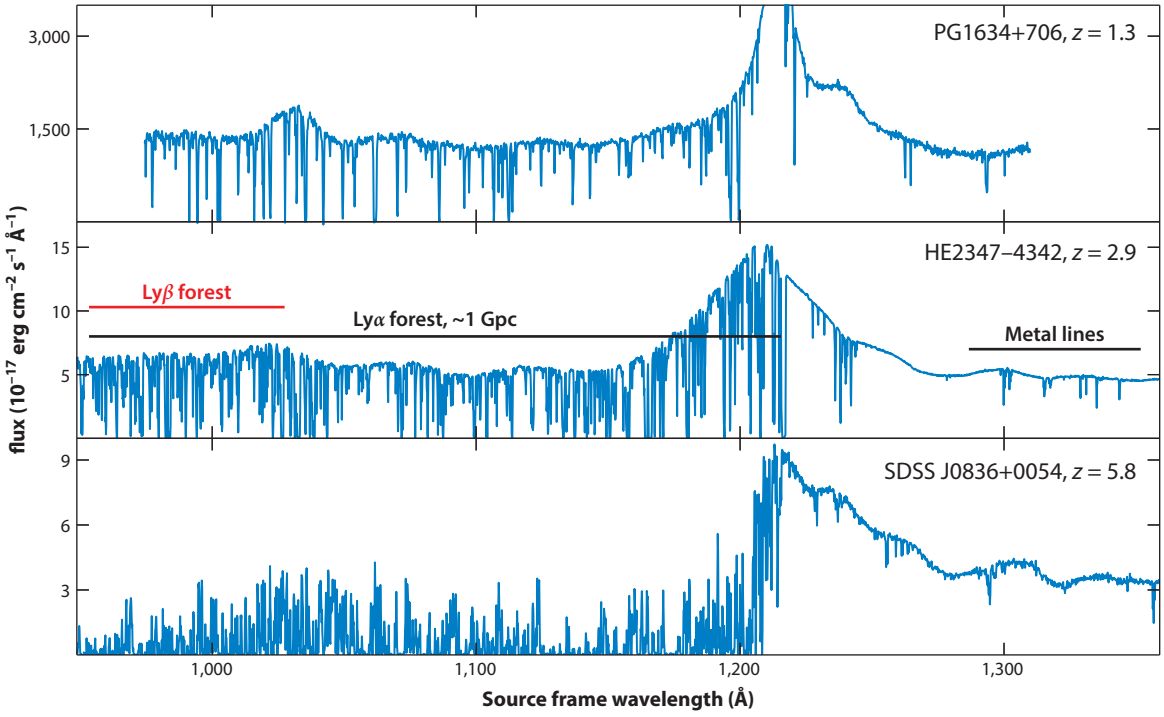

Figure 2

Lyα forest spectral region for three quasars chosen to span a large range in redshift. The HST/STIS spectrum of PG1634+706 was provided by X. Prochaska, the VLT/UVES spectrum of HE2347-4342 by C. Fechner (Fechner & Reimers 2007), and the VLT/X-Shooter spectrum by G. Becker (D'Odorico et al. 2013).

except in regions that have been shock heated to $\gtrsim 10^5$–10^6 K such that collisional ionization becomes important. Equation 2 assumes photoionization equilibrium and that $x_{\rm HI} \ll 1$, which both likely hold as the photoionization time $\Gamma^{-1} \sim 30{,}000$ years (a number that, remarkably, is valid over a large range in redshift, $1 \lesssim z \lesssim 5.5$) is much shorter than the recombination time $(\alpha_A n_e)^{-1} \sim 10^{10} \Delta_b^{-1} [(1+z)/4]^{-3}$ years. The photoionization time is also the timescale to reach equilibrium.

Inference from the Lyα forest spectra is complicated by the fact that there is no reliable analytic model for the mildly nonlinear densities probed by the forest. All analyses require a comparison with large cosmological simulations (see the sidebar Cosmological Simulations of the IGM). **Figure 3**, from Weinberg et al. (2003), shows just such a comparison. The top two panels show the Lyα forest transmission of a real quasar observed with the HIRES instrument on the Keck I telescope, zooming in on several select regions. The other panels show the Lyα forest extracted from cosmological hydrodynamic simulations in three different cosmologies. In addition, the dotted curves in the ΛCDM panels are computed assuming that the gas traces the dark matter, an approximation that nearly reproduces the absorption seen in the full hydrodynamic calculation (*solid curve*). Thus, the absorption structures in the Lyα forest largely follow the underlying voids, sheets, and filaments in the dark matter (e.g., Meiksin & White 2001).

Figure 3 shows that the ΛCDM model predicts a forest that is qualitatively similar to that seen in observations. To make this comparison more quantitative (as well as to appreciate the

COSMOLOGICAL SIMULATIONS OF THE IGM

At early times the matter overdensity fluctuations in the Universe, $\delta \equiv \Delta_b - 1$, were small such that $\delta \ll 1$, with properties that are understood from observations of the CMB as well as other probes of large-scale structure. Their smallness allows one to solve for their evolution using simple perturbative equations. The matter overdensity fluctuations grow with time and eventually become nonperturbative, requiring a simulation. The typical collisionless matter-only (or N-body) cosmological simulation starts with a grid of particles for the dark matter at time zero (the limit in which $\delta = 0$) and, assuming periodic boundary conditions, displaces them using perturbation theory to their positions at redshifts of a hundred or so [when the fluctuations in the density at the grid resolution are $\mathcal{O}(0.1)$ such that perturbation theory is still applicable; Klypin & Shandarin 1983, White et al. 1983, Kuhlen et al. 2012]. From there, the evolution of the dark matter particles is evolved using the full nonlinear dynamics. In linear perturbation theory (which is the order used to set the initial displacements in the majority of simulations), the Fourier series of the initial displacements equals $-i\tilde{\delta}_k/k$ (Zel'dovich 1970), where the δ_k are the Nyquist-sampled Fourier series expansions of $\delta(\boldsymbol{x})$ in the box. Each of the $\tilde{\delta}_k$ in the simulation box is a Gaussian deviate with standard deviation in modulus of $P_{\rm L}(k, z)V^{-1}$ and random phase, where V is the simulation volume and $P_{\rm L}(k, z)$ is the linear-theory matter power spectrum (which can be easily calculated with widely used codes such as CAMB; **http://camb.info**).

When the dynamics of the gas is included, in addition to following the trajectories of collisionless dark matter particles, a hydro solver is employed for the gaseous evolution. To study the IGM, the gas also needs to be heated and cooled appropriately. Except for the small set of simulations that attempts to model reionization with radiative transfer, the bulk of cosmological simulations employ a uniform ionizing background that determines the ionization states and temperatures of the gas (see Section 2.4). These simulations also incorporate the cooling rates for all processes relevant for primordial gas (Katz et al. 1992), with some also incorporating cooling due to metals (e.g., Wiersma et al. 2009).

Accurate simulations are necessary for modern Lyα forest analyses. Although different methods for solving the hydrodynamics and gravity yield nearly identical predictions (Regan et al. 2007, Bird et al. 2013, Lukić et al. 2015), numerical convergence in box size and in resolution is notoriously tricky (Meiksin & White 2004, McDonald et al. 2005b, Bolton & Becker 2009, Tytler et al. 2009, Lidz et al. 2010, Lukić et al. 2015). A typical modern simulation used to study the Lyα forest has of order $N_{\rm side}^3 = 1{,}000^3$ gas resolution elements and dark matter particles, although some have reached a few times larger $N_{\rm side}$ employing Eulerian hydro grids (e.g., Lukić et al. 2015). With $1{,}000^3$ elements, a box size of $\approx$20 comoving Mpc is required to resolve 10^6-$M_\odot$ structures, roughly 10^{-4} of the Jeans' mass for mean density gas at $z = 3$, which is the mass resolution studies have found is required for 1–10% accuracy in many forest statistics (Bolton & Becker 2009, Lidz et al. 2010, Lukić et al. 2015). The standard deviation of δ when smoothed over a 20-Mpc cubic volume is $\approx$0.2 at $z = 3$, and so at this level a 20-Mpc box is not representative of the Universe. Large simulations (or extrapolations based on moderate-sized ones) are often necessary for robust inferences.

implications), we need to understand how the simulations model the density structures, the photoionization rates, and the gas temperatures. In addition, analyses must account for common contaminants of the Lyα forest signal. There are a standard set of prescriptions for dealing with each of these:

1. The statistical properties of the gas density field are assumed to be those expected from evolving (via the equations of hydrodynamics and gravity) the cosmological initial conditions subject to a uniform ionizing background that turns on at $z \sim 10$. This posits

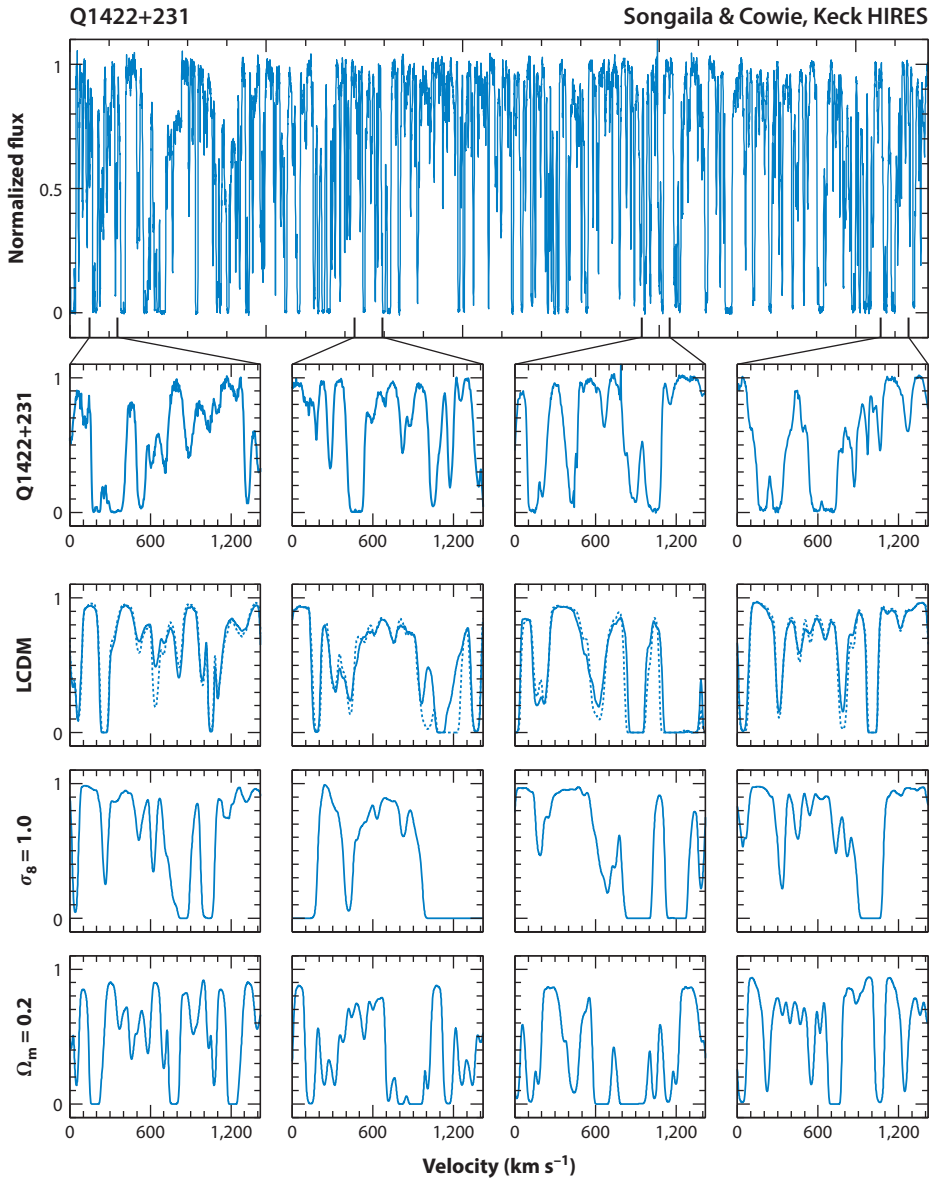

Figure 3

Top two rows show the continuum-normalized Lyα forest spectrum taken with KECK/HIRES of quasar Q1422+231, zooming in on four select regions. The bottom three rows show the absorption in hydrodynamic simulations using three different cosmologies, where the stated parameter is varied from the ΛCDM case taking $\sigma_8 = 0.8$ and $\Omega_m = 0.4$. The same random numbers are used to initialize all simulations. The dotted curves in the ΛCDM panels are from an *N*-body simulation without gas; the absorption of this case is computed assuming that gas traces the *N*-body matter distribution. Adapted from Weinberg et al. (2003) with permission.

that galactic feedback processes—which are known to blow baryons out of galaxies—do not significantly impact the low-density gas seen in the Lyα forest. This supposition is supported by simulations with simple feedback prescriptions (Theuns et al. 2002b, McDonald et al. 2005a, Bertone & White 2006, Kawata & Rauch 2007), although it may not hold to the forecasted precision of upcoming Lyα forest analyses (Viel et al. 2013).

2. The HI photoionization rate Γ (and hence the ionizing background) is assumed to be spatially uniform, which is motivated by the much longer mean free path of ionizing photons relative to the mean distance between sources—a scenario that suppresses fluctuations (Croft 2004, McDonald et al. 2005a). In addition, the amplitude of Γ is adjusted in postprocessing (an approximation justified in Section 2.4) until the simulations match the observed mean amount of absorption in the forest. A by-product of this adjustment is a "flux decrement" measurement of Γ, with Becker & Bolton (2013) finding a remarkably constant $\Gamma \approx 10^{-12\pm0.3}$ s^{-1} over the range $2 < z < 5$ (see also Rauch et al. 1997, Meiksin & White 2003, Bolton et al. 2005, Faucher-Giguère et al. 2008a).
3. The temperature is assumed to be a power-law function of density as motivated in Hui & Gnedin (1997), an assumption that should not apply during and soon after reionization processes (Trac et al. 2008, Furlanetto & Oh 2009, McQuinn et al. 2009). The power-law assumption is in many studies implicit as they use hydrodynamic simulations with a uniform ionizing background that results in a near power-law relation. Often this power law is parameterized in terms of the density in units of the cosmic mean, Δ_b, as

$$T(\Delta_b) = T_0 \Delta_b^{\gamma-1}, \tag{3}$$

with T_0 and $\gamma - 1$ being parameters that are varied to fit the observations. We discuss the physics of what sets T_0 and $\gamma - 1$ as well as the latest constraints on the temperature in Section 2.3. Many studies adjust the temperatures in postprocessing rather than use the temperatures generated in the simulation, which captures temperature's effect on thermal broadening but not on the gas pressure. (The smoothing from gas pressure is the smaller of these effects for most Lyα forest statistics.) Others inject heat into the simulated gas in a way that achieves a specified T_0 and γ (e.g., Bolton et al. 2008).
4. It is assumed that the Lyα forest absorption can be extracted sufficiently well that metal line contamination, errors in the estimate of the quasar's intrinsic continuum, and damping wing absorption do not bias inference. Each of these contaminants comes with its own set of issues and techniques for addressing them:

   Metal lines are responsible for 10% of the absorption in the Lyα forest spectral region at $z = 2$, with a decreasing fraction toward higher redshifts (Schaye et al. 2003, Kirkman et al. 2005, Section 2.6). Metal absorption can be isolated or corrected for by studying the absorption redward of the forest or, for high-quality data, within the forest itself, often using the doublet structure of prominent ions.

   The quasar continuum is fit by finding low-absorption points and interpolating between them in high-quality spectra. This method leads to quantifiable errors (e.g., Bolton et al. 2005, Faucher-Giguère et al. 2008a), which increase with redshift and, for many analyses, are small enough to safely ignore.

   Damping wing absorption becomes significant for dense systems with $N_{\rm HI} \gtrsim 10^{19}$ cm^{-2}, with one system occurring every several Lyα forest spectra at $z \sim 3$. Systems with significant damping wings are not captured reliably in standard cosmological simulations. These systems often can be removed visually.

In high S/N, high-resolution spectra, all of these issues are easier to diagnose/eliminate. For Sloan spectra, more sophisticated techniques than those listed above are often required (e.g., McDonald et al. 2005b).

Many studies have found that, once these prescriptions are adopted, mocks extracted from simulations are able to describe the standard set of statistics applied to the Lyα forest data, and some have even leveraged this result to constrain cosmological parameters. However, others have found potential discrepancies. We now discuss the state of this comparison for the three most studied statistics.

2.1.1. The line-of-sight power spectrum. The line-of-sight Lyα forest power spectrum is the most studied of all Lyα forest statistics, defined as $P_F(k) \equiv L^{-1}|\tilde{\delta}_F(k)|^2$, where $\delta_F(x) \equiv F(x)/\langle F(x)\rangle - 1$ is the overdensity in the transmission at position x over a sightline of length L and $\tilde{\delta}_F(k)$ is its Fourier transform. (Often the transmission is called the normalized flux.) **Figure 4*a*** shows for a multitude of redshifts $\Delta_F(k)^2 \equiv kP_F(k)/\pi$, a combination whose integral over $d\log k$

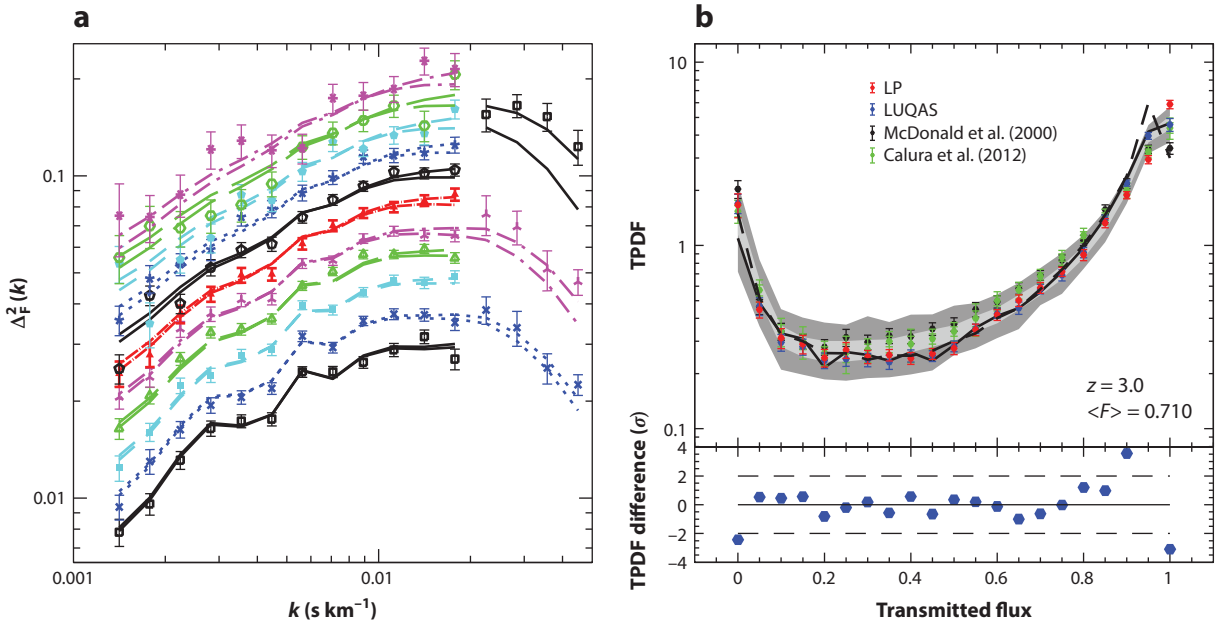

Figure 4

The two statistics that are most commonly applied to the Lyα forest. (*a*) The power spectrum of the normalized flux, showing kP_F/π, from Seljak et al. (2006). The points with error bars are measurements using 3,000 Sloan quasar spectra for $k < 0.02$ s km^{-1} (with the lowest set being $z = 2.2$ and the highest $z = 4.2$, in increments of $\Delta z = 0.2$) and eight high-resolution quasar spectra at higher wavenumbers (showing $z = 2.4$, 3.0, and 3.9). The underlying curves are the predictions of the cold dark matter model (*thick curves*) and of a model in which a 6.5-keV sterile neutrino is the dark matter (*thin curves*). (*b*) The top part of the panel shows the Lyα forest transmission probability distribution function (TPDF) at $z = 3$. The points with error bars show three measurements of this statistic, the solid curve is this statistic estimated from a simulation, and the shaded regions represent bootstrap error estimates matching the sampling of the measurement of Bergeron et al. (2004), labeled "LP," and calculated by sampling skewers from the simulation (with the shading indicating the 1σ and 2σ errors). Adapted from Rollinde et al. (2013) with permission. The bottom part of the panel shows the residuals between the LP measurement and the simulations in units of the 1σ bootstrap error. Abbreviation: LUQAS, Large Sample of UVES Quasar Absorption Spectra.

is the variance in the transmission overdensity (from Seljak et al. 2005). At high wavenumbers $k \gtrsim 0.02$ s km^{-1}, $P_F(k)$ is sensitive to the small-scale smoothing of the gas (constraining the gas temperature as well as the warmness of the dark matter), whereas smaller wavenumbers are primarily sensitive to the large-scale density distribution of matter. Many other (astrophysical) effects that could potentially affect P_F have been found to be small in physically motivated models. These include spatial variations in $T(\Delta_b)$, spatial variations in the ionizing background, and galactic feedback processes (Croft 2004, Meiksin & White 2004, McDonald et al. 2005b, Lai et al. 2006, McQuinn et al. 2011a). This robustness to messy astrophysical processes potentially allows one to use P_F to constrain cosmological parameters.

Studies find that the predictions of simulations of the Lyα forest agree with the observed P_F, a confirmation of the standard model for the forest (Croft et al. 1999, 2002; McDonald et al. 2000; Tytler et al. 2004). This exercise has been conducted with an increasing level of precision, finding over the range of $2 \lesssim z \lesssim 4.5$ that, when tuning the IGM $T - \Delta_b$ relation and cosmological parameters within allowed bounds, the standard simulations yield good χ^2 values even when the estimate uses 3,000 (McDonald et al. 2005b) and, recently, 14,000 Sloan spectra (Palanque-Delabrouille et al. 2013, 2015). The former measurement is featured in **Figure 4*a***, showing the P_F estimates and best-fit model in the range of $2.2 < z < 4.2$ in increments of $\Delta z = 0.2$. These measurements are so precise that by themselves they constrain the amplitude of density fluctuations (σ_8), the matter density (Ω_m), and the tilt of the primordial power spectrum (n_s) to 5–10% (Viel & Haehnelt 2006). These constraints derive from smaller comoving scales than the constraints from other cosmological probes (down to ∼1 Mpc, a decade beyond other techniques). The agreement between cosmological parameters inferred from the forest and other methods is a fabulous consistency test of the inflation+ΛCDM paradigm, in which there is nearly zero parametric freedom in how density fluctuations on disparate scales are connected. The bottom three rows in **Figure 3** illustrate how the absorption in the forest changes in the concordance cosmology relative to cosmologies with a low Ω_m and a high σ_8. Although it is debated whether to trust cosmological parameter determinations from P_F (with skeptics pointing to the high value of σ_8, the seemingly unphysical temperatures that the analyses favor, or discrepancies between their mean transmission inferences and more direct measurements; Viel & Haehnelt 2006, Becker & Bolton 2013), at the $\lesssim$10% level the Lyα forest power spectrum is consistent with the favored ΛCDM cosmology. The 1D power spectrum is also well suited for constraining warm dark matter models that act to truncate the power at high wavenumbers. The lower curves in **Figure 4*a*** show a 6.5-keV sterile neutrino warm dark matter model that is clearly ruled out (Seljak et al. 2006; see also Viel et al. 2013.)

2.1.2. The probability distribution function of transmission. After the Lyα forest power spectrum, the Lyα forest transmission probability distribution function (TPDF) is the most studied statistic (e.g., McDonald et al. 2000, Lidz et al. 2006, Kim et al. 2007, Lee et al. 2015). This statistic is shown in **Figure 4*b***. Bolton et al. (2008) and Calura et al. (2012) argued that the measured TPDF over $2 \lesssim z \lesssim 3$ disagrees with estimates from cosmological simulations. Studies have proposed several potential resolutions, including the temperature-density relation of the IGM being "inverted" such that $\gamma - 1 < 0$ (Bolton et al. 2008, Puchwein et al. 2012), that the difference is due to continuum fitting errors (Lee 2012), or that the quoted error bars in previous analyses underestimated the sample variance (Rollinde et al. 2013). The latter solution is shown in **Figure 4*b***. Rollinde et al. (2013) found that several previous independent measurements of the TPDF (which had used ∼10–20 Lα forest sightlines broken into a few redshift bins) were inconsistent in each transmission bin at a few standard deviations using their quoted errors. Furthermore, when Rollinde et al. measured the TPDF using a large simulation but emulating the sampling statistics of the measurements, their bootstrap error estimates were much larger than the errors reported

on previous measurements and large enough to yield good χ^2 values. This result suggests that there is no tension between the data and simulations regarding the TPDF.

2.1.3. The line-width distribution. A final Lyα forest statistic that is often encountered is the line-width PDF (Hu et al. 1995, Davé et al. 1997, Theuns et al. 1998, Hui & Rutledge 1999). There have also been claimed discrepancies in this statistic between the observations and simulations, with Tytler et al. (2009) finding a 10% difference. We are not worried about this level of discrepancy. The line-width PDF is very sensitive to the thermal history, which is only crudely modeled in standard simulations. Indeed, the line widths themselves are used to measure the thermal history (Schaye et al. 2000, Bolton et al. 2014; see Section 2.3), suggesting that with the correct thermal history the simulations' line widths may match the observed distribution.

In conclusion, our vanilla models of the forest agree with the observations to $\lesssim$10% in the standard statistics, with no convincing discrepancies. Future progress can be made by increasing the precision of the measurements and targeting new statistics (as the standard three statistics could be insensitive to interesting effects). One such statistic is the two-point transmission correlation function between adjacent sightlines, which studies have found can be more sensitive to astrophysical effects than the 1D statistics discussed here (McDonald & Eisenstein 2007, White et al. 2010, McQuinn & White 2011, Gontcho et al. 2014, Pontzen et al. 2014, Arinyo-i-Prats et al. 2015).

2.2. The HI Column Density Distribution

The column density distribution of HI absorbers—the number of absorbers per unit column density per unit path length—is another statistic that is often measured from quasar absorption spectra. The method used to measure this statistic depends strongly on column. The lowest HI columns ($N_{\rm HI} \lesssim 10^{14}$ cm^{-2}) are measured using just Lyα absorption. At $10^{14} \lesssim N_{\rm HI} \lesssim 10^{17}$ cm^{-2}, the column density of an HI absorber is inferred by also using absorption from higher Lyman-series lines. Around $N_{\rm HI} \sim 10^{17}$ cm^{-2}, breaks from continuum absorption of HI in the spectrum are used (or, statistically, by stacking around source-frame 912 Å; Prochaska et al. 2009). Finally, at $N_{\rm HI} \gtrsim 10^{19}$ cm^{-2}, the damping wing of the Lyα line is exploited. The somewhat tedious terminology for systems in different column density ranges, which we avoid here, is given in the margin. This combination of methods has been used to measure the HI column density distribution over the entire range that occurs in nature (most recently by Fumagalli et al. 2013, Kim et al. 2013, Rudie et al. 2013, Worseck et al. 2014b). The points with error bars in **Figure 5** show select previous measurements.

Lyman limit: $10^{17.2}$–10^{19} cm^{-2}

Super Lyman limit: 10^{19}–$10^{20.3}$ cm^{-2}

Damped Lyα (DLA): $N_{\rm HI} > 10^{20.3}$ cm^{-2}

The HI column density distribution is a diagnostic of the distribution of gas densities in the Universe. A useful model for the relationship between column density, size, and physical density for overdense absorbers that cannot self-shield to the background (i.e., $\lesssim 10^{17}$ cm^{-2}) was proposed by Schaye (2001b). This study argued that the size of an absorber was on average set by the distance a sound wave travels in the dynamical time ($t_{\rm dyn} \sim 1/\sqrt{G\rho} \sim H^{-1}\Delta_b^{-1/2}$). This distance is also known as the Jeans' length. Assuming a photoionization rate and a temperature allows one to then relate the density of an absorber to its column density via (Schaye 2001b)

$$\Delta_b = 200 \left(\frac{1+z}{4}\right)^{-3} \left(\frac{N_{\rm HI}}{10^{17}\ {\rm cm}^{-2}}\ \frac{\Gamma}{10^{-12}\ {\rm s}^{-1}}\right)^{2/3} \left(\frac{T}{10^4\ {\rm K}}\right)^{0.17}. \quad (4)$$

Note that $\Gamma \sim 10^{-12}$ s^{-1} is the HI photoionization rate that is measured over the range $2 < z < 5$. This model has been verified using cosmological simulations (Altay et al. 2011, McQuinn et al. 2011b), and shows that the type of system that yields a certain $N_{\rm HI}$ varies dramatically over time,

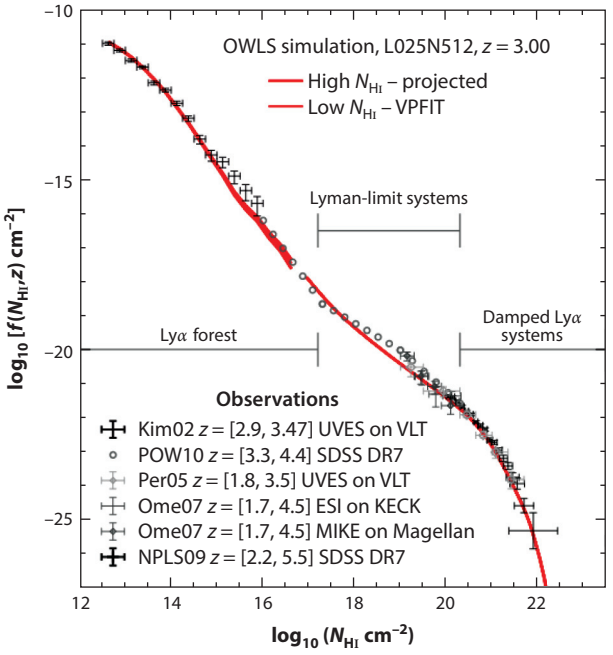

Figure 5

Log_{10} of the number of HI systems per $\mathrm{d}N_{\mathrm{HI}}$ per $\mathrm{d}X \equiv (1+z)^{1/2}\Omega_m^{-1/2}\mathrm{d}z$, measured from cosmological simulations (*red curve*) and from quasar absorption spectra (*points with error bars*). Adapted from Altay et al. (2011) with permission. Abbreviation: OWLS, OverWhelmingly Large Simulations project.

with absorbers having $N_{\mathrm{HI}} \lesssim 10^{17}[(1+z)/4]^3$ cm^{-2} corresponding to the $\Delta_b < 200$ gas that is likely to be intergalactic. Even though they are not necessarily intergalactic, the properties of systems with $N_{\mathrm{HI}} \sim \sigma_{\mathrm{HI}}^{-1}(\nu = 1\mathrm{Ry}/h) = 1.6 \times 10^{17}$ cm^{-2} are always important for the IGM because they set the mean free path of HI-ionizing photons.

Higher column systems owe to denser gas, and the denser the gas is, the closer it lies to a galaxy on average. The closer it lies to a galaxy, the more likely astrophysical effects may enter and change the gas distribution from the numerical models that ignore such effects. Thus, the column density distribution at higher columns than those probed by the Lyα forest may be a more promising diagnostic than the Lyα forest of galactic feedback. Several studies have investigated how well the column density distribution is reproduced in simulations over various N_{HI} ranges (Katz et al. 1996; Theuns et al. 1998; Kohler & Gnedin 2007; Altay et al. 2011, 2013; McQuinn et al. 2011b; Rahmati et al. 2013a). **Figure 5** shows a comparison of $f(X, N_{\mathrm{HI}})$—the number of absorbers per $\mathrm{d}N_{\mathrm{HI}}$ per $\mathrm{d}X \equiv (1+z)^{1/2}\Omega_m^{-1/2}\ \mathrm{d}z$—between a simulation at $z = 3$ and a compilation of measurements (from Altay et al. 2011). If the comoving number density and physical cross section of absorbers at a given column do not evolve, $f(X, N_{\mathrm{HI}})$ is constant with redshift when $\Omega_m \approx 1$, and both observations and simulations find that $f(X, N_{\mathrm{HI}})$ is constant at the factor-of-two level over the range $2 < z < 5$ (Prochaska et al. 2010, McQuinn et al. 2011b). The major features in $f(X, N_{\mathrm{HI}})$ are a transition to a power-law functional form above columns of $N_{\mathrm{HI}} \sim 10^{14}$ cm^{-2} owing to the power-law density profile that develops around collapsed structures, a break in the slope at $N_{\mathrm{HI}} \sim \sigma_{\mathrm{HI}}^{-1}(\nu = 1\mathrm{Ry}/h) = 1.6 \times 10^{17}$ cm^{-2} owing to systems self-shielding at higher columns (Zheng & Miralda-Escudé 2002), and a roll off at the highest columns owing to the transition to the formation of molecules and the depletion of diffuse gas onto stars (Schaye 2001a).

To better than a factor of two, the simulations and measurements agree over the columns shown (even remarkably at the higher columns that probe denser circumgalactic and galactic gas). This result has also been shown to hold down to $z = 0$ and to even be fairly robust to galactic feedback recipes (Altay et al. 2013, Rahmati et al. 2013a; see Section 2.6 for more description of these recipes). Unfortunately, we are unaware of a quantitative comparison between simulations and measurements at columns higher than those probed by the Lyα forest but that are still intergalactic ($10^{14} \lesssim N_{\rm HI} \lesssim 10^{17}$ cm^{-2} at $z \sim 3$). Such a comparison would be interesting in light of recent, more precise measurements (Kim et al. 2013, Rudie et al. 2013).

Another useful statistic for probing the distribution of HI around galaxies is to measure the amount of HI absorption in quasar spectra as a function of the distance to spectroscopic galaxies. This statistic was investigated by Adelberger et al. (2005) and Rakic et al. (2012), who detected an enhancement in absorption out to a few physical megaparsecs from galaxies but with a large amount of scatter. (The scatter at <0.2 physical Mpc had initially been attributed to galactic feedback, generating much excitement.) Rakic et al. (2013) found that the median absorption profile in HI is consistent with the predictions of standard cosmological simulations (and relatively insensitive to the galactic feedback prescriptions they employed in the simulations).

2.3. The Thermal History of the IGM

There has been a recent resurgence in work to reconstruct the thermal history of the low-density IGM over intermediate redshifts (Lidz et al. 2010, Becker et al. 2011, Garzilli et al. 2012, Rudie et al. 2012, Boera et al. 2014, Bolton et al. 2014), following up on the seminal investigations from over a decade ago (Schaye et al. 2000, Ricotti et al. 2000, McDonald et al. 2001, Zaldarriaga et al. 2001, Theuns et al. 2002a, Hui & Haiman 2003). Temperature measurements are interesting because they constrain different energy injection processes into the IGM and because the IGM temperature sets the minimum mass of galaxies (see the sidebar The Minimum Mass of Galaxies). Temperature measurements rely on the width of Lyα absorption features from the low-density IGM being broader with higher temperatures, because of both thermal broadening and, to a lesser extent, the broadening owing to pressure effects. A variety of methods to determine temperature are used, ranging from directly fitting for the width of absorption lines as a function of $N_{\rm HI}$ (Schaye et al. 1999) to measuring the suppression at high wavenumbers in the Lyα forest power spectrum that owes principally to thermal broadening (Theuns et al. 2000, Zaldarriaga et al. 2001). All methods must be calibrated with simulations. The spate of IGM temperature measurements near the turn of the century generally found fairly high temperatures over the range $2 < z < 4$, with temperatures at the mean density of $T_0 = (20\text{–}30) \times 10^3$ K, although with a large amount of scatter and large statistical errors of $\sim(5\text{–}10) \times 10^3$ K. Recent measurements have led to a more concordant picture with $T_0 = (10\text{–}20) \times 10^3$ K, with the concordance arising because of the general agreement among several studies (Becker et al. 2011, Garzilli et al. 2012, Boera et al. 2014, Bolton et al. 2014; albeit with significant collaborative overlap) and with the past study by Schaye et al. (2000). In addition, led by Becker et al. (2011), some studies have chosen to estimate the temperature at the density where the variance in the estimate is minimized rather than at $\Delta_b = 1$, resulting in smaller errors. However, there is still some tension among recent measurements (Lidz et al. 2010, Becker et al. 2011).

In the standard story, the temperature history primarily constrains the reionization history of the IGM. When an ionization front swept through and reionized the intergalactic hydrogen, this ionization photoheated the cold IGM. Estimates are that the IGM was heated to $(17\text{–}25) \times 10^3$ K, with the exact value depending on the hardness of the incident spectrum and the velocity of the ionization front (Miralda-Escudé & Rees 1994, McQuinn 2012). The reionization of the second

THE MINIMUM MASS OF GALAXIES

The IGM thermal history also shapes the minimum mass of galaxies. Before reionization, the pressure of the IGM was negligible and so whether a galaxy formed in a halo was determined simply by whether the virialized halo gas had sufficient time to cool and condense. Reionization heated the gas to $\sim 10^4$K, making the IGM Jeans' mass larger than the mass threshold for cooling (Rees 1986, Thoul & Weinberg 1996). Indeed, the first models for this suppression were based on comparing the halo mass with the IGM Jeans' mass or the analogous mass for an expanding universe (termed the "filtering mass"; Shapiro et al. 1994, Gnedin & Hui 1998, Gnedin 2000). More recent studies have noted that the gas that would make it onto a halo typically does not reach a density within an order of magnitude of the mean density at collapse, and so a higher density and hence smaller Jeans' mass are more applicable (although not necessarily smaller than the filtering mass; Hoeft et al. 2006, Okamoto et al. 2008, Noh & McQuinn 2014). These studies find that the mass scale where pressure inhibits accretion is a strong function of time, suppressing $\approx 10^9$ $M_\odot$ (10^{10} $M_\odot$) halos at $z = 6$ ($z = 1.5$) for a region reionized at $z \sim 10$.

This suppression of accretion onto galaxies from the pressure of an ionized IGM, often attributed to the "ultraviolet background" or "reionization", is invoked to help explain the missing satellite problem: In the cold dark matter picture, the Milky Way should have thousands of subhalos massive enough that the gas could have cooled and formed stars, but observations of satellite galaxies suggest that ultimately only a small fraction of them were able to form stars. IGM pressure can raise the mass threshold above which subhalos can accrete gas and form stars (Quinn et al. 1996, Bullock et al. 2000, Bovill & Ricotti 2009). Intriguingly, some of the ultra-faint dwarf satellite galaxies of the Milky Way appear to have formed their stars by the time the Universe was $\sim$1 Gyr old (Brown et al. 2012, Weisz et al. 2014), which may indicate that accretion was shut off by the pressure of a photoionized IGM.

electron of helium (HeII reionization) is another major heating event, likely driven by the harder emissions of quasars. During HeII reionization by quasars (which is discussed in more detail in Section 2.5), HeIII bubbles are blown around quasars, and the IGM is additionally heated by (5–10) $\times$ 10^3 K (McQuinn et al. 2009, Compostella et al. 2013). After each of these reionization processes the IGM cooled, mainly through the adiabatic cosmic expansion and through Compton cooling off of the CMB (which is especially important at $z \gtrsim 5$), although recombination and free-free cooling are important at the 10% level. Cooling after reionization drives most of the gas to a ridiculously tight power-law relationship with $T = T_{0,\rm lim}\Delta_b^{0.6}$ for $\Delta_b \lesssim 10$ within a doubling of the scale factor (Hui & Gnedin 1997), as described in the sidebar Asymptotic Temperature-Density Relation.

The points with error bars in **Figure 6** show recent estimates of the IGM temperature (Becker et al. 2011, Boera et al. 2014). Also shown is the average temperature in semianalytic calculations that model the optically thick photoheating from reionization processes and subsequent optically thin photoheating plus cooling. The Becker et al. and Boera et al. measurements do not directly constrain T_0 but rather constrain the temperature at a redshift-dependent Δ_b. The $T - \Delta_b$ relation in the intermediate model in **Figure 6*a*** is used to extrapolate these measurements to T_0 in this figure, although it matters little which model is chosen. See Upton Sanderbeck et al. (2016) for additional details and Puchwein et al. (2016) for a related study. These semianalytic models predict a distribution of T (Δ_b) at any redshift (as must be true in the actual IGM), but Upton Sanderbeck et al. (2016) find that what is measured is effectively the average temperature. **Figure 6*a*** shows the dependence on the spectral index of the postreionization ionizing background, and **Figure 6*b*** shows the duration of HeII reionization assuming linear histories spanning $2.8 < z < 4$ (*dashed curve*) and $2.8 < z < 5$ (*solid curve*)—the two most important dependences found by Upton Sanderbeck et al. (2015). The temperature peak in the models (and likely in the data) is due to HeII reionization, which occurs at $z \approx 3$ without any fine-tuning of the quasar emissivity history (the models in

ASYMPTOTIC TEMPERATURE-DENSITY RELATION

The evolution of temperature of an unshocked ionized Lagrangian fluid element follows from the first law of thermodynamics:

$$\frac{\mathrm{d}T}{\mathrm{d}t} = -2HT + \frac{2T}{3\Delta_b}\frac{\mathrm{d}\Delta_b}{\mathrm{d}t} + \frac{2}{3k_B n_b}\frac{\mathrm{d}Q}{\mathrm{d}t}, \tag{5}$$

where n_b is the number density of all free "baryonic" particles in the plasma (including electrons; Miralda-Escudé & Rees 1994, Hui & Gnedin 1997). In an ionized IGM, the dominant processes are photoheating and Compton cooling such that $\mathrm{d}Q/\mathrm{d}t \approx \Delta E\,\Gamma n_{\rm HI} + Cn_e$, where ΔE is the amount of energy per photoionization, $C(z)$ is a coefficient that describes Compton cooling off of the CMB, and in photoionization equilibrium $n_{\rm HI} \approx \alpha_A n_e/\Gamma$ (with the recombination coefficient scaling as $\alpha_A \propto T^{-0.7}$). Using these relations, Equation 5 can be solved for arbitrary $\Delta_b(t)$, yielding

$$T = \left[\left(\frac{Z^3\Delta_b}{Z_i^3\Delta_{b,i}}\right)^{2/3\times1.7} T_i^{1.7} e^{(Z/7.1)^{5/2}-(Z_i/7.1)^{5/2}} + T_{0,\rm lim}^{1.7}\Delta_b\right]^{1/1.7} \underset{\text{late times}}{\longrightarrow} T_{0,\rm lim}\,\Delta_b^{1/1.7}, \tag{6}$$

where $Z \equiv 1+z$, and subscript i denotes the initial state of the gas parcel at time z_i (McQuinn & Upton Sanderbeck 2016). The first term in the parentheses is sensitive to the initial temperature from a passing ionization front (the exponential factor, which acts to erase memory of the initial temperature, is due to Compton cooling), and the second term encodes the limiting temperature from the balance between photoheating and cooling processes. The function $T_{0,\rm lim}$ has an extremely weak dependence on the prior density evolution of a gas parcel such that regardless of how the density evolves $T_{0,\rm lim} \approx 10^4[(1+z)/4]$ K before HeII reionization and twice this value after, with additionally a weak dependence on the ionizing background spectrum. Thus, all unshocked gas with $\Delta_b \lesssim 10$ (densities below where collisional cooling is important) is driven to a single $T-\Delta_b$ relation with index $\gamma - 1 = 1/1.7 = 0.6$, with almost negligible dispersion (Hui & Gnedin 1997). Within a doubling of the scale factor, this evolution erases the memory of an earlier state, which just after hydrogen reionization should have had a lot of dispersion in temperature (Trac et al. 2008, Furlanetto & Oh 2009), with HeII reionization regenerating dispersion at $z \sim 3$ (McQuinn et al. 2009, Compostella et al. 2013). This behavior has motivated the power-law parameterizations of the $T-\Delta_b$ relation used in many IGM analyses.

Figure 6*a* use the luminosity function of Hopkins et al. 2007). The shorter duration models (which are more consistent with most measurements of the quasar emissivity history) and softer ionizing background models are more consistent with the data. Without HeII reionization occurring at $z \sim 3$, such models would predict a monotonically decreasing temperature with time after reionization.

Thus, the standard model for the thermal history with a late reionization of HeII seems consistent with the Becker et al. (2011) and Boera et al. (2014) measurements, which span $1.6 < z < 4.8$. This consistency limits the amount of heating from mechanisms other than photoheating, such as proposals associated with TeV blazers, cosmic rays, dust, or dark matter annihilations (Inoue & Kamaya 2003, Samui et al. 2005, Chang et al. 2012, Lacki 2015). This consistency does not constrain hydrogen reionization at $z > 6$, as the IGM has cooled by $z = 4.8$—the highest redshift where the temperature has been measured—to an asymptotic temperature that does not retain much memory of earlier times. Constraints on hydrogen reionization would be vastly improved by a temperature measurement at somewhat higher redshifts (Lidz & Malloy 2014, Upton Sanderbeck et al. 2016).

Our understanding of the thermal history can also be improved by measuring the slope of the $T-\Delta_b$ relation, $\gamma - 1$, the IGM pressure smoothing length at $\Delta_b \sim 1$, as well as fluctuations

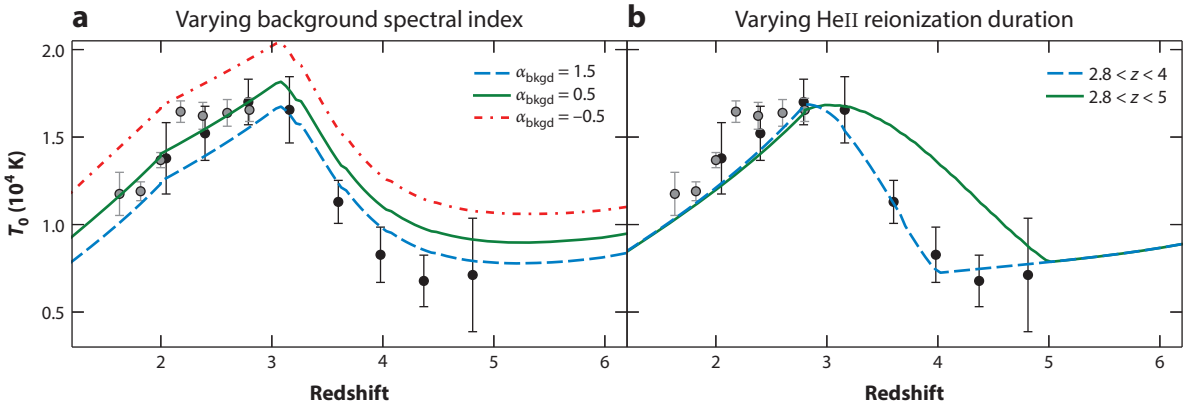

Figure 6

Intergalactic medium (IGM) temperature measurements of Becker et al. (2011) and Boera et al. (2014) compared with semianalytic model predictions for the average temperature thermal history of the IGM, varying two of the most important model parameters. (*a*) The dependence on the spectral index of the postreionization ionizing background. (*b*) The dependence on the duration of HeII reionization assuming linear-in-redshift histories. The temperature peak in the models (and likely in the data) is due to HeII reionization. Adapted from Upton Sanderbeck et al. (2016) with permission.

in the IGM temperature. Forecasts are that $\gamma - 1$ tends to zero or even negative values during reionization processes (Trac et al. 2008, Furlanetto & Oh 2009), with $\gamma - 1 \to 0.6$ afterward (see the sidebar Asymptotic Temperature-Density Relation). Only at $z = 2.4$ is $\gamma - 1$ reasonably well measured with the constraint $\gamma - 1 \approx 0.54 \pm 0.11$ (Rudie et al. 2012, Bolton et al. 2014), so there is substantial room for improvement in $\gamma - 1$ determinations. Secondly, the length scale over which fluctuations are smoothed by pressure effects is sensitive to the temperature temporally averaged over a dynamical time, which is roughly the Hubble time at $\Delta_b \sim 1$ (rather than the instantaneous temperature that the line-of-sight forest primarily constrains). Quasars at small angular separations potentially allow a measurement of this pressure-smoothing scale (Rorai et al. 2013, Kulkarni et al. 2015). Finally, relic fluctuations in the IGM temperature are an inevitable by-product of the inhomogeneous nature of reionization processes. Unfortunately at $z < 5$ the fluctuations appear not to be large enough in theoretical models to manifest in a detectable signal (McQuinn et al. 2011a), explaining why searches for these fluctuations have not turned up any evidence (Theuns & Zaroubi 2000, Lidz et al. 2010). At $z > 5$, a detection of temperature fluctuations in the Lyα forest may be more possible (D'Aloisio et al. 2015; see Section 3.3.1).

2.4. Synthesis Cosmic Ultraviolet Background Models

Following earlier work (Miralda-Escudé & Ostriker 1990, Giroux & Shapiro 1996), Haardt & Madau (1996) developed models that synthesized observations of the sources (namely quasars and galaxies) and the sinks of ionizing photons to make predictions for the properties of the extragalactic ionizing background. Subsequent efforts have developed these models further (Fardal et al. 1998, Faucher-Giguère et al. 2009, Haardt & Madau 2012). These models are adopted in essentially all nonadiabatic cosmological hydrodynamic simulations of the postreionization IGM to compute the ionization state and photoheating rates of intergalactic gas, and they are also widely used in the modeling of intergalactic and circumgalactic absorption.

Built into these models are the assumptions that sink positions are uncorrelated and that the ionizing background is spatially uniform. Uncorrelated positions is typically justified because the Poisson fluctuations in the number of sinks generally far exceed their clustered fluctuations.

Spatial uniformity of the background is justified at many redshifts as the mean free paths of ionizing photons, $\lambda_{\rm mfp}$, soon after the cosmological reionization of the species being ionized becomes much longer than the average distance between sources, a situation that suppresses variations (e.g., Meiksin & White 2004). From these assumptions, calculating the ionizing background for a given emissivity history and HI column density distribution is straightforward, although somewhat less so at wavelengths affected by HeII continuum absorption. The mathematics behind these models is described in the sidebar Homogeneous Ionizing Backgrounds.

HOMOGENEOUS IONIZING BACKGROUNDS

The assumption of spatial uniformity and uncorrelated absorbing clouds of fixed column allows one to calculate the background specific intensity, I_ν, with two inputs, the column density distribution of absorbing clouds, $\partial^2\mathcal{N}/\partial x \partial N_{\rm HI}$, where x is the comoving distance, and the physical specific emissivity of the sources, $\epsilon(\boldsymbol{x}, \nu, z)$. The spatially averaged solution to the cosmological radiative transfer equation $\mathrm{d}[I_\nu/\nu^3]/\mathrm{d}t = c\epsilon_\nu/[4\pi\nu^3] - c\sum_X \sigma_X n_X [I_\nu/\nu^3]$—just a Boltzmann equation for the (unnormalized) phase space density I_ν/ν^3 with sources and sinks on the right-hand side—where $X \in \{\mathrm{HI}, \mathrm{HeI}, \mathrm{HeII}\}$ and $\sigma_X(\nu)$ is the photoionization cross section, is easily derived via the method of Green's functions:

$$J_{\nu_0}(z_0) = \frac{c}{4\pi}\int_{z_0}^{\infty} \frac{\mathrm{d}z}{H(z)(1+z)} \left(\frac{1+z_0}{1+z}\right)^3 \langle\epsilon(\boldsymbol{x}, \nu, z)\rangle\, e^{-\tau_{\rm eff}(\nu_0, z, z_0)}, \tag{7}$$

where $\nu = \nu_0(1+z)/(1+z_0)$, $J_{\nu_0}(z_0) \equiv (4\pi)^{-1}\int \mathrm{d}\Omega\, I_{\nu_0}$ is the angularly averaged background intensity at ν_0 as seen by an observer at redshift z_0, and the effective optical depth, $\tau_{\rm eff}$, is defined as $e^{-\tau_{\rm eff}} \equiv \langle e^{-\tau}\rangle$, where brackets are a spatial average and $\tau = \int_{x(z)}^{x(z_0)} \mathrm{d}x \sum_X \sigma_X n_X$. This average yields

$$\tau_{\rm eff}(\nu_0, z, z_0) = \int_{x(z)}^{x(z_0)} \mathrm{d}x \overbrace{\int_0^\infty \mathrm{d}N_{\rm HI}\left[1 - e^{-\sum_X \sigma_X(\nu) N_X(N_{\rm HI}, J_\nu)}\right] \frac{\partial^2\mathcal{N}}{\partial x \partial N_{\rm HI}}}^{\equiv a\lambda_{\rm mfp}^{-1}(\nu)}, \tag{8}$$

where $N_X(N_{\rm HI}, J_\nu)$ is the column density in ion X (Paresce et al. 1980). All previous background models calculate N_X by treating the absorbers as single-density planar slabs (often using Equation 4 for Δ_b). In addition to continuum absorption, models generally treat the emission and absorption from atomic transitions of H and He. These transitions are generally of secondary importance, with the most important being ionizing HI recombination radiation, which contributes 5–20% to Γ (Faucher-Giguère et al. 2009).

In the limit that photons do not redshift significantly between emission and absorption (which applies for $\nu \sim^+ \nu_{\rm HI}$ at $z > 3$), Equation 7 simplifies to

$$J_\nu = \frac{1}{4\pi}\langle\epsilon(\boldsymbol{x}, \nu, z)\rangle\, \lambda_{\rm mfp}(\nu). \tag{9}$$

Specializing to the case of just HI absorption, $J_\nu \propto \nu^{-\alpha+3[\beta-1]}$ for $\partial^2\mathcal{N}/\partial x \partial N_{\rm HI} \propto N_{\rm HI}^{-\beta}$ and $\epsilon \propto \nu^{-\alpha}$. This scaling also lets us simplify the expressions for the photoionization and photoheating rates, which, specializing to the case of HI and using that $n_{\rm HI} = \alpha_A n_e/\Gamma$ and $\sigma_{\rm HI} \propto \nu^{-3}$, become

$$\Gamma \equiv 4\pi\int_{\nu_{\rm HI}}^\infty \frac{\mathrm{d}\nu}{h\nu}\sigma_{\rm HI}(\nu)J_\nu \approx \frac{4\pi\sigma_{\rm HI}(\nu_{\rm HI})J_{\nu_{\rm HI}}}{h(6+\alpha-3\beta)}; \quad \frac{\mathrm{d}Q}{\mathrm{d}t} \equiv 4\pi n_{\rm HI}\int_{\nu_{\rm HI}}^\infty \frac{\mathrm{d}\nu}{\nu}\sigma_{\rm HI}(\nu)J_\nu(\nu-\nu_{\rm HI}) \approx \frac{h\nu_{\rm HI}\alpha_A n_e}{5+\alpha-3\beta}. \tag{10}$$

The photoheating rate does not depend on the amplitude of J_ν, which justifies the postprocessing adjustments to Γ in Lyα forest analyses and limits the sensitivity of numerical simulations to the exact $J_\nu(z)$.

J_ν: angularly averaged specific intensity of ionizing background

Γ: photoionization rate of HI

$\lambda_{\rm mfp}(\nu)$: photon mean free path

Previous background models tune the assumed emissivity for the ionizing sources (consisting of galaxies and quasars) to reproduce the transmission in the HI Lyα forest. The emissivity of quasars, which can be estimated to a factor of $\sim$2 accuracy, is roughly consistent at $z \sim 2$–3 with that needed to source the entire ionizing background (Haardt & Madau 1996, 2012; Faucher-Giguère et al. 2008b). However, the known population of quasars is likely unable to maintain the backgrounds at higher redshifts, so it is generally assumed that stars make up the deficit (an assumption discussed further in Section 3.1). These models then typically take the ionizing emissivity associated with the observed cosmological star-formation history, tuning the escape fraction of ionizing photons so that the background calculation reproduces measurements of $\Gamma(z)$. Once the emissivity history of the sources is prescribed at $\nu \sim \nu_{\rm HI}$, these models are then solved using our best guesses for the frequency dependences of the sources' spectra and using the latest measurements of the HI column density distribution. Until recently, to redshift-dependent normalization factors, background models used a power-law source spectra with specific luminosity parameterized as $L_\nu \propto \nu^{-\alpha}$ and a power-law distribution of absorbers parameterized as $\partial^2\mathcal{N}/\partial x \partial N_{\rm HI} = A N_{\rm HI}^{-\beta}$, where the choices of A and β are motivated by observations. With these parameterizations, taking the limit that the mean free paths satisfy $\lambda_{\rm mfp} \ll cH^{-1}$ valid at $z \gtrsim 3$ and ignoring resonant processes (which are of secondary importance), the spectrum between 1 and 4 Ry and then also above 4 Ry scales as $\nu^{-\alpha+3(\beta-1)}$ (see the sidebar Homogeneous Ionizing Backgrounds). The modeling has been improved in the most recent models by using population synthesis calculations for the stellar emission spectrum and HI column density distributions that are not single power laws (Haardt & Madau 2012). **Figure 7** shows the ionizing background model of Haardt & Madau (2012) over the range

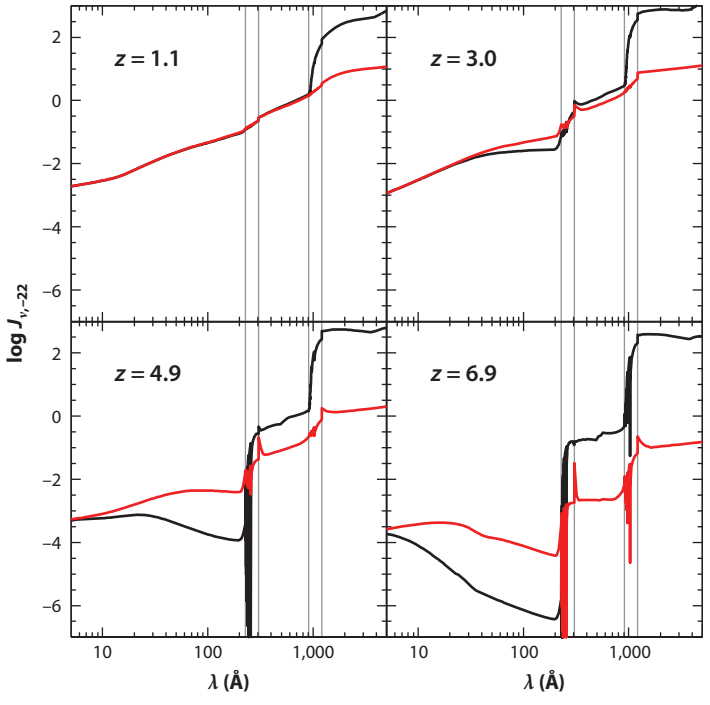

Figure 7

Haardt & Madau (2012) uniform ultraviolet background models. The black curve is their full model that includes emissions from galaxies and quasars, and the red curve is their "quasar only" model. The vertical lines correspond to the Lyα and Lyman-continuum wavelengths of both HI (1216 Å and 912 Å) and HeII (304 Å and 228 Å). Adapted from Haardt & Madau (2012) with permission.

$1 < z < 7$. The black curve is their full model that includes emissions from galaxies and quasars, and the red curve is their "quasar only" model. The major breaks in the spectrum are at the ionization edges of HI and HeII at 912 Å and 228 Å, respectively.

It is difficult to gauge the fidelity with which uniform ionizing background models describe the actual ionizing background. Around $z \approx 2$, the shape of the ionizing background has been constrained observationally using metal line systems in Agafonova et al. (2007) and Fechner (2011), with the latter finding agreement with some models. At most redshifts these models have not been tested. However, we know that uniform ionizing background models must err at certain redshifts and in certain locations. For example, near dense systems with $N_{\rm HI} \gtrsim 10^{18}$ cm^{-2}, local sources of radiation should be important (Miralda-Escudé 2005, Rahmati et al. 2013b). In addition, uniform background models also break down if $n^{1/3}\lambda_{\rm mfp}(\nu) \lesssim 1$ because spatial fluctuations in J_ν will be large, where n is the number density of sources. At $h\nu \sim 4$ Ry, energies that set the HeII photoionization rate, $\lambda_{\rm mfp}$ becomes small enough ($\lesssim$100 comoving Mpc) to result in $\mathcal{O}(1)$ fractional variance in J_ν at $z \gtrsim 2.5$ if quasars source this background (for which effectively $n \sim 10^{-5}$ comoving Mpc^{-3}; Bolton et al. 2006, Furlanetto 2009, McQuinn & Worseck 2014). There is also evidence that fluctuations on the order of unity or greater are occurring in the HI Lyα forest at $z > 5.5$ (Becker et al. 2015; see Section 3.3.1). Lastly, large spatial fluctuations should occur in J_ν for ν above the ionization potential of an ion during its reionization.

2.5. The HeII Lyα Forest

The Lyα resonance of HeII at 304 Å is the only other intergalactic absorption line that has been observed from an element created in the Big Bang, elements which of course have huge modeling advantages. Because the HeII Lyα line falls blueward of 912 Å, this spectral region is prone to foreground continuum absorption from neutral hydrogen. Such foreground absorption means that the HeII forest can only be observed at $z > 2$ as the HeII forest from lower redshift clouds is absorbed by the $\gtrsim 10^{19}$ cm^{-2} HI columns through our galaxy. It also means that intervening systems with $N_{\rm HI} \gtrsim 10^{17}$ cm^{-2} absorb parts of the HeII Lyα spectral region; quasar sightlines that by chance intersect fewer of these systems have more useable HeII Lyα forest spectra. About 1% of $z \sim 3$ quasars show enough transmission in the HeII forest to be useful (Syphers et al. 2009, Worseck & Prochaska 2011). At present, the HeII Lyα forest has been observed toward about twenty quasars spanning the range $2.7 < z < 3.8$ (Hogan et al. 1997, Reimers et al. 1997, Heap et al. 2000, Zheng et al. 2004, Worseck et al. 2011, Syphers et al. 2012), a number that has increased significantly in the past few years with the installation of the ultraviolet-sensitive Cosmic Origins Spectrograph (COS) on the *Hubble Space Telescope* (HST).

The HST/COS HeII Lyα forest spectrum of the brightest quasar, HE2347-4342 ($z = 2.9$), in the far ultraviolet is shown in **Figure 8** (Shull et al. 2010). Also shown is a high-resolution Very Large Telescope spectrum of this sightline's coeval HI Lyα forest from Fechner & Reimers (2007). The HeII spectrum illustrates several features generic to the existing HeII Lyα forest sightlines. At high redshifts, much of the HeII absorption is saturated. Indeed, Gunn-Peterson troughs, defined as regions with no detected transmission, are seen in the spectrum of HE2347-4342 at $2.7 < z < 2.9$, with the largest trough spanning $\Delta z \sim 0.05$ or ~30 comoving Mpc (Shull et al. 2010). (The *yellow highlighted regions* in **Figure 8** identify segments with nearly zero transmission.) Higher-redshift HeII sightlines, famously Q0302-003, show even more significant troughs (Heap et al. 2000, Syphers & Shull 2014). These troughs make way for a forest of transmission at lower redshifts. Even at these lower redshifts, there is ≈100 times more HeII than HI at any location (Fechner & Reimers 2007, Worseck et al. 2011), resulting in the HeII Lyα transmission coming largely from the deepest voids.

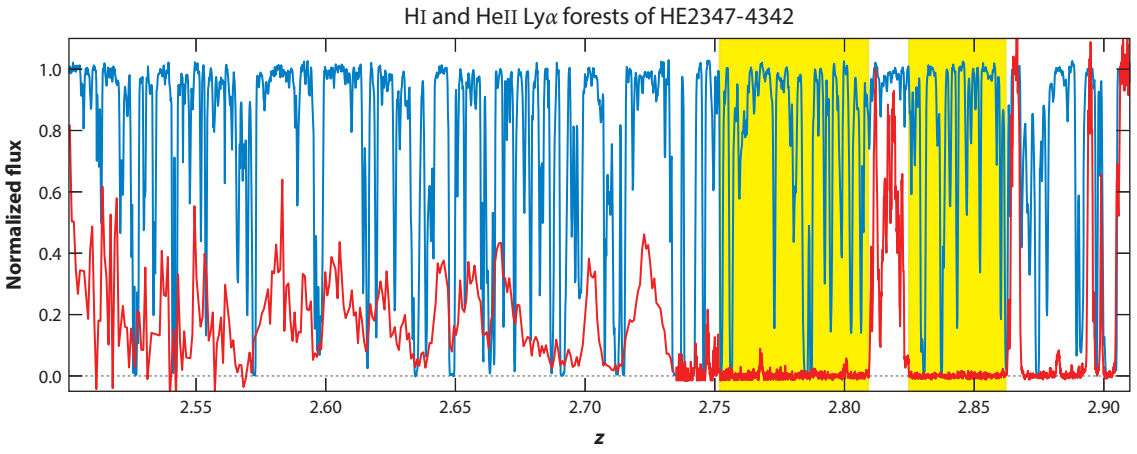

Figure 8

Continuum-normalized spectra of the brightest quasar in the far ultraviolet, HE2347-4342. The blue curve is the HI Lyα forest transmission of Fechner & Reimers (2007) using VLT/UVES, and the red curve is the coeval HeII Lyα forest obtained with HST/COS by Shull et al. (2010) using the reduction of Worseck et al. (2011). This spectrum illustrates the finding by HeII Lyα forest studies that the HeII absorption is much stronger than the coeval HI absorption, with large swaths of highly absorbed regions at $z \gtrsim 2.7$ (*highlighted in yellow*). The HST/COS spectrum has resolution of $\lambda/\Delta\lambda \approx 1{,}500$ at $z < 2.73$ and $\lambda/\Delta\lambda \approx 20{,}000$ at higher redshifts, whereas the VLT/UVES spectrum has $\lambda/\Delta\lambda \approx 50{,}000$.

HeII Lyα forest spectra shed light on the process of HeII→HeIII reionization, termed HeII reionization, a process that chronicles the history of intergalactic >4-Ry backgrounds (Miralda-Escudé 1993). The leading picture is that intergalactic >4-Ry radiation is due to quasars. This picture is supported by most measurements of the quasar spectral energy distribution and luminosity function (Hopkins et al. 2007, Willott et al. 2010; see Section 3.1 for related discussion), which are consistent with quasars producing enough photons to reionize the HeII around $z \approx 3$ (Wyithe & Loeb 2003, Furlanetto & Oh 2008). The HeII Lyα Gunn-Peterson troughs directly imply that small-scale void regions (which can be localized using HI Lyα absorption) are $\gtrsim$1% HeII. Because the gas is either photoionized or fully HeII (and noting that the voids seen in the HI Lyα forest are roughly a tenth of the mean density), this bound implies that the HeII fraction at the mean density is $\gtrsim$10% (McQuinn 2009). (The ∼100-kpc-scale voids in the forest cannot experience much different ionizing background than mean density regions.) Greater than 10% is a strong constraint; this argument shows that HeII has not been reionized fully in these trough regions. These troughs are observed to occur at $z \gtrsim 2.7$ (Shull et al. 2010; although there are only two HeII spectra that provide useful spectra at $z \lesssim 2.7$). Accordingly, this redshift is often taken to mark the end of HeII reionization. Studies have also attempted to understand the implications of the evolution in the mean HeII Lyα opacity for the timing of HeII reionization, which shows significant evolution at $z > 2.8$ in addition to large fluctuations about the mean in ∼10 comoving Mpc segments (Worseck et al. 2011, 2014a; Davies & Furlanetto 2014). These studies have been less conclusive because the mean HeII Lyα opacity is difficult to model.

At observable redshifts that occur after the HeII reionization was complete ($2 < z \lesssim 2.7$), the HeII Lyα forest is useful for constraining the hardness of the metagalactic ionizing background, as the ratio between HI Lyα and HeII Lyα optical depths directly measures the local ratio between the HeII and HI photoionization rates (informing ionizing background models). Many studies have attempted this exercise using the brightest two HeII quasars, HS1700+6416 and

HE2347-4342. Early work found mysterious order-of-magnitude spatial fluctuations in this ratio (Shull et al. 2004, 2010; Zheng et al. 2004), much larger fluctuations than the nearly uniform prediction of models for the postreionization ionizing backgrounds. This result has not been confirmed by more recent work (Fechner & Reimers 2007, McQuinn & Worseck 2014), which found that the $z \sim 2.5$ data are consistent with background models as long as quasars contribute half or more of the HI-ionizing background.

2.6. Metal Absorption Lines and the Enrichment of the IGM

Once stars formed in the Universe, not only did their ionizing emissions ionize all of the hydrogen but their radiation pressure and their supernovae powered winds into the IGM, enriching the cosmic volume. These winds may even have been particularly efficient at evacuating the halos of the first galaxies, which had shallow potential wells. Observationally, galactic disks contain only a fraction of the metals synthesized by their stars (e.g., Dalcanton 2007, Davé et al. 2011), with the fraction of metals retained in a galaxy's ISM estimated to be ∼20% across a large range of stellar masses at $z \sim 0$ (with an uncertain percentile also residing in the circumgalactic medium; e.g., Peeples et al. 2014). The rest must have escaped into the IGM.

Metal absorption that falls redward of the forest is annotated in the quasar absorption spectrum shown in the middle panel of **Figure 2**. The strongest metal absorbers that appear in this figure, with optical depths $\gtrsim$1, are likely of galactic or circumgalactic origin. (An exception is a curious population(s) of abundant, highly enriched, and diminutive overdense absorbers [$Z = 0.1 - 1$ $Z_\odot$, $L \sim 100$ pc, $\Delta_b \sim 100$–1,000] reported in Simcoe et al. 2006 and Schaye et al. 2007 that may reflect how the IGM was enriched.) Indeed, if only familiar with the previous content in this review, one might guess that the typical metal line optical depth in the IGM is zero: Vanilla models for the Lyα forest are an astonishing success; galactic winds cannot significantly redistribute mass or this redistribution would change the statistical properties of the forest. Contrary to this intuition, studies find that half or so by mass of the intergalactic gas have been enriched to a detectable level of [O, C/H] > -3.5, where, e.g., [C/H] denotes $\log_{10}$ of this ratio relative to the Solar ratio.

Two methods have been used to establish this result, both utilizing the highest S/N high-resolution quasar spectra. The first is the so-called pixel optical depth method (Cowie & Songaila 1998, Ellison et al. 2000, Aguirre et al. 2002), which tabulates at fixed optical depth in HI Lyα the optical depth of a given metal ion at the same location in the IGM, correcting for noise and other contaminants. The second method involves carefully fitting individual metal absorption lines associated with an HI absorber and, then, performing a survival analysis to quantify the probability of false detections (Simcoe et al. 2004). The resulting metal ion optical depths from both methods are largely in agreement, although the second method is somewhat less sensitive. These methods have been used to infer an approximately lognormal distribution of optical depths for the prominent metal lines at fixed $\tau_{\mathrm{Ly}\alpha}$ (and hence fixed Δ_b assuming the model of Schaye 2001b). In particular, Schaye et al. (2003) found a median optical depth in CIV at $z \approx 2.5$ of $\tau_{\mathrm{CIV}} = 0.1\Delta_b^{3/2}$ for $\Delta_b \gtrsim 0.5$ with a large standard deviation of ≈0.8 dex, and Aguirre et al. (2004, 2008) found similar optical depth distributions for OVI and SiIV.

One of the most interesting results of these analyses is the fraction of cosmic gas that has been enriched. Simcoe et al. (2004) estimated from their survival analysis that 60–70% of systems with $N_{\mathrm{HI}} \geq 10^{13.6}$ cm^{-2} (or $\Delta_b > 2.6$ using Equation 4) show metal absorption. The fraction of absorbers enriched to a given metallicity is shown in **Figure 9*b*** (from Simcoe et al. 2004). If the metals for each system are well mixed, such observations imply that at least half of all gas by mass and ≈5% by volume have been enriched to a detectable level (Pieri & Haehnelt 2004, Simcoe et al. 2004).

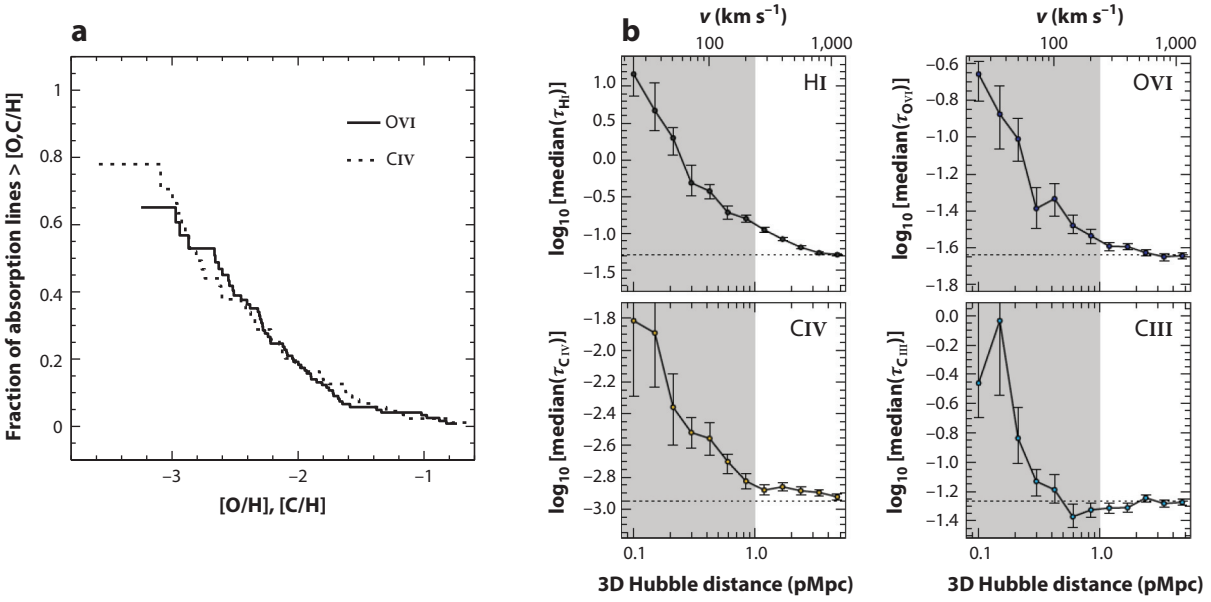

Figure 9

(*a*) Fraction of Lyα lines with $N_{\rm HI} > 10^{13.6}$ cm^{-2} (corresponding to $\Delta_b \gtrsim 3$) that are enriched above the quoted metallicity using OVI absorption (*solid histogram*), or with $N_{\rm HI} > 10^{14}$cm^{-2} ($\Delta_b \gtrsim 5$) using CIV absorption (*dashed histogram*). Adapted from Simcoe et al. (2004) with permission. (*b*) Median pixel optical depth at $z \approx 2.4$ of the named ion as a function of the physical separation between galaxy and absorber (assuming Hubble flow velocities in the line-of-sight direction, which ignores the redshift-space distortions that significantly affect the regions highlighted in gray). Adapted from Turner et al. (2014) with permission.

Translating metal line optical depths to median metallicities requires assumptions about the incident ultraviolet background and the gas temperature. All inferences use uniform background models in the vein of Haardt & Madau (1996) and assume $\sim 10^4$ K photoionized gas. Over the range $2 \lesssim z \lesssim 4$, Schaye et al. (2003) and Aguirre et al. (2008) find a median metallicity of $[{\rm C/H}] = -3.5 + 0.1[z-3] + 0.7[\log(\Delta_b - 1) - 1]$, an oxygen-to-carbon ratio of $[{\rm O/C}] = 0.7 \pm 0.2$, and a logarithmic standard deviation of $\sigma([{\rm C, O/H}]) \sim 0.8$ dex. These numbers are in general agreement at $z \approx 2.4$ with the measurements of Simcoe et al. (2004), aside from the Δ_b dependence of the median metallicity, which was not detected there. Plausible changes to the ionizing background model change the metallicity estimates by a few tenths of dex. Simcoe (2011) repeated the Simcoe et al. (2004) analysis on CIV but for $z \approx 4.3$ rather than $z \approx 2.4$, finding a median metallicity for slightly overdense gas that is a factor of 2–3 smaller, suggesting that much of the enrichment occurred between these redshifts.

Another approach to understanding the enrichment of the IGM is to look at the statistics of absorbers in quasar spectra as a function of their distance to Lyman break–selected galaxies in the foreground of the quasar. Turner et al. (2014) recently investigated this statistic at $z \approx 2.4$ using pixel optical depth methods with galaxy separation taking the place of $\tau_{{\rm Ly}\alpha}$. The median absorption they measure as a function of the 3D separation (which is calculated by adding in quadrature the transverse and line-of-sight distances assuming pure Hubble flow) from galaxies is shown in **Figure 9*b*** for the most prominent ions. Turner et al. (2014) detected correlations out to a proper megaparsec for the standard metal ions. At proper megaparsec-scales these correlations likely owe to the clustering of galaxies, but at shorter distances they should reflect the extent of

each galaxy's own enrichment. However, disentangling these effects (as well as interpreting most metal line diagnostics) requires detailed modeling.

Most theoretical models of chemical enrichment use large simulations of a cosmological volume that attempt to capture galaxy formation. These simulations adopt "feedback" recipes for how star formation (and sometimes quasar activity) expels gas (Aguirre et al. 2001a,b; Oppenheimer & Davé 2006; Wiersma et al. 2010, 2011; Tescari et al. 2011). There is much freedom in how feedback is implemented in these simulations. Some eject from galaxies one to a few solar masses in "wind" particles with a specified velocity for every solar mass formed in stars, tuning the exact numbers to match observations of winds, galaxy stellar masses, and other observables. Others inject momentum/energy around star-formation sites and try to follow the development of galactic winds more organically. Generally in these simulations, the intergalactic metal yield tends to trace the star-formation history, with enrichment contributed by galaxies over a broad range in stellar mass and extending hundreds of kiloparsecs from galaxies. However, certain feedback recipes provide a better match to observations, with some able to reproduce the gross properties of intergalactic metal lines (e.g., Wiersma et al. 2011). Describing these comparisons in detail would require its own review.

3. THE IGM AT HIGH REDSHIFTS, $z > 5$, AND REIONIZATION

The diagnostics of the IGM at $z > 5$ differ from those at lower redshifts, partly because our star diagnostic, Lyα forest absorption, is becoming very saturated in most pixels. At $z > 5$ it is not possible to detect the HeII Lyα forest, and the detected metal absorbers (namely OI and CIV) are likely associated with dense gas around galaxies rather than the diffuse IGM (Keating et al. 2014). The focus shifts to a new set of observables that is sensitive to a neutral IGM and cosmological reionization.

3.1. The Sources of Reionization

The consensus model is that galaxies drove the reionization of intergalactic hydrogen (e.g., Madau et al. 1999, Shapiro et al. 1994, Faucher-Giguère et al. 2008b, Becker & Bolton 2013). This model is supported by observations of high-redshift galaxies, which find approximately enough ultraviolet emission at $z = 6$ to reionize the Universe if a substantial fraction of the associated ionizing radiation escaped into the IGM (Robertson et al. 2010, Finkelstein et al. 2012a). Alternatively, the steep faint-end slope of the observed UV luminosity function also supports unseen low-mass galaxies being responsible for reionization. (The sidebar Exotic Reionization Models discusses other models that have been previously considered.) To reionize the IGM in a time $t_{\rm SFR}$ requires a comoving galactic star-formation rate density of

$$\dot{\rho}_{\rm SFR} = 3.6\times10^{-2}\, N_{\gamma/b}\left(\frac{1+z}{8}\right)^{3/2}\left[\frac{t_{\rm SFR}}{0.5t_{\rm uni}(z)}\right]^{-1}\left(\frac{f_{\rm esc}}{0.1}\frac{\xi_{\rm ion}}{4{,}000}\right)^{-1}{\rm M}_\odot\,{\rm year}^{-1}\,{\rm Mpc}^{-3}, \qquad (11)$$

where $t_{\rm SFR}/t_{\rm uni}(z)$ is the timescale of star formation relative to the age of the Universe, $N_{\gamma/b}$ is the required number of ionizing photons per hydrogen atom to complete reionization (studies find 1–3; Section 3.2), $f_{\rm esc}$ is the highly uncertain fraction of ionizing photons that escaped from their galactic sites of production into the IGM, $\xi_{\rm ion}$ is the number of ionizing photons that are emitted for each stellar baryon, and $\dot{\rho}_{\rm SFR}$ is the star-formation rate density in comoving space. Much numerical work has focused on the difficult problem of calculating $f_{\rm esc}$ (which requires the daunting task of resolving the multiphase ISM), but answers essentially range from zero to one (Gnedin et al. 2008, Wise & Cen 2009) with some recent simulations finding average values of

EXOTIC REIONIZATION MODELS

Starting with Arons & McCray (1970), another source that has often been mentioned as potentially responsible for reionization is quasars. Quasar reionization scenarios have generally been argued against because most observations show quasar numbers to be declining with increasing redshift above $z = 3$ (e.g., Hopkins et al. 2007, Willott et al. 2010). This decline seems consistent with the merger hypothesis for quasars and the decreasing abundance of massive galaxies, as the quasar luminosity scales strongly with galaxy stellar mass in models (e.g., Hopkins et al. 2008). However, Giallongo et al. (2015) recently claimed to have found a sufficient abundance of quasars at $z \sim 6$ for them to be able to reionize the Universe, partially driving a resurgence of quasar-reionization models (Chardin et al. 2015, Madau & Haardt 2015). An issue with this model is that, if quasars reionized the hydrogen, their hard spectrum would also doubly ionize the helium by $z = 4$ (Madau & Haardt 2015), which is in conflict with the HeII Gunn-Peterson trough detections and the IGM temperature measurements (Sections 2.5 and 2.3, respectively).

In addition, X-rays from high-mass X-ray binaries (Furlanetto 2006, Mirabel et al. 2011), supernovae shocks (Johnson & Khochfar 2011), supernova-accelerated electronic cosmic rays (Oh 2001), and even more exotic processes such as dark matter annihilations (Belikov & Hooper 2009) may contribute some fraction of the ionizations (Dijkstra et al. 2004, McQuinn 2012). X-ray photons have two advantages relative to ultraviolet ones when it comes to reionization. First, a single X-ray can convert as much as 30% of its energy into ionizations (with this fraction decreasing with x_i; Shull & van Steenberg 1985). Second, X-rays should have no problem escaping from their sites of production into the IGM, with $h\nu \lesssim 1.5\bar{x}_{\rm H}\sqrt{(1+z)/10}$ keV photons absorbed within a Hubble distance. Because they penetrate much further into the IGM, early X-rays should have established a relatively uniform ionization floor before ultraviolet photons finished the job, with empirically motivated models predicting a floor of 0.1–1% (Furlanetto 2006, Pober et al. 2015), although the modeling uncertainties are immense.

$f_{\rm esc} \sim 10\%$ (Kimm & Cen 2014, Ma et al. 2015). There have also been attempts to measure the escape of ionizing photons from $z \lesssim 3$ galaxies, which yield a confusing picture as well (Iwata et al. 2009, Siana et al. 2010, 2015). In addition, $\xi_{\rm ion}$ equals 4,000 for an empirically motivated stellar initial mass function (IMF), although with a factor of two theoretical uncertainty (Shull et al. 2012a). A metal-free, top-heavy IMF produces a factor of ten more ionizing photons per stellar baryon (Bromm et al. 2001, Venkatesan et al. 2003).

Equation 11 is slightly different than the more widely used metric, the critical star-formation rate density to maintain reionization. This metric compares with the comoving $\dot{\rho}_{\rm SFR}$ that produces enough ionizing photons to balance the number of intergalactic recombinations for a reionized IGM (Madau et al. 1999):

$$\dot{\rho}_{\rm SFR} = 3.1\times10^{-2}\left(\frac{1+z}{8}\right)^3\left(\frac{C/2}{f_{\rm esc}/0.1}\right)\left(\frac{\xi_{\rm ion}}{4{,}000}\right)^{-1}\ {\rm M}_\odot\ {\rm year}^{-1}\ {\rm Mpc}^{-3}. \qquad (12)$$

Studies find a gas clumping factor of $C \equiv \langle\Delta^2 T_4^{-0.7}\rangle_V \sim 2$–3 at $z \sim 7$, where $\langle ...\rangle_V$ denotes an average over the volume and T_4 is the temperature in units of 10^4 K (Pawlik et al. 2009, McQuinn et al. 2011b, Kaurov & Gnedin 2015). Because the recombination time at $z \sim 6$ is roughly the age of the Universe, Equations 11 and 12 require similar $\dot{\rho}_{\rm SFR}$.

There has been much discussion on whether the observed population of high-redshift galaxies was responsible for reionization. Observationally, the luminosity function of ultraviolet dropout-selected galaxies at source-frame ~1500 Å has been measured at $z > 6$ with HST (Bouwens et al. 2012, Finkelstein et al. 2012b, Ellis et al. 2013, McLure et al. 2013). The ultraviolet dropout technique uses the break in a high-redshift spectrum that occurs at source-frame Lyα owing to intergalactic Lyα absorption. These measurements have been improved in recent years with the

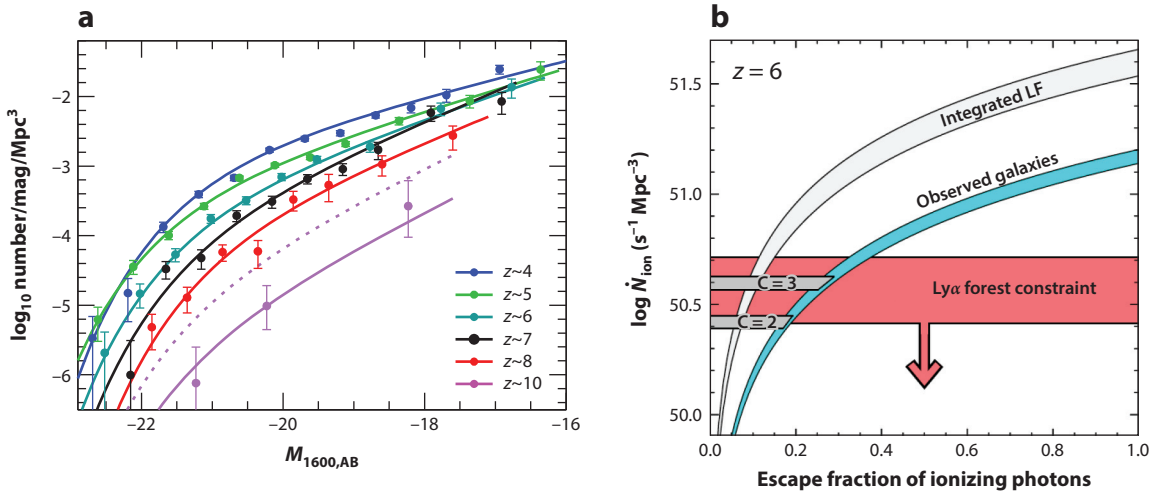

Figure 10

(*a*) Luminosity function of *Hubble Space Telescope* dropout-selected galaxies. The points with error bars are the measurements, and the solid curves are the best-fit Schechter functions. Adapted from Bouwens et al. (2015b) with permission. (*b*) Comparison of $z = 6$ estimates for the emissivity of ionizing photons, from the observed population of galaxies and from integrating the luminosity function below the detection threshold, as a function of the assumed f_{esc}. These numbers are compared against the ionizing emissivities required to maintain reionization with clumping factors of 2 or 3 and against the emissivities inferred by Kuhlen & Faucher-Giguère (2012) using Γ and λ_{mfp} estimates. Recent constraints from Becker & Bolton (2013) allow up to a factor of three higher emissivities than Kuhlen & Faucher-Giguère (2012). Adapted from Finkelstein et al. (2012a) with permission.

installation of the near-infrared sensitive Wide Field Camera 3 on HST during the 2009 servicing mission, extending luminosity function estimates to redshifts as high as $z = 10$. **Figure 10*a*** shows the luminosity function of HST dropout-selected galaxies at $z = 4$–10, from Bouwens et al. (2015b). There is a decline in the luminosity function over this redshift (especially at $z > 6$). Such a decline is not surprising as the abundance of the halos that host these galaxies evolves similarly at $z > 6$.

The final step to infer the total ionizing flux of the population is to estimate the conversion from the observed flux at ∼1500 Å to the amount of ionizing flux. This conversion involves matching the spectral slope of these galaxies' emissions to the slopes in stellar population synthesis models (e.g., Robertson et al. 2013). The conversion estimate combined with the best-fit ∼1500-Å luminosity function allows one to estimate the ionizing photon emissivity. The results of this exercise are that for $f_{esc} \gtrsim 0.2$ the observed population of galaxies can maintain reionization at $z \sim 6$. The curved bands in **Figure 10*b*** show the estimated photon emissivity from the observed galaxies as a function of their f_{esc} (from Finkelstein et al. 2012a; see also Bouwens et al. 2015a). These numbers are compared against the ionizing emissivities required to maintain reionization with clumping factors of 2 or 3 and against the emissivity range inferred from the Lyα forest (a constraint discussed below).

However, it is possible that $f_{esc} \lesssim 0.2$ and that less luminous galaxies than those observed reionized the Universe. The observed population of galaxies shows a steep faint-end slope of $\alpha = -1.8 \pm 0.2$ (Kuhlen & Faucher-Giguère 2012, McLure et al. 2013, Bouwens et al. 2015b). For luminosity-independent f_{esc}, $\alpha = -1.8$ results in about a factor of two more ionizing flux from fainter galaxies than those observed (see the "integrated" band in **Figure 10*b***), but of course $\alpha = -2$ is logarithmically divergent. Theoretical models predict that there should be some star

formation in halos down to $\sim 10^8$ $M_\odot$, which (if $\alpha = -1.8$ is maintained the entire way) fall 6–10 astronomical magnitudes beyond those observed (Kuhlen & Faucher-Giguère 2012). However, it might also be surprising if galaxies in such diminutive halos reionized the Universe. Star formation at low redshifts seems progressively less efficient as the halo mass of a system decreases because of stellar feedback. Models in which reionization was driven by $\sim 10^8$ $M_\odot$ halos—the smallest halos that can cool atomically—with a standard IMF appear to be ruled out as they overproduce the observed stellar masses of the ultra-faint dwarf galaxies (Boylan-Kolchin et al. 2014).

In addition to directly observing high-redshift sources, the global amount of ionizing photons they emit as a function of redshift can be inferred from quasar absorption line studies. In particular, as shown in Section 2.4 (c.f. Equation 9), the emissivity of the sources is proportional to the often well-constrained amplitude of the hydrogen ionizing background times the mean free path of ionizing photons—which is set by the observationally constrained number of systems with $N_{\rm HI} \sim 10^{17}$ cm^{-2}. Miralda-Escudé (2003) estimated the ionizing emissivity in this way, showing that the emissivity, even at $z = 4$, was not much higher than that required to reionize hydrogen. Later, Bolton & Haehnelt (2007) extended this result to $z \approx 6$, estimating 1.5–3 ionizing photons per hydrogen atom were being emitted per Gyr (the age of the Universe at $z = 6$ is 0.94 Gyr) and coining the phrase "photon-starved reionization" to describe this result. In addition, Bolton & Haehnelt (2007) found an emissivity history that was remarkably constant over $z = 3$–6, as Miralda-Escudé (2003) had surmised. This result has held up in some subsequent studies (Faucher-Giguère et al. 2008b, Kuhlen & Faucher-Giguère 2012, Becker & Bolton 2013). Recently this photon-starved result has been revisited by Becker & Bolton (2013), using higher-redshift $\lambda_{\rm mfp}$ estimates and more rigorously tracking the sources of uncertainty. The Becker & Bolton (2013) analysis found that the data allow 3–10 ionizing photons per hydrogen atom atom per gigayear at $z \approx 5$, suggesting that reionization might not be so photon starved after all.

However, there is still a compelling case for reionization to be photon starved. Another approach to inferring the emissivity is to calculate the clumping factor of ionized gas in cosmological simulations that use an empirically motivated Γ and that account for self-shielding. Integrating the cosmological radiative transfer equation (see text above Equation 7) over $d^3x\, d\Omega\, d\nu\, \nu^2$ yields

$$\bar{\epsilon}_\gamma = \overbrace{\left(\dot{\bar{n}}_{\rm HI} + C\alpha_{B,4}\,\bar{n}_e\bar{n}_{\rm HII}\right)}^{\Gamma\bar{n}_{\rm HI}} + 4\pi/c\dot{J}_\gamma, \tag{13}$$

where an overbar denotes a spatial average, a subscript γ indicates the quantity in terms of the total number of ionizing photons, and $\alpha_{B,4} \equiv \alpha_B(T = 10^4\ {\rm K})$. To simplify, first note that $\dot{n}_{\rm HI}$ is small after reionization. Additionally, because $J_\gamma \approx \lambda_{\rm mfp}\epsilon_\gamma/4\pi$, the latter term is smaller by the factor $\lambda_{\rm mfp}/[cft_{\rm uni}]$, where f is the fraction of $t_{\rm uni}$ over which the background is evolving (the background at $2 \lesssim z \lesssim 6$ evolves remarkably little and so $f \sim 1$). Thus, Equation 13 simplifies to $\bar{\epsilon}_\gamma \approx C\alpha_4\bar{n}_e\bar{n}_H$, such that if $C = 2$ this implies ≈2 ionizing photons per hydrogen atom per gigayear at $z = 6$ because at this time $(\alpha_{B,4}\, n_e)^{-1} = 1.1$ Gyr. Simulations with radiative transfer to capture self-shielding suggest small clumping factors of only 2–3 at $z \sim 6$ for ionizing backgrounds in the range of those allowed (McQuinn et al. 2011b, Kaurov & Gnedin 2015). For regions that have been reionized within $\Delta z \approx 2$ and hence have not had time to relax, the gas can have somewhat higher clumping factors (Pawlik et al. 2009).

3.2. Models of Reionization

Almost every observable of reionization is tied to the structure of this process, making models critical for interpreting the observations. There has been substantial effort directed toward modeling reionization (Gnedin & Ostriker 1997; Ciardi et al. 2003, 2012; Furlanetto & Oh 2005;

Iliev et al. 2006; McQuinn et al. 2007b; Trac & Cen 2007; Finlator et al. 2009; Thomas et al. 2009; Santos et al. 2010; Mesinger et al. 2011; Gnedin 2014; Pawlik et al. 2015). Existing models for the structure of reionization are almost exclusively in the prevailing galactic source paradigm. Generically in these models, ionization fronts propagate outward from galaxies and, much like with HII regions in the ISM, there is a sharp boundary between where gas is ionized and where it is neutral. This width is $\sim 1\Delta_b^{-1}$ physical kpc during reionization, a scale that is generally much smaller than the size of the HII regions themselves (and often unresolved). Thus, a typical region in the IGM during reionization is expected to be either highly ionized or nearly neutral, leading to the term patchy reionization. The ionization fronts also heat the gas from likely hundreds of Kelvin to more than 10^4 K, causing the gas to evaporate from $<$10-km s^{-1} potential wells (Barkana & Loeb 1999, Shapiro et al. 2004, Okamoto et al. 2008; see also the sidebar The Minimum Mass of Galaxies in Section 2.3).

Most predictions for the structure of reionization come from semianalytic models or large-box radiative transfer simulations (typically performed with ray-tracing algorithms). "Large box" is used here to mean box sizes that are $\gtrsim$100 Mpc, roughly the scale studies have shown is required to have a sufficient sample of structures (and to not be biased by missing large-scale modes) to make accurate statistical statements about reionization (Barkana & Loeb 2004, Furlanetto et al. 2004, Iliev et al. 2006). The predictions for the structure of reionization in semianalytic models and large-box simulations have been shown to be in fantastic agreement with one another (Zahn et al. 2007, 2011; Santos et al. 2008), although these models themselves are not without controversy, as discussed below. The semianalytic models and large-box simulations predict that the structure of reionization is driven mostly by the clustering of the galactic sources. The most striking prediction of these models is that the bubble sizes reach many megaparsecs in size, engulfing thousands and even millions of galaxies (Barkana & Loeb 2004, Furlanetto et al. 2004, Iliev et al. 2006). Because these overdensities of galaxies trace large-scale matter overdensities, these simulations also established that on large scales reionization should be "inside-out," meaning that on megaparsec scales and greater, overdense regions are ionized first rather than outside-in as can happen on smaller scales [see the sidebar The Miralda-Escudé et al. Model for Reionization]. Even when the global hydrogen ionized fraction is only $\sim$10%, these models tend to find that much of the ionized volume is subsumed by $\sim$10 comoving Mpc bubbles. Many semianalytic models even find $>$100 comoving Mpc bubbles by the time the intergalactic hydrogen is $\sim$90% ionized (Furlanetto et al. 2004, Zaroubi et al. 2012). **Figure 11** shows a light cone image of a large-box reionization simulation (from Mellema et al. 2006).

Large-box calculations have also been used to explore how reionization models depend on the properties of the sources or on unresolved overdense structures that can act as sinks of ionizing

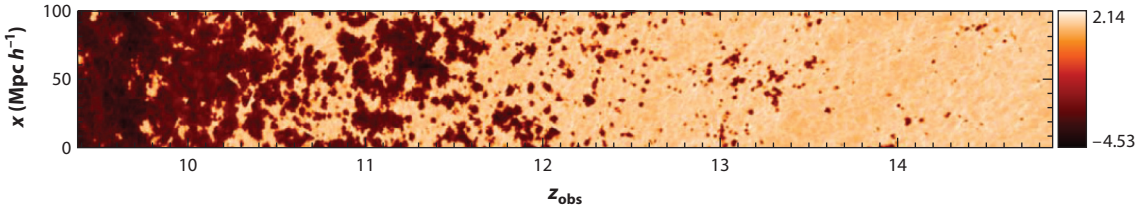

Figure 11

Image of a 100-Mpc h^{-1} radiative transfer simulation of reionization. Shown is a slice through the 21-cm emission signal on the light cone (showing $\log_{10}$ of the brightness temperature). Darker regions are ionized and brighter ones are neutral. Adapted from Mellema et al. (2006) with permission.

THE MIRALDA-ESCUDÉ ET AL. MODEL FOR REIONIZATION

On large scales, reionization should have been "inside-out," meaning that overdense regions that host more galaxies were ionized first. However, as the ionized bubbles grew, the ionizing background within them increased, resulting in an "outside-in" process also occurring as dense, self-shielding clumps became progressively more ionized. Miralda-Escudé et al. (2000) proposed an elegant model for this outside-in process; it is able to characterize many of the essential aspects with a single parameter, the sources' ionizing emissivity ϵ_γ. This model makes the ansatz that all gas is ionized up to a critical density, $\Delta_{b,*}$, after which it becomes neutral. This critical overdensity is calculable using the PDF of Δ_b, $P(\Delta_b)$, which can be estimated from cosmological simulations (Miralda-Escudé et al. 2000, Bolton & Becker 2009), as the emissivity of the sources balances the rate density of recombinations (see Equation 13): $\epsilon_\gamma = \alpha_B \bar{n}_e^2 \int_0^{\Delta_{b,*}} d\Delta_b P(\Delta_b) \Delta_b^2 \propto \Delta_{b,*}^{3-n}$, where the proportionality assumes $P(\Delta_b) \propto \Delta_b^{-n}$ as simulations find is applicable at high densities. The ansatz of a critical overdensity has been subsequently tested in several studies, finding that it works very well (Faucher-Giguère et al. 2010, McQuinn et al. 2011b, Yajima et al. 2012), and, indeed, it is often used as a simple way to incorporate self-shielding in cosmological simulations (e.g., Nagamine et al. 2010). Next, to estimate $\lambda_{\rm mfp}$, Miralda-Escudé et al. (2000) made a second ansatz that the number density and shape of absorbers do not change with Γ, which implies that the mean free path must scale as the fraction of the volume that is neutral, $\int_{\Delta_{b,*}}^{\infty} d\Delta_b P(\Delta_b) \propto \Delta_{b,*}^{1-n}$, to the $-2/3$ power. The scaling coefficient can be measured using simulations or by matching to $\lambda_{\rm mfp}$ measurements. Finally, to close the equations requires an expression for the photoionization rate:

$$\Gamma = \frac{\sigma_{\rm HI}(\nu_{\rm HI})(3\beta - 3 + \alpha)}{3 + \alpha} \epsilon_\gamma \lambda_{\rm mfp}(\nu_{\rm HI}) \propto \Delta_{b,*}^{(7-n)/3} \propto \epsilon_\gamma^{\frac{7-n}{9-3n}} \propto \epsilon_\gamma^{1/(2-\beta)}, \quad (14)$$

where α is the spectral index of the sources and β the power-law scaling of $\partial^2\mathcal{N}/\partial N_{\rm HI}\partial z$ at $N_{\rm HI} = 10^{17}$ cm^{-2} (see McQuinn et al. 2011b). Miralda-Escudé et al. (2000) used this model to demonstrate that the number of recombinations per H atom during reionization is likely small. More recently, this model has been used to (1) calculate the HII bubble radii above which recombinations retard their growth (Furlanetto & Oh 2005), (2) model ionizing background fluctuations (Davies & Furlanetto 2015), and (3) model the postreionization IGM (Bolton & Haehnelt 2007, Muñoz et al. 2016).

Interestingly, β is found to be fairly steep with values of 1.7–1.8 in simulations (Altay et al. 2011, McQuinn et al. 2011b) and tentatively the observations (Prochaska et al. 2010, Rudie et al. 2013). By using Equation 14, this suggests that $\Gamma \propto \epsilon_\gamma^{3-5}$, making it even more curious why Γ is measured to be rather constant over the range of $2 < z < 5$. However, this strong scaling potentially helps explain the quick evolution in the IGM Lyα opacity at $z \approx 6$ (McQuinn et al. 2011b, Muñoz et al. 2016).

photons. Regarding the source properties, studies find that as more massive galaxies reionized the Universe, the sizes of HII regions increased owing to the enhanced source clustering (Furlanetto et al. 2005, McQuinn et al. 2007b), and they also find modest changes for more complex source prescriptions such as tying some of the ionizing emissivity to major mergers (Cohn & Chang 2007). Regarding the unresolved dense structures that act as sinks of ionizing photons, studies find that the sinks act to cap the maximum ionized bubble size at roughly the photon mean free path to intersect a sink (Furlanetto & Oh 2005, McQuinn et al. 2007b, Alvarez & Abel 2012, Sobacchi & Mesinger 2014).

A criticism of large-box models is that these dense sinks of ionizing radiation are not self-consistently captured, unlike potentially in small-box, higher spatial resolution simulations such as that conducted by Gnedin & Fan (2006). (Conversely, the small-box simulations are unable to capture the large-scale structure of reionization.) We describe the physics that shapes the sinks in the sidebar The Miralda-Escudé et al. Model for Reionization. These sinks are often

imprecisely referred to as Lyman-limit systems, which are systems defined to have $N_{\rm HI} > 1.6 \times 10^{17}$ cm^{-2} and which correspond to regions with $\Delta_b \gtrsim 10[(1+z)/10]^{-3}\Gamma_{12}^{-1}$ (Equation 4). (At lower redshifts, Lyman limits contribute about half of the opacity for ionizing photons.) Some contributions to the sinks include photoevaporating minihalos (defined as halos below the threshold to cool atomically) and other thermally relaxing gaseous structures (Iliev et al. 2005, Ciardi et al. 2006, McQuinn et al. 2006). An unfortunate ramification of not self-consistently capturing the sinks is that large-box simulations are unable to address the final phase of reionization in which the IGM transitioned to the highly ionized state seen in the Lyα forest. A related problem is that most previous simulations prescribed source emissivities that were far from being photon-starved (Section 3.1). In this very emissive source limit, the impact of dense systems/recombinations should be reduced, potentially skewing the predictions for the structure of reionization (Furlanetto & Oh 2005, Choudhury et al. 2009, Ciardi et al. 20012).

A generic result of modern reionization models is that $N_{\gamma/b}$—the ratio of ionizing photons produced to the number of hydrogen atoms needed to complete reionization—is within a factor of two or so of its absolute minimum value of one. For example, Choudhury et al. (2009) predicted values that range from 1.2–2 for this ratio. (We define $N_{\gamma/b}$ to exclude the absorption of ionizing photons in the ISM/circumgalactic medium of the source galaxy. Such absorption is handled by $f_{\rm esc}$. This distinction explains some much higher numbers for $N_{\gamma/b}$ that have appeared previously in the literature.) The small values of this ratio can be understood from the reionization occurring in most models primarily at $6 < z < 10$ and spanning a few hundred million years, a duration that is shorter than or comparable to the effective recombination timescale, $[C\alpha_B \bar{n}_e(z)]^{-1}$, at these redshifts.

3.3. Observables of Cosmological Reionization

The main observables of cosmological reionization are the Lyα forest (Section 3.3.1), anisotropies in the CMB (Section 3.3.2), diagnostics of damping wing absorption of intergalactic hydrogen (Section 3.3.3), and highly redshifted 21-cm radiation (Section 3.3.4). Studies have quoted a variety of constraints on reionization, typically on the global neutral fraction, using all of the aforementioned probes. Two of these constraints (the mean redshift of reionization from the CMB and the end redshift of reionization from the Lyα forest) are quite robust. Many of the other constraints are controversial or model dependent. Here we discuss what each of these probes may be revealing about reionization as well as each's future prospects.

3.3.1. The $z > 5$ Lyman-series forest. At $z \sim 6$, the cosmic mean density saturates in Lyα absorption for $x_{\rm HI} \sim 10^{-5}$ (Equation 1), with Lyβ and Lyγ forests extending the range to $x_{\rm HI} \sim 10^{-4}$. Therefore, the Lyman-series forests are insensitive to the $\mathcal{O}(1)$ fluctuations in the neutral fraction that define reionization. Even though this saturation means that the Lyman-series forests cannot be used to directly detect neutral regions (although see Malloy & Lidz 2015), the $z > 5$ Lyman-series forest exhibits dramatic evolution in the mean opacity as well as extremely large spatial fluctuations in the transmission (Becker et al. 2001, 2015; Fan et al. 2002, 2006; Mortlock et al. 2011). These trends must contain information about reionization and the transition to a highly ionized IGM, but there is currently little consensus in the interpretation.

Figure 12*a* shows the Lyα forest toward 19 of the highest redshift quasars that have been identified, from Fan et al. (2006). These spectra have been used to place a hard limit on the IGM neutral fraction, as any region with detected transmission cannot be fully neutral: **Figure 12*b*** shows a measurement from such spectra of the fraction of 3.3 comoving Mpc regions with no transmission in both the Lyα and Lyβ forests, from McGreer et al. (2015). This measurement constrains this fraction to be $<0.06 \pm 0.05$ at $z = 5.9$, which translates directly to a

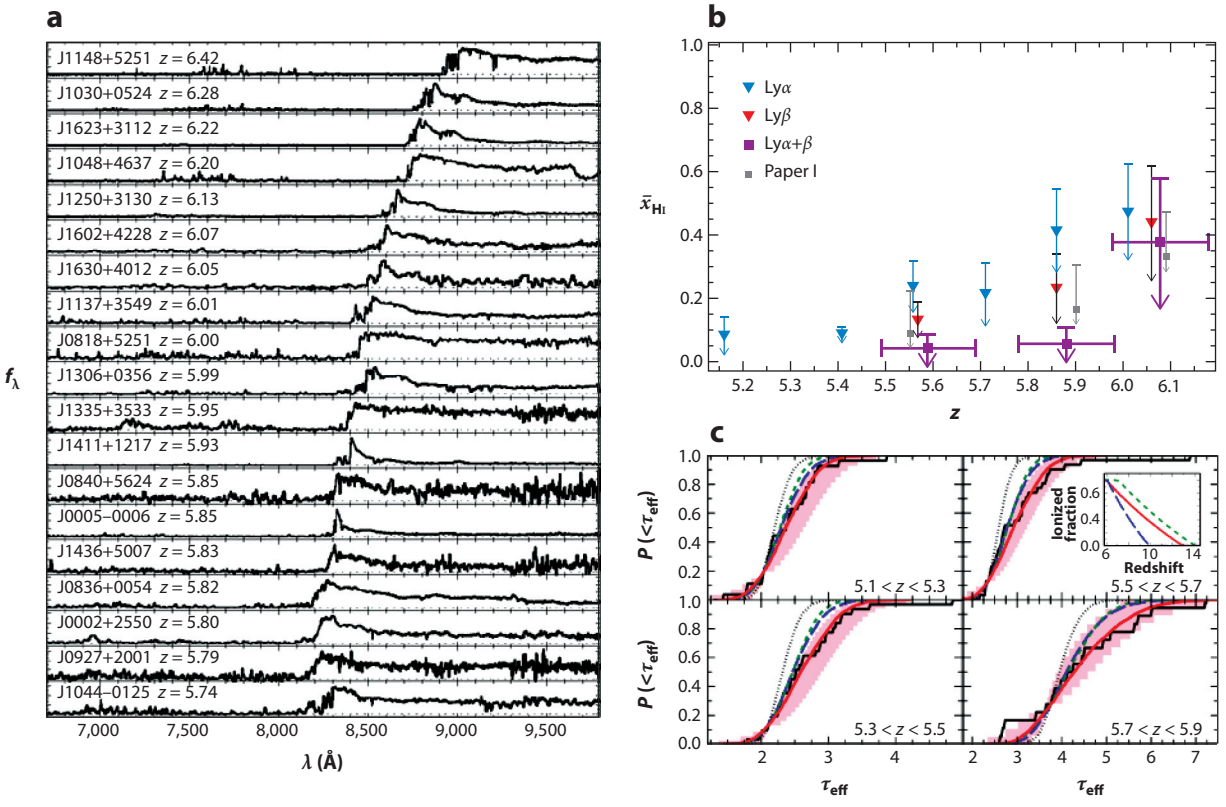

Figure 12

(*a*) Lyα forest spectral region for many of the highest redshift quasars that have been identified. Adapted from Fan et al. (2006) with permission. (*b*) Dark gap bound on the neutral hydrogen fraction, showing the fraction of 3.3 comoving Mpc pixels that show no transmission in Lyα and/or Lyβ. Adapted from McGreer et al. (2015) with permission. (*c*) Panels show the cumulative probability distribution function (PDF) of $\tau_{\rm eff} = -\log(\text{transmission})$ in redshift bins that span $5.1 < z < 5.9$, where the transmission is calculated in 50 comoving Mpc h^{-1} pixels. The histograms show the measurements of Becker et al. (2015). The other curves are the cumulative PDFs in numerical models that include the temperature fluctuations from patchy reionization (*solid curves*) and that do not include them (*dotted curves*). Adapted from D'Aloisio et al. (2015) with permission.

bound on the HI fraction if structures are much larger than 3.3 Mpc (as occurs in most reionization models). This constraint suggests that reionization had completed or was nearly complete by $z \approx 6$.

The high-z Lyα forest spectra in **Figure 12*a*** also illustrate the steeply increasing opacity in the forest with increasing redshift (wavelength). Compare the absorption from gas at $z = 5$, which falls at $\lambda = 7300$ Å, to that at $z = 6$, which falls at 8500 Å. The evolution is even more striking when using Lyβ and Lyγ absorption, with Fan et al. (2006) finding evidence for at least a factor of two increase in the opacity over the short period from $z \approx 5.8$ to $z \approx 6.2$. It has been speculated that the fast increase in the mean opacity arises from the quick evolution that occurs when ionized bubbles overlap and reionization completes (Gnedin 2004). However, it has also been argued that the IGM opacity could evolve over this short timescale even after reionization (see the sidebar The Miralda-Escudé et al. Model for Reionization). However, given other indications that suggest

reionization was ending at $z \sim 6$, it seems likely that this opacity increase is associated with the end of reionization.

More interesting perhaps are the large spatial fluctuations in the Lyα forest opacity at $z > 5$. These opacity fluctuations are larger than those expected in standard models with uniform ionizing backgrounds and power-law temperature-density relations (Fan et al. 2006, Becker et al. 2015). The cumulative PDF of $\tau_{\rm eff} \equiv -\log(\text{Transmission})$ calculated in 50-Mpc h^{-1} comoving pixels is shown with the histograms in **Figure 12*c***. The dotted curves are the predictions from simulations of the standard model for the Lyα forest as described in Section 2.1. Because these curves fall far short of explaining the measured histograms, fluctuations in either the ionizing background, $\propto \Gamma$, and/or the temperature, $T(\Delta_b)$, must source the width of this distribution because $x_{\rm HI} = \alpha(T)n_e/\Gamma$, which is in contrast to the $z < 5$ forest where density inhomogeneities dominate the opacity fluctuations. Becker et al. (2015) and Davies & Furlanetto (2015) attempted to explain the opacity fluctuations with ionizing background fluctuations, showing that models where the mean free path, $\lambda_{\rm mfp}$, is a few smaller at $z = 5.6$ than expected from lower-redshift extrapolations can explain most but not all of the width of the cumulative PDF, especially if one includes spatial fluctuations in the mean free path (Davies & Furlanetto 2015). Rather than a small $\lambda_{\rm mfp}$, larger fluctuations could owe to very rare sources contributing substantially to the background. Chardin et al. (2015) showed that these sources would have to be bright quasars that contribute half or more of the background. Another hypothesis comes from D'Aloisio et al. (2015), who argued that temperature fluctuations could explain the width of the PDF. The solid curves in **Figure 12*c*** show the effect of temperature fluctuations (incorporated using large-box calculations of patchy reionization) for the global ionization histories shown in the inset of **Figure 12*c***. They find that the signal can be explained by temperature fluctuations with relatively extended histories. If temperature fluctuations are their source, the opacity fluctuations in the $z > 5$ forest constrain the duration and structure of reionization.

3.3.2. Anisotropies in the cosmic microwave background from reionization. A model independent constraint on reionization comes from measurements of the average Thomson scattering optical depth through reionization from CMB anisotropies. If the midpoint of reionization occurred at a redshift of $z_{\rm rei}$, then the free electrons generated by this process would result in a Thomson optical depth of $\tau_{\rm es} \approx 0.07\,[z_{\rm rei}/10]^{3/2}$ for CMB photons. This electron "screen" suppresses the anisotropies generated at last scattering by a factor of $\exp(-\tau_{\rm es})$, and more importantly it generates polarization anisotropies at low spherical harmonic multipoles, ℓ. (Spherical harmonics are the favored basis for decomposing the sky in CMB analyses.) In particular, a quadrupole temperature anisotropy (which is always present after recombination owing to the Sachs-Wolfe effect) Thomson scatters off electrons generated at reionization, generating linear polarization (as the electrons shake more orthogonally to the bright axis of the quadrupole). This polarization is correlated over the horizon scale at the redshift of scattering (the correlation length of the quadrupole), which translates to polarization fraction fluctuations at multipoles of $\ell \sim \pi\sqrt{z_{\rm rei}}$. This polarized component of the CMB has fractional amplitude of $\sim\tau_{\rm es}\Delta\phi$, where $\Delta\phi \sim 10^{-5}$ is the typical size of the Sachs-Wolfe quadrupole. In addition, low-ℓ polarization anisotropies are not generated by other means. Measuring this signal and its ℓ dependence constrains the mean redshift of reionization and sets a bound on the duration (Zaldarriaga 1997, Holder et al. 2003, Mortonson & Hu 2008, Zaldarriaga et al. 2008).

This large-scale polarization "bump" was first detected with the WMAP satellite, estimating $\tau_{\rm es} = 0.17 \pm 0.06$ using its first year data, which translates into an average redshift for reionization of $z_{\rm rei} \approx 17 \pm 4$ (Spergel et al. 2003). Modelers of reionization found it difficult to reproduce such an early reionization as there simply was not enough galaxy formation by this redshift in the

concordance ΛCDM cosmology. This tension led to a plethora of exotic solutions (Cen 2003, Haiman & Holder 2003). This high value of τ_{es} (combined with the nearly coincident discovery of $z \approx 6$ quasars with the Sloan Digital Sky-Survey) spawned a period of significant growth in the community working on reionization. However, it turned out that τ_{es} was overestimated in the first year of WMAP analysis owing to a poor foreground model, and by year three the preferred τ_{es} was consistent with the ninth and final year value of $\tau_{es} = 0.088 \pm 0.014$ (Hinshaw et al. 2013), although still 1σ higher than the current best fit value from the Planck satellite of $\tau_{es} = 0.066 \pm 0.016$ (Planck Collaboration et al. 2015). The Planck constraint corresponds to an instantaneous reionization with redshift $z_{rei} = 8.8^{+1.7}_{-1.4}$, which may even be consistent with reionization by the observed population of galaxies (Robertson et al. 2015). The Planck satellite has not yet lived up to forecasts that it would reduce the WMAP error bar on τ_{es} by a factor of 2.5 partly because systematics have prevented the full use of its low-ℓ polarization data. Other than improvements in the Planck analysis (which are rumored to be forthcoming), better estimates of τ_{es} will come with a future large CMB satellite (Zaldarriaga et al. 2008). A cosmic variance-limited E-mode polarization measurement would reduce the current error bar on τ_{es} and z_{rei} by a factor of five and would measure the duration of reionization if this process spanned a redshift interval $\gtrsim 5$ (Zaldarriaga et al. 2008).

The large-scale polarization anisotropies constrain the global reionization history but not the structure of this process. However, reionization is also responsible for small-scale CMB temperature fluctuations from the kinetic Sunyaev-Zel'dovich effect (kSZ), which is due to Doppler scattering off the relative motions of ionized structures (Sunyaev & Zeldovich 1980, Ostriker & Vishniac 1986). These structures could just be postreionization density inhomogeneities or, during reionization, ionized bubbles. In most models, the kSZ effect is smaller than the other important source of secondary temperature anisotropies at high ℓ, the thermal Sunyaev-Zel'dovich effect (tSZ; Zeldovich & Sunyaev 1969), which is due to Compton scattering off hot gas that primarily resides in $>10^{14}$-$M_\odot$ halos. Fortunately, the unique spectral dependence of the tSZ allows it to be separated from the kSZ. Recently, the South Pole Telescope (SPT) has reported a detection of the kSZ with $l^2 C_l/[2\pi] = 2.9 \pm 1.3\ \mu K^2$ at $\ell \approx 3{,}000$ (George et al. 2015). This, kSZ amplitude is not much smaller than their constraint on the tSZ of $l^2 C_l/[2\pi] = 4.1 \pm 0.7\ \mu K^2$ (a surprise given that when the SPT was being planned the tSZ was predicted to be more than an order of magnitude larger).

Most of the kSZ signal likely derives from structures after reionization, but the prediction of reionization calculations is that there should be a significant fraction that is due to reionization (Gruzinov & Hu 1998, Knox et al. 1998, Santos et al. 2003, McQuinn et al. 2005, Zahn et al. 2005, Iliev et al. 2007). The kSZ contribution from after reionization, called the Ostriker-Vishniac effect (Ostriker & Vishniac 1986, Hu 2000), is estimated to have amplitude $l^2 C_l/[2\pi] = 2.2$–$3.9\ \mu K^2$ at $\ell = 3{,}000$, with the exact value depending on how galactic feedback redistributes the baryons around galaxies (Shaw et al. 2012). In light of the SPT measurement, this amplitude range does not leave much room for the kSZ effect from patchy reionization. **Figure 13*a*** compares this limit to three models for the kSZ from Mesinger et al. (2012), assuming a minimal postreionization kSZ of $2.2\ \mu K^2$. All the models are ruled out at 1σ by the SPT bound, and two of the models marginally at 2σ. In most large-box models for reionization, the kSZ signal at $\ell = 3{,}000$ falls in the range of 1–4 μK^2, with the amplitude primarily set by the duration of reionization with other parameters that affect reionization entering at a secondary level (Mesinger et al. 2012, Zahn et al. 2012, Park et al. 2013). Assuming a postreionization kSZ on the low end of estimates, George et al. (2015) constrained the duration of reionization to be $\Delta z < 5.4$ at 95% C.L. using large-box reionization models with a linear-in-redshift reionization history. This bound on the duration is perhaps slightly longer than the duration of reionization in typical models. Constraints on the

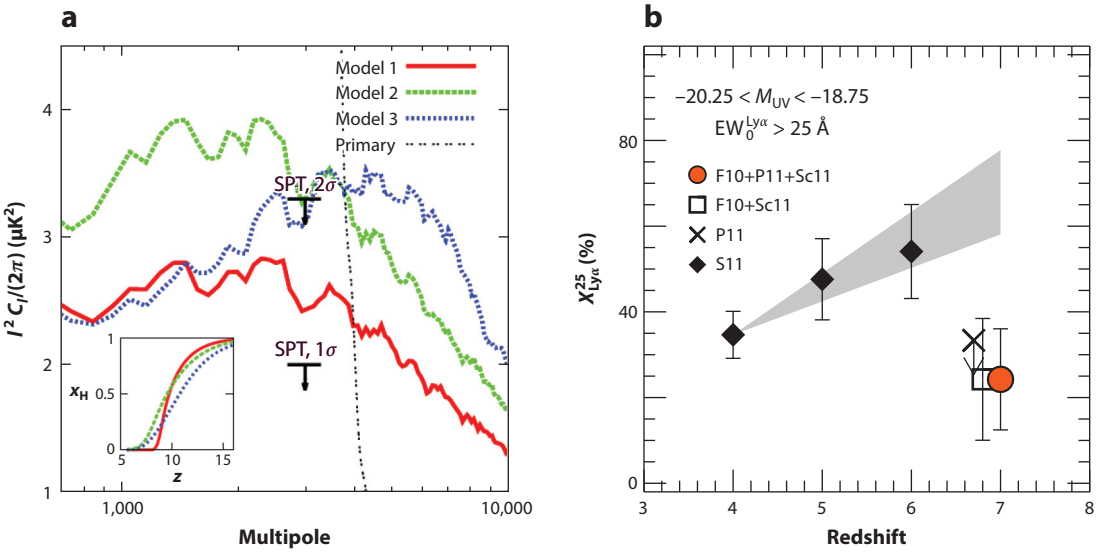

Figure 13

(*a*) Three models for the kinetic Sunyaev-Zel'dovich effect (kSZ) angular power spectrum from patchy reionization presented by Mesinger et al. (2012, their figure 4). The upper bounds are the 1σ and 2σ limits at $\ell = 3{,}000$ on the patchy reionization contribution from the South Pole Telescope (SPT), assuming a minimal postreionization kSZ of 2.2 μK^2. The inset shows the global ionization histories in these models. (*b*) The fraction of dropout-selected galaxies within the quoted magnitude range that show Lyα emission with equivalent width >25 Å. Adapted from Ono et al. (2012) with permission. The rapid falloff at $z > 6$ likely is due to reionization.

kSZ should improve significantly in the next couple years with ACTPol and SPTPol (upgraded receivers on the Atacama Cosmology Telescope and on the SPT; Neimack et al. 2010, Austermann et al. 2012).

Other CMB anisotropies from reionization have also been investigated, namely the non-Gaussianities induced by angular fluctuations in τ_{es} (Dvorkin & Smith 2009, Su et al. 2011), small-scale polarization anisotropies (Hu 2000, Doré et al. 2007), and linear-order Doppler anisotropies that are buried under the primary (Alvarez et al. 2006, Adshead & Furlanetto 2008; the kSZ is second order but dominates over linear order at $\ell \gtrsim 1{,}000$). In standard reionization models, these other anisotropies require at the very least mammoth efforts for a significant detection.

3.3.3. The HI Lyα damping wing of a neutral IGM. If the neutral hydrogen fraction in the $z \sim 8$ IGM is x_{HI}, then the damping wing of the IGM's Lyα line scatters radiation with an optical depth of $\tau_{DW} \sim x_{HI}$ at 10^3 km s^{-1} from the resonance (Miralda-Escudé 1998, McQuinn et al. 2008, Mesinger & Furlanetto 2008a). Thus, scattering from an intergalactic damping wing can extend redward of source-frame Lyα, which is outside of the highly absorbed Lyα forest. Furthermore, the damping wing optical depth from gas in the Hubble flow scales with frequency as ν^{-1} rather than the ν^{-2} for a static cloud (Miralda-Escudé 1998), potentially allowing intergalactic damping wing absorption to be distinguished. The amount of scattering also depends on the size of the ionized bubble around the source, with significant scattering redward of Lyα if the bubble is $\lesssim$1 physical Mpc (i.e., 10^3 km s^{-1} of Hubble flow at $z \sim 8$).

This effect has been used to place constraints on the neutral fraction at $z = 6.3$ using the gamma-ray burst observed on May 9, 2004 (Totani et al. 2006). There have also been claimed detections of the damping wing from a neutral IGM in the spectra of high-redshift quasars (Mesinger &

Static cloud: $\tau_{DW} = 3 \frac{N_{HI}}{10^{21}\,\mathrm{cm}^{-2}} \left(\frac{10^3\,\mathrm{km\,s}^{-1}}{\Delta v}\right)^2$

Neutral IGM: $\tau_{DW} = x_{HI} \left(\frac{1+z}{8.5}\right)^{\frac{3}{2}} \frac{10^3\,\mathrm{km\,s}^{-1}}{\Delta v}$

Haiman 2004), most notably ULASJ1120+0641 at $z = 7.1$, the current redshift record holder (Mortlock et al. 2011). Our assessment of the literature is that these constraints and detections are not sufficiently robust to place much weight. In the case of the May 9, 2004, gamma-ray burst, the large size of the intrinsic DLA prevents a definitive measurement (McQuinn et al. 2008), and in the case of quasar ULASJ1120+0641, uncertainty in the quasar's intrinsic Lyα line profile obscures a clear detection of damping wing absorption (Bosman & Becker 2015). Eventually, we are likely to get lucky and have a spectrum that yields a more convincing detection of a damping wing from neutral patches in the IGM.

The HI Lyα damping wing from a neutral IGM would also scatter Lyα emission lines from galaxies (e.g., Loeb & Rybicki 1999), potentially suppressing the observed abundance of galaxies selected by this often-very-luminous emission line (such galaxies are called Lyα emitters; Haiman & Spaans 1999, Rhoads & Malhotra 2001). This effect may explain the rapid decrease in the number density of Lyα emitters detected above $z = 6$ (Iye et al. 2006). Damping wing scattering should also suppress the Lyα line of dropout-selected galaxies. Several groups have detected a decline with redshift between $z = 6$ and 7, and again between $z = 7$ and 8, in the fraction of dropout galaxies that show significant Lyα emission (Ono et al. 2012, Schenker et al. 2012, Pentericci et al. 2014, Tilvi et al. 2014) after an increase in this quantity between $z = 4$ and $z = 6$ (see **Figure 13*b***). These studies have attributed this decrease to neutral intergalactic gas scattering the Lyα emission line. Although the observed decline likely is due to reionization, the total amount of decline is not yet well constrained, especially because sample variance owing to the modulation of emitters by patchy reionization can be quite large in the small fields in which this decline has been measured (Taylor & Lidz 2014). If the full trend holds, standard reionization models require an uncomfortably rapid evolution in the neutral fraction to explain it (to $x_{\rm HI} > 0.4$ by $z = 7$; Mesinger et al. 2015), although there is debate over whether the dense absorption systems that many of these studies had ignored allows for less rapid evolution (Bolton & Haehnelt 2013, Choudhury et al. 2015, Mesinger et al. 2015). The interpretation of trends in Lyα emission is complicated by the fact that Lyα photons can be blueshifted as the photons scatter out of the host galaxy or "absorbed" by flows onto the host, effects that influence the amount of scattering from a neutral IGM (Santos 2004, Dijkstra et al. 2007).

3.3.4. Redshifted 21-cm radiation. The grand hope of reionization aficionados is that the structures during reionization will be mapped using the 21-cm hyperfine transition of atomic hydrogen (Madau et al. 1997, Ciardi & Madau 2003, Zaldarriaga et al. 2004). This observable has the potential to yield vastly more information about reionization than any other probe (and, with additional effort, the ages that preceded reionization; Furlanetto et al. 2006, Morales & Wyithe 2010, Pritchard & Loeb 2012). Although in principle the 21-cm signal provides a tomographic image of reionization like that shown in **Figure 11**, the first generations of instruments do not have the sensitivity to make images, and we must hope instead to achieve statistical detections of the signal (McQuinn et al. 2006, although see Zaroubi et al. 2012). There is a worldwide effort to detect the $z \sim$ 6–10 21-cm signal using both specialized and multipurpose interferometers, such as the Giant Metrewave Radio Telescope (GMRT) in India, the Mileura Widefield Array (MWA) in Australia, the Precision Array to Probe Epoch of Reionization (PAPER) in South Africa, the Low Frequency Array (LOFAR) primarily in the Netherlands, and the 21-cm Array in China (with planning underway for the next-generation Hydrogen Epoch of Reionization Array (HERA) instrument and the Square Kilometre Array (SKA)-low in South Africa and Australia, respectively; Paciga et al. 2013, van Haarlem et al. 2013, DeBoer et al. 2014, Ali et al. 2015, Dillon et al. 2015, Koopmans et al. 2015). With the exception of the Netherlands, these locations have been chosen to be as isolated as possible from anthropogenic radio transmissions that can easily

contaminate this signal, a signal that from $z = 6$–10 falls in the well-trafficked 130–210 MHz band. There are also efforts afoot attempting to detect the sky-averaged (or global) 21-cm signal from $z = 6$–30 (Bowman & Rogers 2010, Burns et al. 2012, Bernardi et al. 2015). Most of the global instruments consist of a single well-calibrated dipole antenna, which is in stark contrast to the thousands of dipoles that compose the MWA, for example.

The challenges associated with detecting the redshifted 21-cm signal are daunting. The foregrounds scale roughly in brightness temperature as $T_b \sim 500[(1+z)/10]^{2.7}$ K, dwarfing the

$$T_b^{21}(\hat{n}, z) = 9\, x_{\rm HI}\, \Delta_b\, (1+z)^{1/2} \left[1 - \frac{T_{\rm CMB}(z)}{T_{\rm S}}\right] \left[\frac{{\rm d}v/{\rm d}x}{H(z)/(1+z)}\right]^{-1} \ {\rm mK} \qquad (15)$$

signal. All variables on the right-hand side of Equation 15 for which an argument is not given are evaluated in direction $\hat{n}$ and at redshift z, and $T_{\rm S}$ is the spin temperature—the temperature that characterizes the ratio in the excited to ground hyperfine states (e.g., Furlanetto et al. 2006). Fortunately, all appreciable foregrounds (synchrotron and bremsstrahlung) are smooth in frequency, in contrast to the 21-cm signal, allowing the foregrounds to be cleanly separated (Petrovic & Oh 2011). (Such a separation is even thought to be possible for the more slowly varying global 21-cm signal; Bernardi et al. 2015.) Realizing this separation with a real instrument is the largest challenge for 21-cm efforts. Even once the 21-cm signal has been isolated, current instruments geared toward the fluctuating signal (whose sensitivity is due to $\sim 10^3$–$10^4 {\rm m}^2$ of effective collecting area in a few hundred-meter core) require integration times of hundreds of hours to reach sensitivity to the signal in standard reionization models (Morales 2005, McQuinn et al. 2006, Parsons et al. 2012, Beardsley et al. 2013).

The number of publications quoting upper bounds on the 21-cm power spectrum has been rapidly increasing in recent years (most recently for the GMRT, PAPER, and MWA efforts by Paciga et al. 2013, Ali et al. 2015, and Dillon et al. 2015, respectively). A compilation of constraints around a wavenumber of $k = 0.2$ comoving ${\rm Mpc}^{-1}$ are shown in **Figure 14*b***, adapted from Beardsley (2015). (The instrumental sensitivity tends to be maximized at $k = 0.2$ ${\rm Mpc}^{-1}$ as the foreground removal procedure reduces sensitivity at lower wavenumbers, whereas the errors from thermal noise blow up at higher wavenumbers.) Currently PAPER has quoted the strongest upper bound on the 21-cm power spectrum (Ali et al. 2015), but the PAPER bound is still $\sim$2 orders of magnitude below models in the most likely limit of $T_{\rm S} \gg T_{\rm CMB}$. Nevertheless, the PAPER bound rules out some reionization models in which $T_{\rm S} \ll T_{\rm CMB}$, which could occur if the X-rays associated with high-redshift star formation (which are responsible for heating the IGM) fell on the lower range of the values found at low redshifts (Pober et al. 2015). Also of note, the Experiment to Detect the Global EoR Step (EDGES) instrument has placed a bound on the reionization epoch of $\Delta z > 0.06$ using the global signal (Bowman & Rogers 2010). Improvements on 21-cm constraints will come with a better understanding of the instrument and foregrounds, with integrating for longer durations (with errors on the power spectrum decreasing linearly with time if thermal noise dominates), and with building larger arrays (such as HERA and the SKA).

Once a detection of the 21-cm signal from reionization is claimed, it will likely require some convincing for the astrophysical community to believe that the signal is indeed cosmological 21-cm radiation. For the fluctuating signal efforts, such a validation could potentially derive from multiple independent measurements, from a detection in cross-correlation with a cospatial galaxy survey (Furlanetto & Lidz 2007, Lidz et al. 2009), or from a detection of temporal evolution in the signal that is consistent with the predictions of reionization models (Lidz et al. 2008).

A definitive detection of 21-cm radiation from reionization will surely motivate searches for this signal from earlier times as, unlike other probes of the $z > 5$ IGM, 21-cm radiation is not

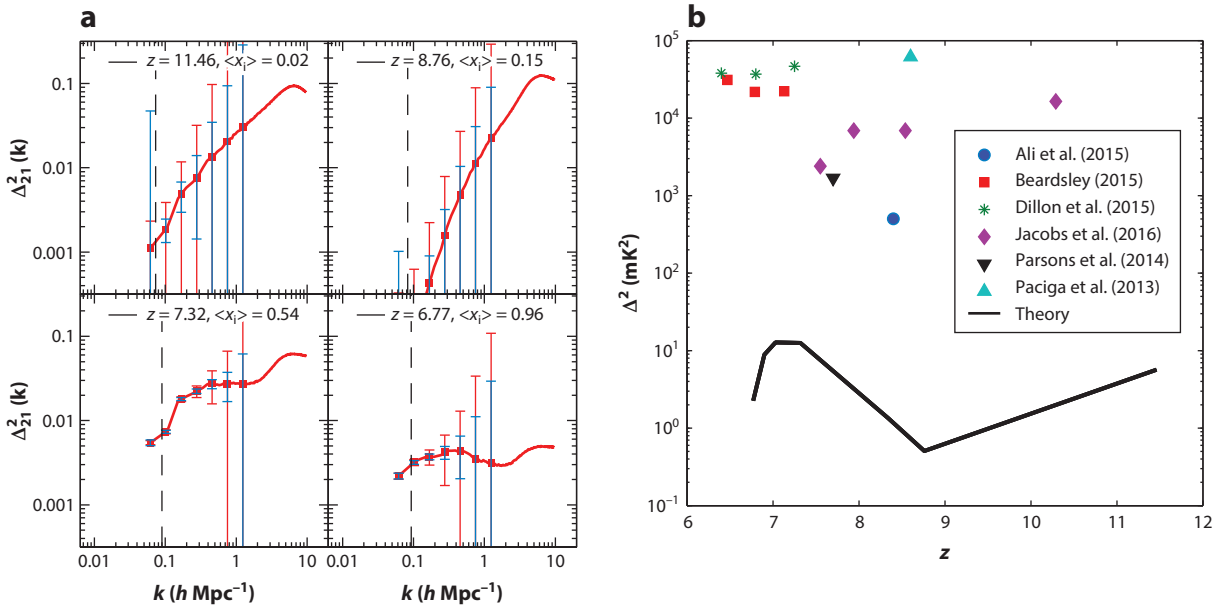

Figure 14

(*a*) Curves show the evolution of the 21-cm dimensionless power spectrum, $\Delta^2_{21} \equiv k^3 P(k)/2\pi^2$, in a large-box reionization simulation. The red error bars are forecasted errors for a 1,000-h integration using an instrument that is five times more sensitive than the current Mileura Widefield Array, assuming perfect foreground removal. Adapted from Lidz et al. (2008) with permission. (*b*) Published upper bounds on the 21-cm dimensionless power spectrum at $k \approx 0.2$ Mpc^{-1}—the wavenumber at which previous analyses are most sensitive. The bounds fall at least two orders of magnitude above the solid theory curve, which is from the same model as panel *a*. Adapted from Beardsley (2015) with permission.

just a reionization-era probe and has the potential to probe all the way to $z \sim 200$ (Madau et al. 1997, Chen & Miralda-Escudé 2004, Furlanetto et al. 2006). Unfortunately, the higher the redshift that is targeted, the brighter is the Galaxy, requiring collecting areas that scale as $\sim\lambda^3$ to maintain the same thermal noise sensitivity to T_b^{21}. The physics that sets T_S and, hence, T_b^{21}, is quite rich (Field 1958, Madau et al. 1997, Chen & Miralda-Escudé 2004, Furlanetto et al. 2006). Once the galaxies formed and the Universe achieved comoving star-formation rate densities of $\sim 10^{-3}$ $M_\odot$ year^{-1} Mpc^{-3} (with only a weak IMF dependence), enough 10.2–13.6 eV photons were produced to couple T_S to the gas kinetic temperature, T_k, through the Wouthuysen-Field effect (Wouthuysen 1952, Field 1958, Furlanetto et al. 2006, McQuinn & O'Leary 2012). Once T_S coupled to T_k, the 21-cm signal became sensitive to how the IGM was preheated before reionization, likely by X-rays associated with the first stellar deaths (Madau et al. 1997, Chen & Miralda-Escudé 2004, Furlanetto 2006; with the signal changing significantly for heating at the level of $\Delta T \sim T_{CMB}$). The amount of X-ray heating from high-redshift galaxies is very uncertain (Fialkov et al. 2014, Pacucci et al. 2014), but scalings based on the X-ray–to–star-formation rate in low-redshift stellar populations suggests that significant heating likely occurred after T_S was coupled to T_k but before reionization (Furlanetto 2006, McQuinn & O'Leary 2012). Thus, the 21-cm signal potentially allows the study of the cosmic gas once the first galaxies turn on, lighting up the gas that is henceforth known as the IGM.

THE $z \sim 0$ HI-IONIZING BACKGROUND

The increasing transmissivity of the HI Lyα forest with decreasing redshift occurs despite HI photoionization rate, Γ, steadily decreasing at $z < 2$ as star formation and quasar activity shut off (in contrast to redshifts of $2 < z < 5$ during which Γ is more or less constant). The effect on Γ of this shutoff is partly compensated by the mean distance ionizing photons transitioning to the photon horizon below $z = 2$, rather than the mean distance to intersect a Lyman-limit system as at higher redshifts (Madau et al. 1999, Faucher-Giguère et al. 2009). The net result is a decrease in Γ by more than an order of magnitude from that inferred at $2 < z < 5$. From tuning Γ in simulations so that they match the observed HI column density distribution, Shull et al. (2015) measured $\Gamma(z) = 5 \times 10^{-14}(1+z)^{4.4}$ s^{-1} over $0 < z < 0.5$. Studies find that this value is consistent with plausible models in which the ionizing background is due to either (*a*) both quasars and galaxies with $f_{esc} \approx 0.05$ (Khaire & Srianand 2015, Shull et al. 2015) or (*b*) just quasars if Γ falls on the lower end of recent estimates (Khaire & Srianand 2015).

4. THE LOW-REDSHIFT IGM ($z < 2$, FOCUSING ON $z \sim 0$)

At lower and lower redshifts, the Lyα forest becomes progressively more transmissive as the Universe is further diluted by cosmological expansion, with an average transmission of $\exp[-\tau_{eff}]$ with $\tau_{eff} = 0.016(1+z)^{1.1}$ over $0 < z < 1.2$, compared with $\tau_{eff} = 0.36$ at $z = 3$ (Meiksin 2006). The evolution of the ionizing background plays some role in the average transmission (see the sidebar The $z \sim 0$ HI-Ionizing Background). Because the redshift evolution in the average transmission is gradual, this review's boundary of $z = 2$ between "low" and "intermediate" redshifts is of no physical significance. (It is the case that at $z \lesssim 2$ the most prominent lines, the Lyman-series and OVI $\lambda\lambda$1032, 1038 Å, fall in the ultraviolet, requiring a space telescope.) Estimates find that only $30 \pm 10\%$ of the $z \sim 0$ gas is seen in Lyα absorption (Shull et al. 2012b) and that $\sim$10% of the baryons lie within galaxies or reside as hot gas inside galaxy clusters. This accounting leaves a large fraction that are "missing." Our inability to observe most of the baryons at $z \sim 0$ is referred to as the missing baryon problem. See Bregman (2007) for a recent review of this problem.

It is not a surprise that a large fraction of the $z \sim 0$ baryons is difficult to observe. Even for photoionized gas, Lyα absorption results in detectable optical depths only for gas with $\Delta_b \gtrsim 10$. In addition, numerical simulations show that 30–50% of the baryons by mass (but only 10% by volume) have been shock-heated into a "warm/hot" 10^5–10^7 K phase (with the fraction of gas roughly constant per interval in $\log T$ over 10^5–10^7 K at $z = 0$) (Cen & Ostriker 1999, 2006; Croft et al. 2001; Davé et al. 2001), temperatures where the hydrogen becomes further ionized by collisions. Most of the warm/hot intergalactic medium (WHIM) is overdense with $\Delta_b \gtrsim 10$, with lower-density gas still predominantly at temperatures characteristic of photoionization. The WHIM is the result of nonlinear structure formation happening at $z \sim 0$ on scales where the potential wells have depths of $\sim$(100 km s^{-1})^2. (There is a relatively tight correlation between potential well depth and comoving scale in our cosmology, and on-average larger scales become nonlinear later.) As a result, the baryons are likely to shock at $\sim$100 km s^{-1}, producing $\sim 10^6$ K gas (Furlanetto & Loeb 2004). The fraction by mass of warm/hot gas is a strong function of redshift with {48, 36, 21, 8}% by mass at $z = \{0, 1, 2, 3\}$, respectively, in the "galactic super-wind" simulation by Cen & Ostriker (2006). These fractions are even more strongly decreasing with increasing redshift for a temperature threshold higher than 10^5 K.

Studies find that outflows from galactic feedback can increase the warm/hot fraction by tens of percent (Davé et al. 2001, Cen & Ostriker 2006). Indeed, the most important problem pertaining to the low-z IGM is not whether the baryons have disappeared between $z = 1,100$ and $z = 0$.

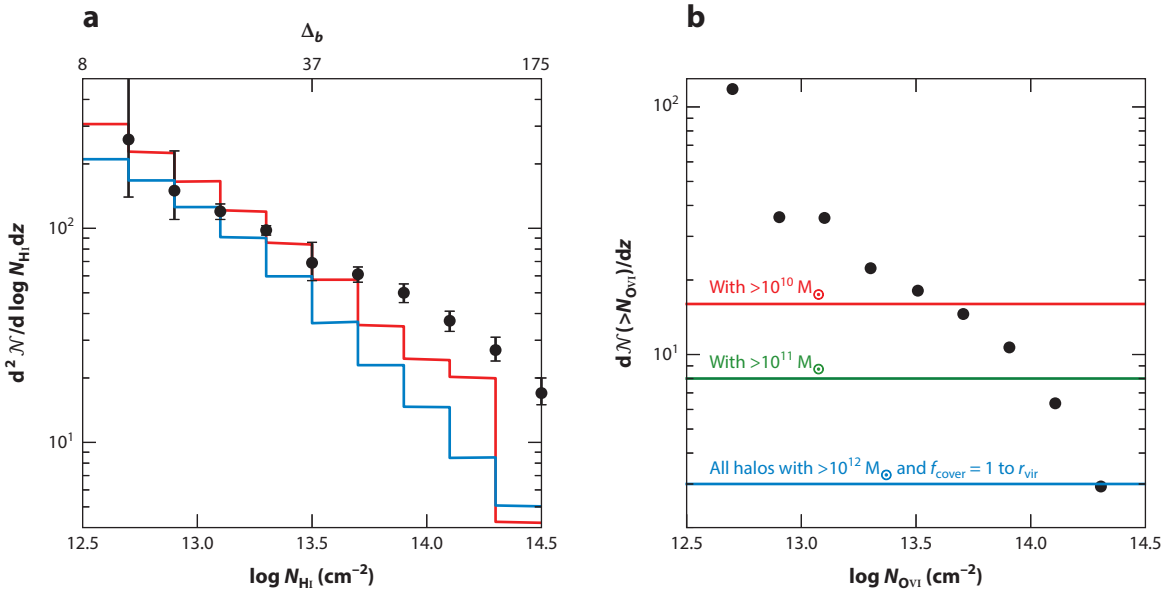

Figure 15

Column density distributions of HI (differential) and OVI (cumulative) at $0 < z < 0.4$. The black dots are the measured distributions from Danforth et al. (2014) using HST/COS data. (*a*) Histograms showing the the HI distribution from the numerical simulations in Kollmeier et al. (2014, *red*) and Shull et al. (2015, *blue*). A second x-axis is included to show the estimated density at a given column using the Schaye (2001b) model. (*b*) Horizontal lines indicate the expected number of absorbers per dz if halos above the specified mass threshold have a covering fraction of unity out to one virial radius.

Instead, it is in understanding how galactic feedback redistributes gas around galaxies (and how this redistribution in turn affects how the IGM feeds galaxies). Only a small fraction, ∼5%, of the gas that should have funneled onto galaxies by $z = 0$ has done so and formed stars (Fukugita & Peebles 2004). Much of this gas has been ejected and redistributed by galactic feedback in a manner that we have yet to fully understand. Currently, the primary observables to understand the impact of feedback on the $z \sim 0$ IGM are HI Lyman-series and OVI λλ1032, 1038-Å absorption (other detectable absorption lines probe denser circumgalactic and galactic gas).

The column density distributions of both HI and OVI are shown in **Figure 15*a*,*b*** for $z \sim 0.2$ using the HST/COS measurements of Danforth et al. (2014). Two simulation predictions for the HI are plotted in **Figure 15*a***; data were taken from Kollmeier et al. (2014) and Shull et al. (2015), using backgrounds with 5× and ≈3× higher Γ than that of Haardt & Madau (2012; see Section 2.4), respectively (see the sidebar Homogeneous Ionizing Backgrounds). Much like at higher redshifts, the HI column density distribution at $N_{HI} \lesssim 10^{14}$ cm^{-2} is found to be only weakly affected by present feedback implementations in simulations (Davé et al. 2010, Shull et al. 2015). However at $N_{HI} \gtrsim 10^{14}$ cm^{-2}, neither simulation shown in **Figure 15** agrees well with the data, which in the adaptive mesh refinement simulations of Shull et al. (2015) likely is due to resolution, but it may reflect differences between the feedback prescription and reality in the smoothed particle hydrodynamics simulations of Kollmeier et al. (2014; also see Davé et al. 2001). This comparison at higher columns should be further investigated, especially in light of these recent HST/COS observations. The upper x-axis in **Figure 15*a*** shows an estimate for the overdensity that corresponds to a given column in the model of Schaye (2001b).

Figure 15*b* considers OVI. The horizontal lines show the cross section of the virial radius of halos of different masses. For the most likely scenario in which OVI is due to $\gtrsim 10^{11}$-$M_\odot$ halos that are able to efficiently form stars, the galactic winds must reach a couple virial radii. Tumlinson & Fang (2005) performed a similar analysis, finding that, to explain the OVI absorption, galaxies down to 0.01–0.1 L_* are required to enrich the IGM out to ∼200 kpc. Observations show that $N_{\rm OVI}$ has little or no correlation with $N_{\rm HI}$. This lack of correlation is due to either OVI probing a different gaseous phase of the IGM or to metals not being well mixed. The simulations of Shull et al. (2012b) and of Tepper-García et al. (2011) suggest that OVI probes a mixture of phases (both warm photoionized gas and the WHIM). Aside from the highest metal columns (which are likely probing circumgalactic material), modern simulations are able to reproduce the OVI column density distribution at a factor-of-a-few level (Shull et al. 2012b, Schaye et al. 2015), suggesting that their galactic wind prescriptions result in enriched ejecta that travel roughly the correct distance from galaxies. Such simulations predict that much of the enrichment occurred at relatively high redshifts, with Wiersma et al. (2010) finding that at least half of the $z = 0$ metals were ejected at $z > 2$ (with metals residing in lower-density gas having been ejected earlier).

Going forward, significant improvements in the quality of the HI and OVI measurements over the HST must wait for a future ultraviolet-sensitive space telescope such as the *High-Definition Space Telescope* (HDST) (Dalcanton et al. 2015). An unexplored frontier in understanding the WHIM is mapping the unseen $\gtrsim 10^6$-K phase. (Collisional ionizations destroy the OVI by these temperatures.) Such mapping may be possible (1) with observations of the soft X-ray background (predicted to constitute 1–10% of the total observed background; Cen & Ostriker 1999, Croft et al. 2001, Kuntz et al. 2001), (2) by isolating the tSZ CMB anisotropy that is due to the WHIM (Atrio-Barandela & Mücket 2006, Génova-Santos et al. 2013, Planck Collaboration et al. 2013), and (3) with studies of OVII and OVIII absorption (Hellsten et al. 1998, Bregman 2007). Limits on WHIM emission from the soft X-ray background are currently on the upper end of model forecasts, and there have been purported detections of field OVII absorption with the *Chandra X-ray Observatory* and the *X-ray Multi-Mirror Mission-Newton* (Bregman 2007). However, a statistical sample of robust OVII and OVIII absorption detections requires a future spectroscopic X-ray satellite. The aforementioned probes of $\gtrsim 10^6$-K gas will be most sensitive to dense gas either within or at the outskirts of galactic halos, further informing models of galactic feedback and flows between galaxies and the IGM. Such information may even solve the great mystery of why an increasing number of galaxies at low redshifts are red and dead, with no recent star formation.

5. CONCLUDING REMARKS

The success of our models at reproducing the HI Lyα forest at $z = 2$–5 shows that much is known about the low-density IGM at intermediate redshifts. The same models also appear to be consistent with the HI column density distribution (all the way to galactic columns) and with some recent IGM temperature measurements (assuming a late HeII reionization), although these comparisons are less exact. Despite these successes, there is plenty of room for additional precision in the measurements, in the models, and in their comparison over $z = 2$–5. There are several established and hypothesized processes that could source a detectable departure from our vanilla IGM models.

At much lower and higher redshifts (as well as near galaxies at all redshifts), our understanding of the IGM is far from complete. At low redshifts and around galaxies, likely the most important unresolved questions are (1) how galactic feedback shapes the IGM and (2) how this in turn affects galaxy formation. We currently have many measurements that constrain the answers, including measurements of the statistics of HI and OVI absorbers at $z \sim 0$, of the distribution of metal absorbers

around massive galaxies at $z \sim 2.5$, and (though beyond the scope of this review) of circumgalactic medium absorption (e.g., Tumlinson et al. 2011, Stocke et al. 2013, Werk et al. 2014). However, there is still much to do on both the observational and theoretical fronts as highlighted throughout this review. At high redshifts, the IGM is shaped by the process of reionization. We have tenuous indications from several distinct observables that hydrogen reionization ended around $z = 6$ and that it extended to higher redshifts. Yet, we know little about the structure and duration of this important process. Future observations and more in-depth study of the high-redshift Lyα forest, of secondary anisotropies in the CMB, of Lyα emitters, and (ultimately) of redshifted 21-cm radiation promise to provide the details that complete this missing chapter in our cosmological narrative.

DISCLOSURE STATEMENT

The authors are not aware of any affiliations, memberships, funding, or financial holdings that might be perceived as affecting the objectivity of this review.

ACKNOWLEDGMENTS

We thank G. Altay, A. Beardsley, A. D'Aloisio, G. Becker, R. Bouwens, X. Fan, C. Fechner, S. Finkelstein, F. Haardt, J. Hennawi, A. Lidz, P. Madau, I. McGreer, G. Mellema, A. Mesinger, Y. Ono, J. Prochaska, E. Rollinde, P. Upton Sanderbeck, J. Schaye, U. Seljak, R. Simcoe, M. Turner, M. Walther, D. Weinberg, G. Worseck, and J. Yeh for sharing figures and spectra and/or providing comments on the manuscript. This work is supported by NSF grants AST-1514734 and AST-1312724 as well as by NASA through Space Telescope Science Institute grant HST-AR-13903.00. Some of this work was performed at the Aspen Center for Physics, which is supported by National Science Foundation grant PHY-1066293.

LITERATURE CITED

Abel T, Bryan GL, Norman ML. 2002. *Science* 295:93–98
Adelberger KL, Shapley AE, Steidel CC, et al. 2005. *Ap. J.* 629:636–53
Adshead PJ, Furlanetto SR. 2008. *MNRAS* 384:291–304
Agafonova II, Levshakov SA, Reimers D, et al. 2007. *Astron. Astrophys.* 461:893–909
Aguirre A, Dow-Hygelund C, Schaye J, Theuns T. 2008. *Ap. J.* 689:851–64
Aguirre A, Hernquist L, Schaye J, et al. 2001a. *Ap. J.* 561:521–49
Aguirre A, Hernquist L, Schaye J, et al. 2001b. *Ap. J.* 560:599–605
Aguirre A, Schaye J, Kim TS, et al. 2004. *Ap. J.* 602:38–50
Aguirre A, Schaye J, Theuns T. 2002. *Ap. J.* 576:1–20
Ali ZS, Parsons AR, Zheng H, et al. 2015. *Ap. J.* 809:61
Altay G, Theuns T, Schaye J, Booth CM, Dalla Vecchia C. 2013. *MNRAS* 436:2689–707
Altay G, Theuns T, Schaye J, Crighton NHM, Dalla Vecchia C. 2011. *Ap. J. Lett.* 737:L37
Alvarez MA, Abel T. 2012. *Ap. J.* 747:126
Alvarez MA, Komatsu E, Doré O, Shapiro PR. 2006. *Ap. J.* 647:840–52
Arinyo-i-Prats A, Miralda-Escudé J, Viel M, Cen R. 2015. *J. Cosmol. Astropart. Phys.* 12:017
Arons J, McCray R. 1970. *Ap. J. Lett.* 5:L123
Atrio-Barandela F, Mücket JP. 2006. *Ap. J.* 643:1–7
Austermann JE, Aird KA, Beall JA, et al. 2012. In *Millimeter, Submillimeter, and Far-Infrared Detectors and Instrumentation for Astronomy VI*, ed. WS Holland, J Zmuidinas. *Proc. SPIE Conf. Ser.* 8452:84521E. Bellingham, WA: SPIE
Bahcall JN, Salpeter EE. 1965. *Ap. J.* 142:1677–80
Barkana R, Loeb A. 1999. *Ap. J.* 523:54–65

Barkana R, Loeb A. 2001. *Phys. Rep.* 349:125–238
Barkana R, Loeb A. 2004. *Ap. J.* 609:474–81
Beardsley AP. 2015. Ph.D. thesis, University of Washington, Seattle
Beardsley AP, Hazelton BJ, Morales MF, et al. 2013. *MNRAS* 429:L5–9
Becker GD, Bolton JS. 2013. *MNRAS* 436:1023–39
Becker GD, Bolton JS, Haehnelt MG, Sargent WLW. 2011. *MNRAS* 410:1096–112
Becker GD, Bolton JS, Madau P, et al. 2015. *MNRAS* 447:3402–19
Becker RH, Fan X, White RL, et al. 2001. *Astron. J.* 122:2850–57
Behroozi PS, Silk J. 2015. *Ap. J.* 799:32
Belikov AV, Hooper D. 2009. *Phys. Rev. D* 80:035007
Bergeron J, Petitjean P, Aracil B. 2004. *Messenger* 118:40
Bernardi G, McQuinn M, Greenhill LJ. 2015. *Ap. J.* 799:90
Bertone S, White SDM. 2006. *MNRAS* 367:247–58
Bi HG, Boerner G, Chu Y. 1992. *Astron. Astrophys.* 266:1–5
Bird S, Vogelsberger M, Sijacki D, et al. 2013. *MNRAS* 429:3341–52
Boera E, Murphy MT, Becker GD, Bolton JS. 2014. *MNRAS* 441:1916–33
Bolton JS, Becker GD. 2009. *MNRAS* 398:L26–30
Bolton JS, Becker GD, Haehnelt MG, Viel M. 2014. *MNRAS* 438:2499–507
Bolton JS, Haehnelt MG. 2007. *MNRAS* 382:325–41
Bolton JS, Haehnelt MG. 2013. *MNRAS* 429:1695–704
Bolton JS, Haehnelt MG, Viel M, Carswell RF. 2006. *MNRAS* 366:1378–90
Bolton JS, Haehnelt MG, Viel M, Springel V. 2005. *MNRAS* 357:1178–88
Bolton JS, Viel M, Kim T, Haehnelt MG, Carswell RF. 2008. *MNRAS* 386:1131–44
Bosman SEI, Becker GD. 2015. *MNRAS* 452:1105–11
Bouwens RJ, Illingworth GD, Oesch PA, et al. 2015a. *Ap. J.* 811:140
Bouwens RJ, Illingworth GD, Oesch PA, et al. 2012. *Ap. J.* 754:83
Bouwens RJ, Illingworth GD, Oesch PA, et al. 2015b. *Ap. J.* 803:34
Bovill MS, Ricotti M. 2009. *Ap. J.* 693:1859–70
Bowman JD, Rogers AEE. 2010. *Nature* 468:796–98
Boylan-Kolchin M, Bullock JS, Garrison-Kimmel S. 2014. *MNRAS* 443:L44–48
Bregman JN. 2007. *Annu. Rev. Astron. Astrophys.* 45:221–59
Bromm V, Kudritzki RP, Loeb A. 2001. *Ap. J.* 552:464–72
Bromm V, Larson RB. 2004. *Annu. Rev. Astron. Astrophys.* 42:79–118
Bromm V, Yoshida N. 2011. *Annu. Rev. Astron. Astrophys.* 49:373–407
Brown TM, Tumlinson J, Geha M, et al. 2012. *Ap. J. Lett.* 753:L21
Bullock JS, Kravtsov AV, Weinberg DH. 2000. *Ap. J.* 539:517–21
Burns JO, Lazio J, Bale S, et al. 2012. *Adv. Space Res.* 49:433–50
Calura F, Tescari E, D'Odorico V, et al. 2012. *MNRAS* 422:3019–36
Cen R. 2003. *Ap. J.* 591:12–37
Cen R, Miralda-Escudé J, Ostriker JP, Rauch M. 1994. *Ap. J. Lett.* 437:L9–12
Cen R, Ostriker J. 1992. *Ap. J.* 393:22–41
Cen R, Ostriker JP. 1999. *Ap. J.* 514:1–6
Cen R, Ostriker JP. 2006. *Ap. J.* 650:560–72
Chang P, Broderick AE, Pfrommer C. 2012. *Ap. J.* 752:23
Chardin J, Haehnelt MG, Aubert D, Puchwein E. 2015. *MNRAS* 453:2943
Chen X, Miralda-Escudé J. 2004. *Ap. J.* 602:1–11
Choudhury TR, Haehnelt MG, Regan J. 2009. *MNRAS* 394:960–77
Choudhury TR, Puchwein E, Haehnelt MG, Bolton JS. 2015. *MNRAS* 452:261–77
Ciardi G, Bolton JS, Maselli A, Graziani L. 2012. *MNRAS* 423:558–74
Ciardi G, Madau P. 2003. *Ap. J.* 596:1–8
Ciardi G, Scannapieco E, Stoehr F, et al. 2006. *MNRAS* 366:689–96
Ciardi G, Stoehr E, White SDM. 2003. *MNRAS* 343:1101–9
Cohn JD, Chang TC. 2007. *MNRAS* 374:72–94

Compostella M, Cantalupo S, Porciani C. 2013. *MNRAS* 435:3169–90
Cowie LL, Songaila A. 1998. *Nature* 394:44–46
Croft RAC. 2004. *Ap. J.* 610:642–62
Croft RAC, Di Matteo T, Davé R, et al. 2001. *Ap. J.* 557:67–87
Croft RAC, Weinberg DH, Bolte M, et al. 2002. *Ap. J.* 581:20–52
Croft RAC, Weinberg DH, Pettini M, Hernquist L, Katz N. 1999. *Ap. J.* 520:1–23
D'Aloisio A, McQuinn MJ, Trac H. 2015. *Ap. J. Lett.* 813:L38
D'Odorico V, Cupani G, Cristiani S, et al. 2013. *MNRAS* 435:1198–232
Dalcanton J, Seager S, Aigrain S, et al. 2015. *From cosmic birth to living earths: the future of UVOIR space astronomy*. AURA Rep. 072715, Assoc. Univ. Res. Astron., Washington, DC. **http://www.hdstvision.org/report**
Dalcanton JJ. 2007. *Ap. J.* 658:941–59
Danforth CW, Keeney BA, Tilton EM, et al. 2016. *Ap. J.* 817:111
Davé R, Cen R, Ostriker JP, et al. 2001. *Ap. J.* 552:473–83
Davé R, Finlator K, Oppenheimer BD. 2011. *MNRAS* 416:1354–76
Davé R, Hernquist L, Weinberg DH, Katz N. 1997. *Ap. J.* 477:21–26
Davé R, Oppenheimer BD, Katz N, Kollmeier JA, Weinberg DH. 2010. *MNRAS* 408:2051–70
Davies FB, Furlanetto SR. 2014. *MNRAS* 437:1141–54
Davies FB, Furlanetto SR. 2015. arXiv:1509.07131
DeBoer D, Bowman JD, Jacobs D, et al. 2014. In *Exascale Radio Astronomy* 1:10304
Dijkstra M, Haiman Z, Loeb A. 2004. *Ap. J.* 613:646–54
Dijkstra M, Lidz A, Wyithe JSB. 2007. *MNRAS* 377:1175–86
Dillon JS, Neben AR, Hewitt JN, et al. 2015. *Phys. Rev. D* 91:123011
Dodelson S. 2003. *Modern Cosmology*. San Diego, CA: Academic
Doré O, Holder G, Alvarez M, et al. 2007. *Phys. Rev. D* 76:043002
Dvorkin C, Smith KM. 2009. *Phys. Rev. D* 79:043003
Efstathiou G. 1992. *MNRAS* 256:43P–47P
Ellis RS, McLure RJ, Dunlop JS, et al. 2013. *Ap. J. Lett.* 763:L7
Ellison SL, Songaila A, Schaye J, Pettini M. 2000. *Astron. J.* 120:1175–91
Fan X, Carilli CL, Keating B. 2006. *Annu. Rev. Astron. Astrophys.* 44:415–62
Fan X, Narayanan VK, Strauss MA, et al. 2002. *Astron. J.* 123:1247–57
Fan X, Strauss MA, Becker RH, et al. 2006. *Astron. J.* 132:117–36
Fardal MA, Giroux ML, Shull JM. 1998. *Astron. J.* 115:2206–30
Faucher-Giguère C, Lidz A, Zaldarriaga M, Hernquist L. 2009. *Ap. J.* 703:1416–43
Faucher-Giguère C, Prochaska JX, Lidz A, Hernquist L, Zaldarriaga M. 2008a. *Ap. J.* 681:831–55
Faucher-Giguère CA, Keres D, Dijkstra M, Hernquist L, Zaldarriaga M. 2010. *Ap. J.* 725:633–57
Faucher-Giguère CA, Lidz A, Hernquist L, Zaldarriaga M. 2008b. *Ap. J.* 688:85–107
Fechner C. 2011. *Astron. Astrophys.* 532:A62
Fechner C, Reimers D. 2007. *Astron. Astrophys.* 461:847–59
Fialkov A, Barkana R, Visbal E. 2014. *Nature* 506:197–99
Field GB. 1958. *Proc. IRE* 46:240
Fields B, Sarkar S. 2006. *J. Phys. G* 33:1
Finkelstein SL, Papovich C, Ryan RE, et al. 2012a. *Ap. J.* 758:93
Finkelstein SL, Papovich C, Salmon B, et al. 2012b. *Ap. J.* 756:164
Finlator K, Özel F, Davé R, Oppenheimer BD. 2009. *MNRAS* 400:1049–61
Fukugita M, Peebles PJE. 2004. *Ap. J.* 616:643–68
Fumagalli M, O'Meara JM, Prochaska JX, Worseck G. 2013. *Ap. J.* 775:78
Furlanetto SR. 2006. *MNRAS* 371:867–78
Furlanetto SR. 2009. *Ap. J.* 703:702–16
Furlanetto SR, Hernquist L, Zaldarriaga M. 2004. *MNRAS* 354:695–707
Furlanetto SR, Lidz A. 2007. *Ap. J.* 660:1030–38
Furlanetto SR, Loeb A. 2004. *Ap. J.* 611:642–54
Furlanetto SR, McQuinn M, Hernquist L. 2005. *MNRAS* 365:115
Furlanetto SR, Oh SP. 2005. *MNRAS* 363:1031–48

Furlanetto SR, Oh SP. 2008. *Ap. J.* 681:1–17
Furlanetto SR, Oh SP. 2009. *Ap. J.* 701:94–104
Furlanetto SR, Oh SP, Briggs FH. 2006. *Phys. Rep.* 433:181–301
Furlanetto SR, Zaldarriaga M, Hernquist L. 2004. *Ap. J.* 613:1–15
Garzilli A, Bolton JS, Kim TS, Leach S, Viel M. 2012. *MNRAS* 424:1723–36
Génova-Santos R, Suárez-Velásquez I, Atrio-Barandela F, Mücket JP. 2013. *MNRAS* 432:2480–87
George EM, Reichardt CL, Aird KA, et al. 2015. *Ap. J.* 799:177
Giallongo E, Grazian A, Fiore F, et al. 2015. *Astron. Astrophys.* 578:A83
Giroux ML, Shapiro PR. 1996. *Ap. J. Suppl.* 102:191
Gnedin NY. 2000. *Ap. J.* 542:535–41
Gnedin NY. 2004. *Ap. J.* 610:9–13
Gnedin NY. 2014. *Ap. J.* 793:29
Gnedin NY, Fan X. 2006. *Ap. J.* 648:1–6
Gnedin NY, Hui L. 1998. *MNRAS* 296:44–55
Gnedin NY, Kravtsov AV, Chen HW. 2008. *Ap. J.* 672:765–75
Gnedin NY, Ostriker JP. 1997. *Ap. J.* 486:581–98
Gontcho A, Gontcho S, Miralda-Escudé J, Busca NG. 2014. *MNRAS* 442:187–95
Greif TH, Springel V, White SDM, et al. 2011. *Ap. J.* 737:75
Gruzinov A, Hu W. 1998. *Ap. J.* 508:435–39
Gunn JE, Peterson BA. 1965. *Ap. J.* 142:1633–36
Haardt F, Madau P. 1996. *Ap. J.* 461:20
Haardt F, Madau P. 2012. *Ap. J.* 746:125
Haiman Z, Abel T, Rees MJ. 2000. *Ap. J.* 534:11–24
Haiman Z, Holder GP. 2003. *Ap. J.* 595:1–12
Haiman Z, Spaans M. 1999. *Ap. J.* 518:138–44
Heap SR, Williger GM, Smette A, et al. 2000. *Ap. J.* 534:69–89
Heger A, Woosley SE. 2002. *Ap. J.* 567:532–43
Hellsten U, Gnedin NY, Miralda-Escudé J. 1998. *Ap. J.* 509:56–61
Hernquist L, Katz N, Weinberg DH, Miralda-Escudé J. 1996. *Ap. J. Lett.* 457:L51
Hinshaw G, Larson D, Komatsu E, et al. 2013. *Ap. J. Suppl.* 208:19
Hoeft M, Yepes G, Gottlöber S, Springel V. 2006. *MNRAS* 371:401–14
Hogan CJ, Anderson SF, Rugers MH. 1997. *Astron. J.* 113:1495–504
Holder GP, Haiman Z, Kaplinghat M, Knox L. 2003. *Ap. J.* 595:13–18
Hopkins PF, Hernquist L, Cox TJ, Keres D. 2008. *Ap. J. Suppl.* 175:356–89
Hopkins PF, Richards GT, Hernquist L. 2007. *Ap. J.* 654:731–53
Hu EM, Kim TS, Cowie LL, Songaila A, Rauch M. 1995. *Astron. J.* 110:1526
Hu W. 2000. *Ap. J.* 529:12–25
Hui L, Gnedin NY. 1997. *MNRAS* 292:27–42
Hui L, Haiman Z. 2003. *Ap. J.* 596:9–18
Hui L, Rutledge RE. 1999. *Ap. J.* 517:541–48
Iliev IT, Mellema G, Pen UL, et al. 2006. *MNRAS* 369:1625–38
Iliev IT, Pen UL, Bond JR, Mellema G, Shapiro PR. 2007. *Ap. J.* 660:933–44
Iliev IT, Shapiro PR, Raga AC. 2005. *MNRAS* 361:405–14
Inoue AK, Kamaya H. 2003. *MNRAS* 341:L7–11
Iwata I, Inoue AK, Matsuda Y, et al. 2009. *Ap. J.* 692:1287–93
Iye M, Ota K, Kashikawa N, et al. 2006. *Nature* 443:186–88
Jacobs DC, Hazelton BJ, Trott CM, et al. 2016. *Ap. J.* 825:114
Johnson JL, Khochfar S. 2011. *Ap. J.* 743:126
Katz N, Hernquist L, Weinberg DH. 1992. *Ap. J. Lett.* 399:L109–12
Katz N, Weinberg DH, Hernquist L, Miralda-Escudé J. 1996. *Ap. J. Lett.* 457:L57
Kaurov AA, Gnedin NY. 2015. *Ap. J.* 810:154
Kawata D, Rauch M. 2007. *Ap. J.* 663:38–52
Keating LC, Haehnelt MG, Becker GD, Bolton JS. 2014. *MNRAS* 438:1820–31

Kereš D, Katz N, Weinberg DH, Davé R. 2005. *MNRAS* 363:2–28
Khaire V, Srianand R. 2015. *MNRAS* 451:L30–34
Kim T, Bolton JS, Viel M, Haehnelt MG, Carswell RF. 2007. *MNRAS* 382:1657–74
Kim TS, Hu EM, Cowie LL, Songaila A. 1997. *Astron. J.* 114:1–13
Kim TS, Partl AM, Carswell RF, Müller V. 2013. *Astron. Astrophys.* 552:A77
Kimm T, Cen R. 2014. *Ap. J.* 788:121
Kirkman D, Tytler D. 1997. *Ap. J.* 484:672–94
Kirkman D, Tytler D, Suzuki N, et al. 2005. *MNRAS* 360:1373–80
Klypin AA, Shandarin SF. 1983. *MNRAS* 204:891–907
Knox L, Scoccimarro R, Dodelson S. 1998. *Phys. Rev. Lett.* 81:2004–7
Kohler K, Gnedin NY. 2007. *Ap. J.* 655:685–90
Kollmeier JA, Weinberg DH, Oppenheimer BD, et al. 2014. *Ap. J. Lett.* 789:L32
Koopmans L, Pritchard J, Mellema G, et al. 2015. Presented at *Advancing Astrophysics with the Square Kilometre Array (AASKA14), Giardini Naxos, Italy, June 9–13*, No. 1. **http://pos.sissa.it/archive/conferences/215/001/AASKA14_001.pdf**
Kravtsov AV, Borgani S. 2012. *Annu. Rev. Astron. Astrophys.* 50:353–409
Kuhlen M, Faucher-Giguère CA. 2012. *MNRAS* 423:862–76
Kuhlen M, Vogelsberger M, Angulo R. 2012. *Phys. Dark Univ.* 1:50–93
Kulkarni G, Hennawi JF, Oñorbe J, Rorai A, Springel V. 2015. *Ap. J.* 812:30
Kulkarni G, Rollinde E, Hennawi JF, Vangioni E. 2013. *Ap. J.* 772:93
Kuntz KD, Snowden SL, Mushotzky RF. 2001. *Ap. J. Lett.* 548:L119–22
Lacki BC. 2015. *MNRAS* 448:L20–24
Lai K, Lidz A, Hernquist L, Zaldarriaga M. 2006. *Ap. J.* 644:61–70
Lee KG. 2012. *Ap. J.* 753:136
Lee KG, Bailey S, Bartsch LE, et al. 2013. *Astron. J.* 145:69
Lee KG, Hennawi JF, Spergel DN, et al. 2015. *Ap. J.* 799:196
Lidz A, Faucher-Giguère C, Dall'Aglio A, et al. 2010. *Ap. J.* 718:199–230
Lidz A, Heitmann K, Hui L, et al. 2006. *Ap. J.* 638:27–44
Lidz A, Malloy M. 2014. *Ap. J.* 788:175
Lidz A, Zahn O, Furlanetto SR, et al. 2009. *Ap. J.* 690:252–66
Lidz A, Zahn O, McQuinn M, Zaldarriaga M, Hernquist L. 2008. *Ap. J.* 680:962–74
Loeb A, Rybicki GB. 1999. *Ap. J.* 524:527–35
Lukić Z, Stark CW, Nugent P, et al. 2015. *MNRAS* 446:3697–724
Ma X, Kasen D, Hopkins PF, et al. 2015. *MNRAS* 453:960–75
Mac Low MM, Ferrara A. 1999. *Ap. J.* 513:142–55
Madau P, Haardt F. 2015. *Ap. J. Lett.* 813:L8
Madau P, Haardt F, Rees MJ. 1999. *Ap. J.* 514:648–59
Madau P, Meiksin A, Rees MJ. 1997. *Ap. J.* 475:429–44
Malloy M, Lidz A. 2015. *Ap. J.* 799:179
McDonald P, Eisenstein DJ. 2007. *Phys. Rev. D* 76:063009
McDonald P, Miralda-Escudé J, Rauch M, et al. 2000. *Ap. J.* 543:1–23
McDonald P, Miralda-Escudé J, Rauch M, et al. 2001. *Ap. J.* 562:52–75
McDonald P, Seljak U, Cen R, Bode P, Ostriker JP. 2005a. *MNRAS* 360:1471–82
McDonald P, Seljak U, Cen R, et al. 2005b. *Ap. J.* 635:761–83
McGreer ID, Mesinger A, D'Odorico V. 2015. *MNRAS* 447:499–505
McLure RJ, Dunlop JS, Bowler RAA, et al. 2013. *MNRAS* 432:2696–716
McQuinn M. 2009. *Ap. J. Lett.* 704:L89–92
McQuinn M. 2012. *MNRAS* 426:1349–60
McQuinn M, Furlanetto SR, Hernquist L, Zahn O, Zaldarriaga M. 2005. *Ap. J.* 630:643–56
McQuinn M, Hernquist L, Lidz A, Zaldarriaga M. 2011a. *MNRAS* 415:977–92
McQuinn M, Hernquist L, Zaldarriaga M, Dutta S. 2007a. *MNRAS* 381:75–96
McQuinn M, Lidz A, Zahn O, et al. 2007b. *MNRAS* 377:1043–63
McQuinn M, Lidz A, Zaldarriaga M, Hernquist L, Dutta S. 2008. *MNRAS* 388:1101–10

McQuinn M, Lidz A, Zaldarriaga M, et al. 2009. *Ap. J.* 694:842–66
McQuinn M, O'Leary RM. 2012. *Ap. J.* 760:3
McQuinn M, Oh SP, Faucher-Giguère CA. 2011b. *Ap. J.* 743:82
McQuinn M, Upton Sanderbeck P. 2016. *MNRAS* 456:47–54
McQuinn M, White M. 2011. *MNRAS* 415:2257–69
McQuinn M, Worseck G. 2014. *MNRAS* 440:2406–18
McQuinn M, Zahn O, Zaldarriaga M, Hernquist L, Furlanetto SR. 2006. *Ap. J.* 653:815–34
Meiksin A. 2006. *MNRAS* 365:807–12
Meiksin A, White M. 2001. *MNRAS* 324:141–48
Meiksin A, White M. 2003. *MNRAS* 342:1205–14
Meiksin A, White M. 2004. *MNRAS* 350:1107–26
Meiksin AA. 2009. *Rev. Mod. Phys.* 81:1405–69
Mellema G, Iliev IT, Pen UL, Shapiro PR. 2006. *MNRAS* 372:679–92
Mesinger A, Aykutalp A, Vanzella E, et al. 2015. *MNRAS* 446:566–77
Mesinger A, Furlanetto S, Cen R. 2011. *MNRAS* 411:955–72
Mesinger A, Furlanetto SR. 2008a. *MNRAS* 385:1348–58
Mesinger A, Furlanetto SR. 2008b. *MNRAS* 386:1990–2002
Mesinger A, Haiman Z. 2004. *Ap. J. Lett.* 611:L69–72
Mesinger A, McQuinn M, Spergel DN. 2012. *MNRAS* 422:1403–17
Mirabel IF, Dijkstra M, Laurent P, Loeb A, Pritchard JR. 2011. *Astron. Astrophys.* 528:A149
Miralda-Escudé J. 1993. *MNRAS* 262:273–76
Miralda-Escudé J. 1998. *Ap. J.* 501:15–22
Miralda-Escudé J. 2003. *Ap. J.* 597:66–73
Miralda-Escudé J. 2005. *Ap. J. Lett.* 620:L91–94
Miralda-Escudé J, Cen R, Ostriker JP, Rauch M. 1996. *Ap. J.* 471:582–616
Miralda-Escudé J, Haehnelt M, Rees MJ. 2000. *Ap. J.* 530:1–16
Miralda-Escudé J, Ostriker JP. 1990. *Ap. J.* 350:1–22
Miralda-Escudé J, Rees MJ. 1994. *MNRAS* 266:343–52
Morales MF. 2005. *Ap. J.* 619:678–83
Morales MF, Wyithe JSB. 2010. *Annu. Rev. Astron. Astrophys.* 48:127–71
Mortlock DJ, Warren SJ, Venemans BP, et al. 2011. *Nature* 474:616–19
Mortonson MJ, Hu W. 2008. *Ap. J.* 672:737–51
Muñoz JA, Oh SP, Davies FB, Furlanetto SR. 2016. *MNRAS* 455:1385–97
Nagamine K, Choi JH, Yajima H. 2010. *Ap. J. Lett.* 725:L219–22
Naoz S, Noter S, Barkana R. 2006. *MNRAS* 373:L98–102
Niemack MD, Ade PAR, Aguirre J, et al. 2010. In *Millimeter, Submillimeter, and Far-Infrared Detectors and Instrumentation for Astronomy V*, ed. WS Holland, J Zmuidzinas. *Proc. SPIE Conf. Ser.* 7741:77411S. Bellingham, WA: SPIE
Noh Y, McQuinn M. 2014. *MNRAS* 444:503–14
O'Meara JM, Lehner N, Howk JC, et al. 2015. *Astron. J.* 150:111
Oh SP. 2001. *Ap. J.* 553:499–512
Okamoto T, Gao L, Theuns T. 2008. *MNRAS* 390:920–28
Ono Y, Ouchi M, Mobasher B, et al. 2012. *Ap. J.* 744:83
Oppenheimer BD, Davé R. 2006. *MNRAS* 373:1265–92
Ostriker JP, Vishniac ET. 1986. *Ap. J. Lett.* 306:L51–54
Ouchi M, Shimasaku K, Furusawa H, et al. 2010. *Ap. J.* 723:869–94
Paciga G, Albert JG, Bandura K, et al. 2013. *MNRAS* 433:639–47
Pacucci F, Mesinger A, Mineo S, Ferrara A. 2014. *MNRAS* 443:678–86
Palanque-Delabrouille N, Yeche C, Baur J, et al. 2015. *J. Cosmol. Astropart. Phys.* 11:011
Palanque-Delabrouille N, Yèche C, Borde A, et al. 2013. *Astron. Astrophys.* 559:A85
Paresce F, McKee CF, Bowyer S. 1980. *Ap. J.* 240:387–400
Park H, Shapiro PR, Komatsu E, et al. 2013. *Ap. J.* 769:93
Parsons A, Pober J, McQuinn M, Jacobs D, Aguirre J. 2012. *Ap. J.* 753:81

Parsons AR, Liu A, Aguirre JE, et al. 2014. *Ap. J.* 788:106
Pawlik AH, Schaye J, Dalla Vecchia C. 2015. *MNRAS* 451:1586–605
Pawlik AH, Schaye J, van Scherpenzeel E. 2009. *MNRAS* 394:1812–24
Peebles PJE. 1980. *The Large-Scale Structure of the Universe*. Princeton: Princeton Univ. Press
Peeples MS, Werk JK, Tumlinson J, et al. 2014. *Ap. J.* 786:54
Pentericci L, Vanzella E, Fontana A, et al. 2014. *Ap. J.* 793:113
Petrovic N, Oh SP. 2011. *MNRAS* 413:2103–20
Pieri MM, Haehnelt MG. 2004. *MNRAS* 347:985–93
Planck Collaboration, Ade PAR, Aghanim N, Arnaud M, et al. 2013. *Astron. Astrophys.* 550:A134
Planck Collaboration, Ade PAR, Aghanim N, Arnaud M, et al. 2015. *Astron. Astrophys.* Accepted. arXiv:1502.01589
Pober JC, Ali ZS, Parsons AR, et al. 2015. *Ap. J.* 809:62
Pontzen A, Bird S, Peiris H, Verde L. 2014. *Ap. J. Lett.* 792:L34
Pritchard JR, Furlanetto SR, Kamionkowski M. 2007. *MNRAS* 374:159–67
Pritchard JR, Loeb A. 2012. *Rep. Prog. Phys.* 75:086901
Prochaska JX, O'Meara JM, Worseck G. 2010. *Ap. J.* 718:392–416
Prochaska JX, Weiner B, Chen HW, Mulchaey J, Cooksey K. 2011. *Ap. J.* 740:91
Prochaska JX, Worseck G, O'Meara JM. 2009. *Ap. J. Lett.* 705:L113–17
Puchwein E, Bolton JS, Haehnelt MG, et al. 2015. *MNRAS* 450:4081
Puchwein E, Pfrommer C, Springel V, Broderick AE, Chang P. 2012. *MNRAS* 423:149–64
Quinn T, Katz N, Efstathiou G. 1996. *MNRAS* 278:L49–54
Rahmati A, Pawlik AH, Raicevic M, Schaye J. 2013a. *MNRAS* 430:2427–45
Rahmati A, Schaye J, Pawlik AH, Raicevic M. 2013b. *MNRAS* 431:2261–77
Rakic O, Schaye J, Steidel CC, et al. 2013. *MNRAS* 433:3103–14
Rakic O, Schaye J, Steidel CC, Rudie GC. 2012. *Ap. J.* 751:94
Rauch M. 1998. *Annu. Rev. Astron. Astrophys.* 36:267–316
Rauch M, Miralda-Escudé J, Sargent WLW, et al. 1997. *Ap. J.* 489:7–20
Rees MJ. 1986. *MNRAS* 218:25P–30P
Regan JA, Haehnelt MG, Viel M. 2007. *MNRAS* 374:196–205
Reimers D, Kohler S, Wisotzki L, et al. 1997. *Astron. Astrophys.* 327:890–900
Rhoads JE, Malhotra S. 2001. *Ap. J. Lett.* 563:L5–9
Ricotti M, Gnedin NY, Shull JM. 2000. *Ap. J.* 534:41–56
Robertson BE, Ellis RS, Dunlop JS, McLure RJ, Stark DP. 2010. *Nature* 468:49–55
Robertson BE, Ellis RS, Furlanetto SR, Dunlop JS. 2015. *Ap. J. Lett.* 802:L19
Robertson BE, Furlanetto SR, Schneider E, et al. 2013. *Ap. J.* 768:71
Rollinde E, Theuns T, Schaye J, Pâris I, Petitjean P. 2013. *MNRAS* 428:540–50
Rorai A, Hennawi JF, White M. 2013. *Ap. J.* 775:81
Rosati P, Borgani S, Norman C. 2002. *Annu. Rev. Astron. Astrophys.* 40:539–77
Rudie GC, Steidel CC, Pettini M. 2012. *Ap. J. Lett.* 757:L30
Rudie GC, Steidel CC, Shapley AE, Pettini M. 2013. *Ap. J.* 769:146
Samui S, Subramanian K, Srianand R. 2005. In *29th Int. Cosm. Ray Conf.*, Vol. 9, ed. B Sripathi Acharya, S Gupta, P Jagadeesan, A Jain, S Karthikeyan, S Morris, S Tonwar, pp. 215–18. Mumbai: Tata Inst. Fundam. Res.
Santos MG, Amblard A, Pritchard J, et al. 2008. *Ap. J.* 689:1–16
Santos MG, Cooray A, Haiman Z, Knox L, Ma CP. 2003. *Ap. J.* 598:756–66
Santos MG, Ferramacho L, Silva MB, Amblard A, Cooray A. 2010. *MNRAS* 406:2421–32
Santos MR. 2004. *MNRAS* 349:1137
Schaye J. 2001a. *Ap. J. Lett.* 562:L95–98
Schaye J. 2001b. *Ap. J.* 559:507–15
Schaye J, Aguirre A, Kim TS, et al. 2003. *Ap. J.* 596:768–96
Schaye J, Carswell RF, Kim TS. 2007. *MNRAS* 379:1169–94
Schaye J, Crain RA, Bower RG, et al. 2015. *MNRAS* 446:521–54
Schaye J, Theuns T, Leonard A, Efstathiou G. 1999. *MNRAS* 310:57–70

Schaye J, Theuns T, Rauch M, Efstathiou G, Sargent WLW. 2000. *MNRAS* 318:817–26
Schenker MA, Stark DP, Ellis RS, et al. 2012. *Ap. J.* 744:179
Scheuer PAG. 1965. *Nature* 207:963
Schmidt M. 1965. *Ap. J.* 141:1295
Seljak U, Makarov A, McDonald P, Trac H. 2006. *Phys. Rev. Lett.* 97:191303
Seljak U, Makarov A, McDonald P, et al. 2005. *Phys. Rev. D* 71:103515
Shapiro PR, Giroux ML, Babul A. 1994. *Ap. J.* 427:25–50
Shapiro PR, Iliev IT, Raga AC. 2004. *MNRAS* 348:753–82
Shaw LD, Rudd DH, Nagai D. 2012. *Ap. J.* 756:15
Shull JM, France K, Danforth CW, Smith B, Tumlinson J. 2010. *Ap. J.* 722:1312–24
Shull JM, Harness A, Trenti M, Smith BD. 2012a. *Ap. J.* 747:100
Shull JM, Moloney J, Danforth CW, Tilton EM. 2015. *Ap. J.* 811:3
Shull JM, Smith BD, Danforth CW. 2012b. *Ap. J.* 759:23
Shull JM, Tumlinson J, Giroux ML, Kriss GA, Reimers D. 2004. *Ap. J.* 600:570–79
Shull JM, van Steenberg ME. 1985. *Ap. J.* 298:268–74
Siana B, Shapley AE, Kulas KR, et al. 2015. *Ap. J.* 804:17
Siana B, Teplitz HI, Ferguson HC, et al. 2010. *Ap. J.* 723:241–50
Simcoe RA. 2011. *Ap. J.* 738:159
Simcoe RA, Sargent WLW, Rauch M. 2004. *Ap. J.* 606:92–115
Simcoe RA, Sargent WLW, Rauch M, Becker G. 2006. *Ap. J.* 637:648–68
Sobacchi E, Mesinger A. 2014. *MNRAS* 440:1662–73
Sobacchi E, Mesinger A. 2015. *MNRAS* 453:1843–54
Spergel DN, Verde L, Peiris HV, et al. 2003. *Ap. J. Suppl.* 148:175–94
Stocke JT, Keeney BA, Danforth CW, et al. 2013. *Ap. J.* 763:148
Su M, Yadav APS, McQuinn M, Yoo J, Zaldarriaga M. 2011. arXiv:1106.4313
Sunyaev RA, Zeldovich IB. 1980. *MNRAS* 190:413–20
Syphers D, Anderson SF, Zheng W, et al. 2009. *Ap. J.* 690:1181–92
Syphers D, Anderson SF, Zheng W, et al. 2012. *Astron. J.* 143:100
Syphers D, Shull JM. 2014. *Ap. J.* 784:42
Taylor J, Lidz A. 2014. *MNRAS* 437:2542–53
Tepper-García T, Richter P, Schaye J, et al. 2011. *MNRAS* 413:190–212
Tescari E, Viel M, D'Odorico V, et al. 2011. *MNRAS* 411:826–48
Theuns T, Leonard A, Efstathiou G, Pearce FR, Thomas PA. 1998. *MNRAS* 301:478–502
Theuns T, Schaye J, Haehnelt MG. 2000. *MNRAS* 315:600–10
Theuns T, Schaye J, Zaroubi S, et al. 2002a. *Ap. J. Lett.* 567:L103–6
Theuns T, Viel M, Kay S, et al. 2002b. *Ap. J. Lett.* 578:L5–8
Theuns T, Zaroubi S. 2000. *MNRAS* 317:989–95
Thomas RM, Zaroubi S, Ciardi B, et al. 2009. *MNRAS* 393:32–48
Thoul AA, Weinberg DH. 1996. *Ap. J.* 465:608
Tilvi V, Papovich C, Finkelstein SL, et al. 2014. *Ap. J.* 794:5
Totani T, Kawai N, Kosugi G, et al. 2006. *Publ. Astron. Soc. J.* 58:485–98
Trac H, Cen R. 2007. *Ap. J.* 671:1–13
Trac H, Cen R, Loeb A. 2008. *Ap. J. Lett.* 689:L81–84
Trenti M, Stiavelli M. 2009. *Ap. J.* 694:879–92
Tumlinson J, Fang T. 2005. *Ap. J. Lett.* 623:L97–100
Tumlinson J, Thom C, Werk JK, et al. 2011. *Science* 334:948–52
Turner ML, Schaye J, Steidel CC, Rudie GC, Strom AL. 2014. *MNRAS* 445:794–822
Tytler D, Kirkman D, O'Meara JM, et al. 2004. *Ap. J.* 617:1–28
Tytler D, Paschos P, Kirkman D, Norman ML, Jena T. 2009. *MNRAS* 393:723–58
Upton Sanderbeck PR, D'Aloisio A, McQuinn MJ. 2016. *MNRAS* 460:1885–97
van Haarlem MP, Wise MW, Gunst AW, et al. 2013. *Astron. Astrophys.* 556:A2
Venkatesan A, Tumlinson J, Shull JM. 2003. *Ap. J.* 584:621–32
Viel M, Becker GD, Bolton JS, Haehnelt MG. 2013. *Phys. Rev. D* 88:043502

Viel M, Haehnelt MG. 2006. *MNRAS* 365:231–44
Viel M, Lesgourgues J, Haehnelt MG, Matarrese S, Riotto A. 2005. *Phys. Rev. D* 71:063534
Viel M, Schaye J, Booth CM. 2013. *MNRAS* 429:1734–46
Vogt SS, Allen SL, Bigelow BC, et al. 1994. In *Instrumentation in Astronomy VIII*, ed. DL Crawford, ER Craine. *Proc. SPIE Conf. Ser.* 2198:1, June 1994. Bellingham, WA: SPIE; doi:10.1117/12.176725
Weinberg DH, Davé R, Katz N, Kollmeier JA. 2003. In *The Emergence of Cosmic Structure: 13th Astrophysics Conference*, ed. SS Holt, CS Reynolds. *AIP Conf. Ser.* 666:157. Melville, NY: AIP
Weinberg DH, Hernquist L, Katz N, Croft R, Miralda-Escudé J. 1997. In *13th IAP Workshop: Structure and Evolution of the Intergalactic Medium from QSO Absorption Line System*, *Paris*, *France*, *July* 1–5, pp. 157–69
Weisz DR, Dolphin AE, Skillman ED, et al. 2014. *Ap. J.* 789:148
Werk JK, Prochaska JX, Tumlinson J, et al. 2014. *Ap. J.* 792:8
White M, Pope A, Carlson J, et al. 2010. *Ap. J.* 713:383–93
White SDM, Frenk CS, Davis M. 1983. *Ap. J. Lett.* 274:L1–5
Wiersma RPC, Schaye J, Dalla Vecchia C, et al. 2010. *MNRAS* 409:132–44
Wiersma RPC, Schaye J, Smith BD. 2009. *MNRAS* 393:99–107
Wiersma RPC, Schaye J, Theuns T. 2011. *MNRAS* 415:353–71
Willott CJ, Delorme P, Reylé C, et al. 2010. *Astron. J.* 139:906–18
Wise JH, Cen R. 2009. *Ap. J.* 693:984–99
Wolfe AM, Gawiser E, Prochaska JX. 2005. *Annu. Rev. Astron. Astrophys.* 43:861–918
Worseck G, Prochaska JX. 2011. *Ap. J.* 728:23
Worseck G, Prochaska JX, Hennawi JF, McQuinn M. 2014a. *Ap. J.* Accepted. arXiv:1405.7405
Worseck G, Prochaska JX, McQuinn M, et al. 2011. *Ap. J. Lett.* 733:L24
Worseck G, Prochaska JX, O'Meara JM, et al. 2014b. *MNRAS* 445:1745–60
Wouthuysen SA. 1952. *Astron. J.* 57:31
Wyithe JSB, Dijkstra M. 2011. *MNRAS* 415:3929–50
Wyithe JSB, Loeb A. 2003. *Ap. J.* 586:693–708
Yajima H, Choi JH, Nagamine K. 2012. *MNRAS* 427:2889–904
Zahn O, Lidz A, McQuinn M, et al. 2007. *Ap. J.* 654:12–26
Zahn O, Mesinger A, McQuinn M, et al. 2011. *MNRAS* 414:727–38
Zahn O, Reichardt CL, Shaw L, et al. 2012. *Ap. J.* 756:65
Zahn O, Zaldarriaga M, Hernquist L, McQuinn M. 2005. *Ap. J.* 630:657–66
Zaldarriaga M. 1997. *Phys. Rev. D* 55:1822–29
Zaldarriaga M, Colombo L, Komatsu E, et al. 2008. *Reionization science with the cosmic microwave background. CMBPol Mission Concept Study*, *Fermilab*, *IL*, *Jun. 23–26.* arXiv:0811.3918
Zaldarriaga M, Furlanetto SR, Hernquist L. 2004. *Ap. J.* 608:622–35
Zaldarriaga M, Hui L, Tegmark M. 2001. *Ap. J.* 557:519–26
Zaroubi S, de Bruyn AG, Harker G, et al. 2012. *MNRAS* 425:2964–73
Zel'dovich YB. 1970. *Astron. Astrophys.* 5:84–89
Zeldovich YB, Sunyaev RA. 1969. *Astrophys. Space Sci.* 4:301–16
Zhang Y, Anninos P, Norman ML. 1995. *Ap. J. Lett.* 453:L57
Zheng W, Kriss GA, Deharveng JM, et al. 2004. *Ap. J.* 605:631–44
Zheng Z, Miralda-Escudé J. 2002. *Ap. J. Lett.* 568:L71–74

Annual Review of Astronomy and Astrophysics

Volume 54, 2016

Contents

Indexes

Errata

An online log of corrections to *Annual Review of Astronomy and Astrophysics* articles may be found at http://www.annualreviews.org/errata/astro